University of Alberta

Efficient Microwave Susceptor Design for Wafer Bonding Applications

by

Amirali Toossi

A thesis submitted to the Faculty of Graduate Studies and Research
in partial fulfillment of the requirements for the degree of

Master of Science

in

Microsystems and Nanodevices

Electrical and Computer Engineering Department

Fall 2012

Edmonton, Alberta

تقدیم به آنها که سبزی وجودشان امید بودن من است...

Abstract

This MSc Thesis demonstrates the use of a novel efficient metallic susceptor for generating controllable and rapid localized heating for low-cost substrate bonding using commercial microwave ovens. The microwave oven is modeled and enhanced microwave susceptors are designed based on electromagnetic simulations. The designed susceptors are then fabricated using a novel low cost prototyping technique for metal electrode patterning. Proposed prototyping technique utilizes a commercial CO_2 laser cuter for metal patterning. Fabricated efficient susceptors are tested inside a commercial microwave oven and show controllable rapid selective heating. It is demonstrated that by use of proposed susceptors, a PMMA substrate can be heated up to 160 °C in less than 8 seconds. We have also demonstrated that the heat generation is localized and selective, making this technique promising for microfluidic or wafer bonding applications. The designed susceptors are then applied to PMMA microfluidics bonding showing a uniform bond along a 4 cm^2 area. Bond strength characterizations show a minimum of 1.375 MPa failure pressure. Bonded micro-channels show no sign of leakage at flow rates up to 9.7 mL/min.

Acknowledgment

First, I would like to thank my supervisors, Dr. Mojgan Daneshmand and Dr. Dan Sameoto for their insight, guidance, encouragements and support throughout my master's program.

Next I would like to acknowledge Dr. Subir Bhattarcharjee and Dr. Sushanta Mitra for providing access to their laboratory equipment.

Sincere appreciations for University of Alberta Nano-Fab, Mechanical Engineering Department machine shop and Electrical and Computer Engineering Department machine shop staff for their technical support.

Thanks to all my friends that have helped me in this project whom without their help and friendship I would not have been able to advance: Maede Marefat, Aaron Seilis, Hamid Moghadas, Mehdi Rezaei, Walid Khaled, Mehdi Nosrati, Saeed Javidmehr, Naga Siva Kumar Gunda, Mohammadreza Shayegh, Nahid Vahabisani and Brendan Ferguson.

This work was funded by NSERC and nanoBridge.

Finally, I thank my family for their restless love and support.

Table of Contents

List of Tables

List of Figures

List of Acronyms

Abbreviation	Description
BCB	Benzocyclobutene
CAD	Computer-Aided Design
DPI	Dots per Inch
IPA	Isopropyl Alcohol
LOC	Lab On a Chip
LTI	Linear Time-Invariant
MEMS	Micro Electro-Mechanical Systems
MSCD	Magnitude of Surface Current Density
MVCD	Magnitude of Volumetric Current Density
PEC	Perfect Electrical Conductor
PMMA	Polymethylmethacrylate
PPI	Pulses per Inch
RF	Radio Frequency
UV	Ultra Violet
VFM	Variable Frequency Microwave

Chapter 1: Introduction

1.1 Motivation

Wafer bonding or sealing processes can be one of the key fabrication steps in the design of microstructures and integrated systems. While a number of wafer bonding techniques have been developed for common substrates (i.e. glass, silicon), they do not meet the quality and efficiency standards of polymers and other the temperature sensitive devices [2]. Polymers have a wide area of usage in today's microstructure fabrication. Cantilevers, pressure sensors, accelerometers, valves, pumps, actuators and micro/nano tubes are just a small number of polymer materials applications in the fabrication of the microstructures [1]. Available low cost processing techniques and chemical and biological characteristics of the polymers are the major motivations of their current wide use [1]. With more and more applications being fit into polymer microstructure design, improving the quality and efficiency of each fabrication step is an important challenge.

Most common available wafer bonding processes either involve heating the wafers up to the melting point of the bonding material or the use of solvents or adhesive materials. For instance, techniques such as thermo-compressive bonding [3], ultrasonic bonding [4] and solvent bonding [5] can cause deformations, damage or level variations on the wafers which cannot be tolerated in the applications of polymer micro-nano fluidic devices [6]. Excessive heat can sometimes cause irreversible damage to the devices and temperature-sensitive substrates (i.e. polymers). Solvents and adhesives also potentially damage or contaminate the fluidic channels. Additionally, wafer bonding techniques must be done in a cost effective manner to allow for affordable mass-production.

Selective heating of the wafers can be a good solution for this problem. A microwave-bonding technique, originally proposed by Budraa et al. [7], is one of the approaches that can provide selective heating. The concept behind this technique is based on the use of microwave radiation to induce current in a very thin conductive layer. The thickness of the conductive layer is smaller than the skin depth of the material (usually metal) and the induced current flow is the main source of relatively fast heat generation in the conductive layer. For bonding, the above-mentioned conductive layers will be used as intermediate layers (localized heating) in between two substrates (Figure 1-1). Heating selectivity can be achieved for substrates with low RF loss (i.e. silicon[7], polymethylmethacrylate (PMMA) [8]) relative to the susceptor material. Rapid heating of the susceptors is also another effective factor for heating selectivity as it will minimize the effect of conductive heating (from the bonding interface) throughout the substrate during the bonding process [8].

There are several advantages to the microwave bonding technique that has made it a good choice for bonding thermoplastics. Rapid, selective and localized heating will provide the option of bonding substrates with melting points below the melting point of the susceptor materials and the generated heat will not get a chance to transfer through the substrate to the neighboring devices. Furthermore, microwave bonding process can be implemented at relatively low cost compared with ultrasonic and thermal bonding methods.

Section 1.2 will describe several common available wafer bonding techniques in detail and Section 1.3 will discuss the microwave bonding background and earlier

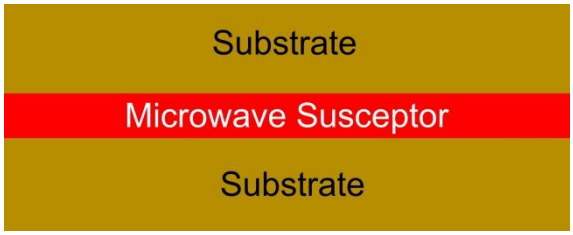

Figure 1-1 - Localized bonding approach using microwave heating

work in this area.

1.2 Wafer Bonding Techniques

Wafer bonding has a wide range of applications from packaging of microstructures to fabrication of microfluidic devices. This section presents common techniques for wafer bonding such as: anodic bonding, thermo-compressive bonding, solvent bonding, adhesive bonding and ultrasonic bonding. Of these, only thermo-compressive, solvent, adhesive and ultrasonic bonding techniques are appropriate for thermoplastic substrates.

- *Anodic Bonding:* Anodic bonding technique, also known as glass-metal bonding, was proposed by Wallis et al. [9] back at 1969. Using this technique the cleaned interface of the wafers (glass and metal) form a bond after heating the wafer stacks under a relatively large applied DC voltage (up to 2000 V), in less than 10 minutes (the heating temperature is between 150-500℃ [10]). A pressure is also applied during the bonding process to ensure good contact between the wafers [11]. The drawback of this technique for low melting point substrates and temperature sensitive devices is the global heating of the wafers up to relatively high temperatures compared to polymers.
- *Thermo-compressive Bonding:* Another approach to bond the wafers together is to use intermediate metallic layers. In [12], a thermo-compressive gold bonding method was used to fabricate Fabry–Pérot microfluidic cavities using Pyrex 7740 substrates. The bonding process of this technique consists of attaching the substrates with gold coating on top of each other followed by applying a holding pressure using aluminum plates and heating the substrates assembled inside a vacuum oven at 10^{-3} Torr to 350℃ for a few hours. Using this technique, a gold-gold diffusion bond is formed with a minimum of 130.557 kPa shear failure pressure.

This technique requires a high temperature step and relatively long processing time which limits its application for temperature sensitive substrates (such as polymers) and devices. Most of the polymers used in microfabrication have glass transition temperatures well below 400℃ [13].

An alternative approach is to melt the intermediate layer for bonding. The glass frit bonding technique uses a low melting point glass intermediate layer and melting the intermediate glass provides a strong hermetic bond. In [14], a thermo-compressive approach is used to melt the intermediate glass frit paste layer and bond two silicon wafers. In their proposed bonding technique, glass frit paste is screen printed (printing thickness of 30 μm and bonded thickness of 10 μm) on the bonding target areas. During the thermo-compressive bonding, the glass melts and the wafers are bonded together when it cools down. The proposed technique provides a bonding strength of 10-30 MPa. The bonding temperature is as high as 430℃.

Alternatively, direct (no intermediate layers) thermo-compressive bonding approach has been applied to polymers. In [15], two PMMA substrates were bonded after the PMMA substrate stack was put inside a convection oven at 108℃ for 10 minutes. PMMA has a glass transition temperature of approximately 105℃. The drawback of polymer microfluidics thermal bonding technique is the resulting deformation in the micro-channels. Zhang et al. [16], have characterized deformation caused by thermal bonding based on the three main variables of this technique: bonding temperature, (holding) pressure and time.

- *Solvent Bonding:* Solvents can be used for bonding polymer substrates to reduce or eliminate the need for elevated bonding temperatures. Substrate material solubility in the selected solvent is the most important factor in the bonding quality [17]. Klank et al. [18] immersed PMMA substrates in ethanol for 10 minutes and then pressed them together while heating at 85℃ (for 90 minutes) for bonding. Hsu et al. [19] used taguchi method

[20] to find the optimized solvent (ethanol, methanol and isopropanol) bonding process (based on the bonding time, pressure and temperature) to achieve minimum structure deformations and maximum PMMA-PMMA bond strength. By their proposed approach PMMA-PMMA bond will have minimum deformations (2-6%) caused by the solvent bonding process (only among the above mentioned solvents) after 5 minutes under 0.25 kg/cm^2 pressure at 60C using isopropanol. Moreover, maximum bond strength (23.5 MPa) will be achieved with ethanol after 9 minutes under 0.25 kg/cm^2 pressure at 100℃.

Although solvents can provide relatively strong bonds [17] they may also damage the substrates if not controlled carefully (large solvent volumes applied or long application time). For instance, in certain situations acetone [5] and alcohol [21] can damage the PMMA substrate in the bonding process. For microfluidics applications solvent damage can also cause channel clogging and deformation. In this respect, Koesdjojo et al [22], have suggested the use of sacrificial layers to protect the channels during the bonding process. In their proposed approach, channels are filled with water and then the channels are cooled down to form ice (sacrificial layer). The PMMA substrates were then bonded with dichlororethane on a cold plate to keep the ice frozen during the bonding process. The channels were heated to remove the water after the bonding process. However, many of these bonding techniques suffer problems in controllability or require high operator skill and are not commercially viable at present.

- *Adhesive Bonding:* Another option for bonding with an intermediate layer is to use glues and epoxies in between. This technique has the advantage of reduced process costs and low temperature processing. Bilenberg et al, [23] used SU-8 intermediate layers to bond Pyrex substrates at different temperatures. In [13], BCB is used to bond two silicon wafers. In the bonding process a 3 μm BCB layer is spun on one of the wafers and is then pre-cured at 65℃ for 5 minutes. After a pre-curing step, the two

wafers with the BCB intermediate layer are attached together with a 2-3 bar holding pressure. Finally, the intermediate layer is cured at 180℃ to form a strong bond. Adhesive bonding with polymers come with drawbacks such as not having hermetic sealing and limited long term stability [24]. Another challenge of adhesive bonding is the leakage of the adhesive material into the devices and channels under bond [17]. In order to control the areas that adhesive (UV adhesive) is applied, silk-screen printing techniques have been used [25]. However even using silk-screen printing, adhesive spreading is still a problem. In this respect, Gutierrez-Rivera et al. [26], used a thin (15 nm) conformal adsorbate film (CAF) as an adhesive for bonding photopolymer layers (KMPR) for microfluidics. A complementary thermo-compressive step is used to cross-link the CAF layer and bond the substrates together. This technique essentially eliminates the adhesive spreading problem.

- *Ultrasonic Bonding:* In [4] ultrasonic energy is used for bonding PMMA substrates. In the bonding process the produced ultrasonic energy is transferred to the bonding interface using designed *energy director* structures (Figure 1-2) providing localized heat (via friction). Energy directors are designed mechanical structures guiding the ultrasonic energy to the desired bonding location (at the substrates' interface). The disadvantage of this technique is that the polymer substrate can be

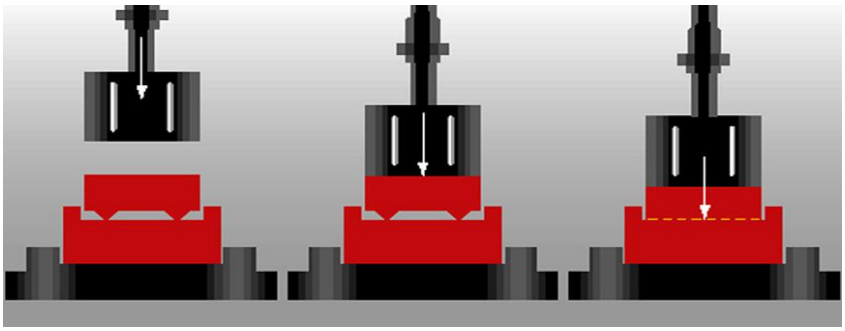

Figure 1-2- Ultrasonic bonding approach using designed energy directors (Reprinted from [4] with permission from Elsevier)

deformed at the energy directors contact proximity (Figure 1-3).

In [27] a wire bonding ultrasonic transducer and horn system is used to bond cellulose acetate substrates using friction. This technique, instead of using energy directors, displacement produced by the ultrasonic horn is used to produce lateral movements for the substrates against each other. Vibration frequency is 60.4 KHz. Using 20 Watts power and a maximum holding pressure of 2.58 MPa, cellulose acetate substrates are bonded after 2 seconds and a hole with 1 mm diameter is encapsulated (Figure 1-4).

In [28], four layers of PMMA substrates (each 1 mm thick) are pre-heated on a hot plate up to 75℃ and then the substrates' stack (held together with 0.16 MPa pressure) undergoes low amplitude (6.6 μm) ultrasound vibrations for 25 seconds for successful bonding. Unlike [4] no energy directors are used and low amplitude vibrations produce heat at the interface.

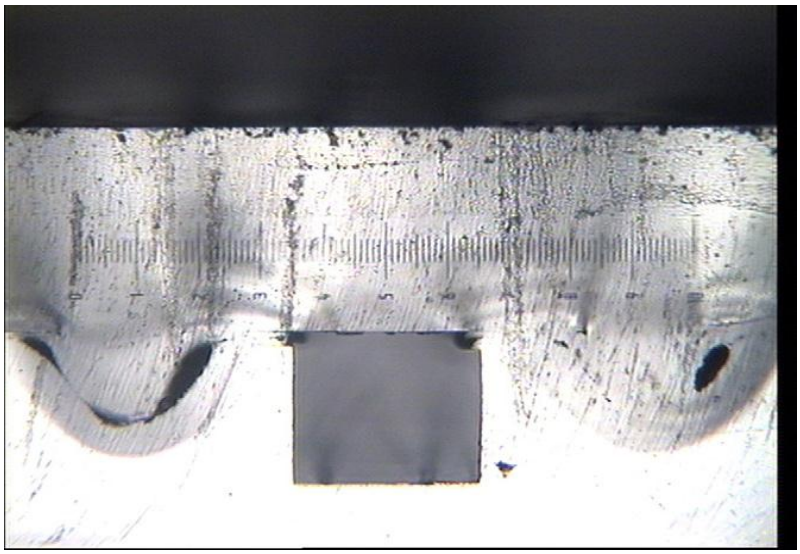

Figure 1-3 – PMMA-PMMA ultrasonic bonding interface showing deformations at the energy directors contact proximity. A 500 μm channel is encapsulated at the center. (Reprinted from [4] with permission from Elsevier)

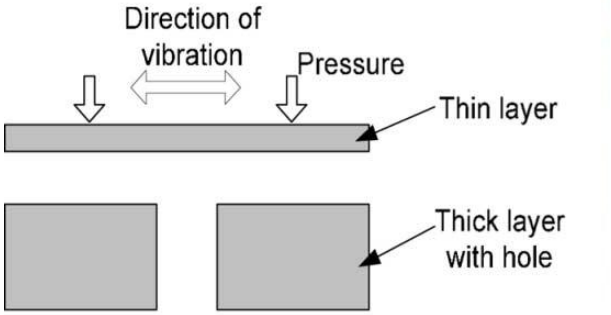

Figure 1-4 – Ultrasonic bonding approach used in [27]to bond cellulose acetate substrates and encapsulate a hole with 1 mm diameter, Copyright © 2009 IEEE.

This section described the details of many common available wafer bonding techniques. Several of the available techniques are not suitable for bonding of temperature sensitive devices or temperature sensitive substrates (i.e. polymers) as most of them include high temperature steps leading to deformations in the device and substrate. The techniques that do not include high temperature steps could potentially damage the substrate in the form of polymer cracking and/or contamination of the devices or microfluidic channels after bonding.

In this regard, microwave bonding approach is advantageous and can potentially offer low cost, low temperature, rapid localized bonding capability. The next section will discuss the microwave bonding technique and the previous works in this area.

1.3 Microwave Bonding Background

In this section, relevant principles of microwave heating will be explained and microwave cavities and their characteristics are described. Later in this section previous works in the microwave bonding area will be reviewed.

1.3.1 Principles of Operation

As mentioned in section 1.1, the microwave bonding technique is based on the use of microwave radiation to induce current in a very thin metallic layer. The induced current flow is the main source of heat generation in the metallic layer. In this section, the basic principles of operation of this technique are described.

1.3.1.1 Microwave Induction and power

Microwave sources (i.e. magnetrons [29]) are the energy source used in microwave heating technique. Microwaves refer to an electromagnetic wave with frequency in the range of 300 MHz and 300 GHz. The behavior of electromagnetic waves can be described by Maxwell's equations [29]:

$$\nabla \times \vec{E} = \frac{-\partial \vec{B}}{\partial t} - \vec{M} \quad (1\text{-}1)$$

$$\nabla \times \vec{H} = \frac{\partial \vec{D}}{\partial t} + \vec{J} \quad (1\text{-}2)$$

$$\nabla \cdot \vec{D} = \rho \quad (1\text{-}3)$$

$$\nabla \cdot \vec{B} = 0 \quad (1\text{-}4)$$

where the symbols are as follows: $\vec{E}$ is the electric field intensity (V/m); $\vec{H}$ is the magnetic field intensity (A/m); $\vec{D}$ is the electric flux density (Coul/m^2);$\vec{B}$ is the magnetic flux density (Wb/m^2); $\vec{M}$ is the magnetic current density (V/m^2); $\vec{J}$ is the electric current density (A/m^2) and ρ is the electric charge density (Coul/m^3).

When an electromagnetic wave reaches the boundary of another medium (i.e. a material being irradiated by the electromagnetic energy in a microwave cavity) part of its energy transmits through the medium, part of it is reflected, another part is stored and the rest will be lost through dielectric, magnetic and conductivity losses [29].

Based on Maxwell's equations, if the material being irradiated by the electromagnetic waves would be a good electrical conductor, the induced electric current mostly flows near the surface (skin effect)[30]. The depth of the conductor at which the magnitude of electric current density reduces to 1/e of its value at the surface of the conductor, is called skin depth and can be derived as ([29], [30]):

$$\delta = \sqrt{\frac{2\rho}{\omega\mu}} \quad (1\text{-}5)$$

where ω is in radians/s and μ is the permeability of the propagation medium.

The skin depth is relatively small for most metals at microwave frequencies. For instance, the skin depth of aluminum at 2.45 GHz is 1.708 μm.

According to [29], the average power dissipated on the good electrical conductor surface (S) can be derived as (Joule's Law):

$$\mathbf{P^t} = \frac{\mathbf{R_s}}{\mathbf{2}} \oint_{\mathbf{S}} \left|\vec{\mathbf{J}}_{\mathbf{s}}\right|^{\mathbf{2}} \mathbf{ds} = \frac{\mathbf{2|E_0|^2 R_s}}{\boldsymbol{\eta_0}^{\mathbf{2}}} \quad (1\text{-}6)$$

$$\mathbf{R_s} = \frac{\mathbf{1}}{\boldsymbol{\sigma\delta}} \quad (1\text{-}7)$$

$$\boldsymbol{\eta_0} = \sqrt{\frac{\boldsymbol{\mu_0}}{\boldsymbol{\varepsilon_0}}} = \mathbf{377}\ \boldsymbol{\Omega} \quad (1\text{-}8)$$

where R_s is the surface resistance of the conductor (defined in equation 1-7), σ is the conductivity ($S \cdot m^{-1}$); J_s is the surface current (A/m); E_0 is electric field amplitude constant; η_0 is the wave impedance in free space (Ω); μ_0 is permeability of free space and ε_0 is the permittivity of free space. With the assumption of uniform power distribution (throughout the surface) based on Joule's law, the heat generation rate (per unit time, per unit area) for the good electrical conductor is equal to P^t value [31]. It is shown that the amount of power loss (resulting in heat generation) in the conductive layer is proportional to the applied field intensity and the surface resistivity of the conductive material

1.3.1.2 Microwave Cavities

Microwave cavities are the structures that are commonly used for irradiation of objects with electromagnetic waves. The basic definition of a microwave cavity is an enclosed structure made up of reflective (for electromagnetic waves) high conductivity material (i.e. metal) boundaries. Microwave cavities are excited by waveguide feeds and support standing waves.

As mentioned earlier, Maxwell's equations describe the behavior of the electromagnetic waves. Thus, solving these equations considering boundary conditions results in different solutions commonly referred to as *modes* [29]. Microwave cavities support TE and/or TM modes:

- *TE Mode:* Transverse Electric Mode which describes travelling electromagnetic waves which do not have electric field component in their propagation direction
- *TM Mode:* Transverse Magnetic Mode which describes travelling electromagnetic waves which do not have magnetic field component in their propagation direction

Based on Maxwell's equations, a sinusoidal electromagnetic wave with the rectangular cavity boundary conditions has the following solution [29], [32]:

$$\mathbf{E_x} = \mathbf{E}_{x0} \cos\frac{\pi m}{a} x \ \sin\frac{\pi n}{b} y \sin\ \frac{\pi l}{d} z \ \mathbf{e}^{\mathbf{j\omega t}} \quad (1\text{-}9)$$

$$\mathbf{E}_y = \mathbf{E}_{y0} \sin\frac{\pi m}{a} x \cos\ \frac{\pi n}{b} y \ \sin\ \frac{\pi l}{d} z \ \mathbf{e}^{\mathbf{j\omega t}} \quad (1\text{-}10)$$

$$\mathbf{E}_z = \mathbf{E}_{z0} \sin\frac{\pi m}{a} x \ \ \sin\frac{\pi n}{b} y \cos\ \frac{\pi l}{d} z \ \mathbf{e}^{\mathbf{j\omega t}} \quad (1\text{-}11)$$

where the symbols are as follows: m, n and l are the (integer) mode indices; a, b and d (W x L x H) are the rectangular cavity dimensions (Figure 1-5(a)); E_{x0}, E_{y0}, E_{z0} are amplitude constants and t is time.

Microwave cavities only support certain electromagnetic wave modes and (resonant) frequencies based on their geometry characteristics [29]. For instance, for a rectangular cavity the resonant frequency can be derived from:

$$f_{mnl} = \frac{C_l}{2\pi\sqrt{\mu_r \epsilon_r}} \sqrt{(\frac{m\pi}{a})^2 + (\frac{n\pi}{b})^2 + (\frac{l\pi}{d})^2} \quad (1\text{-}12)$$

where C_l is the speed of light; ϵ is the permittivity of the propagation medium and μ_r is the relative permeability of the medium. As shown in equation (1-12), only certain modes can be excited in the cavity (based on its physical dimensions).

Cavities are categorized based on the number of modes that they can support: *single mode* and *multimode* cavities. Single mode cavities commonly have physical dimensions close their operating wavelength while multimode cavities have physical dimensions of at least twice the wavelength to allow for multiple mode excitations [33], [34]. Single mode cavities have more distinct (based on design) hot and cold spots (high and low field intensity regions) compared with multimode cavities (Figure 1-5). On the other hand the supported mode in the single mode cavity is generally very sensitive to additional load. However multimode cavities are less sensitive as they can support various modes [33], [34].

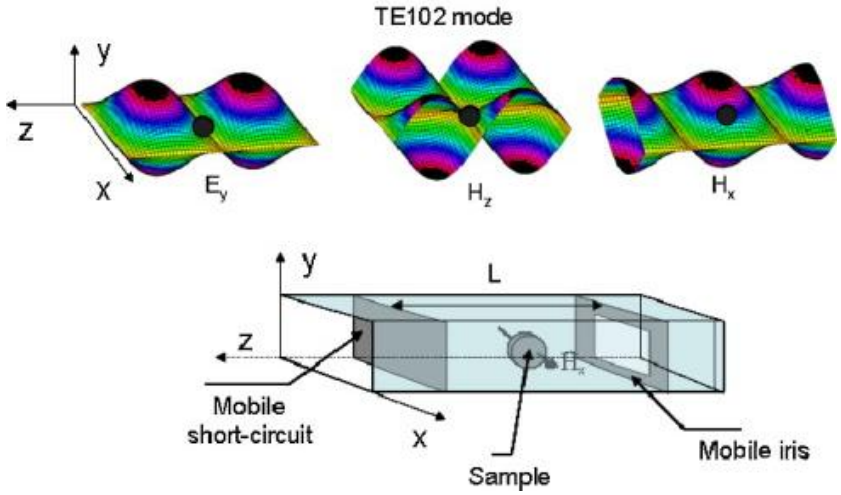

(a)

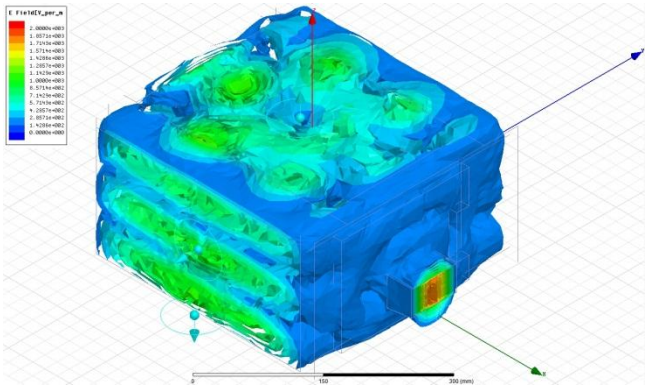

(b)

Figure 1-5 – (a) TE102 mode single mode rectangular cavity and its field distribution (Reprinted from [35] with permission from Elsevier) (b) Electric field simulation of a commercial microwave oven rectangular cavity (multimode cavity)

This is one of the reasons multimode cavities are the most common type of the microwave cavities.

Commercial Microwave Oven: One of the most common multimode cavity applications is in commercial microwave ovens. Commercial microwave ovens consist of a microwave source (magnetron); a waveguide that feeds the cavity (commonly rectangular); multimode cavity connected to the waveguide feed and a glass turn-table rotating on a rotor during the microwave oven operation. As shown in Figure 1-5(b), the excitation of a multimode cavity results in formation of standing waves and therefore uneven field distribution (and uneven heating) inside the cavity. The turn-table acts as a compensator for uneven heating. In addition to turn-tables, some microwave ovens also have a metallic fan blade (also called *mode stirrer*) to change the fields [29].

1.3.1.2 Heat Transfer

The heat generated on the *good electrical conductor* material as a result of microwave radiation, will then transfer through the underlying substrate and the materials in contact with it. Assuming that the thicknesses of the conductor and its substrate are significantly smaller than their length and width, a one dimensional (perpendicular to the surface) heat transfer approximation can be used [36]. Equation 1-13 describes the transient heat transfer of the good electrical conductor material under radiation (Figure 1-6)[36]:

$$\dot{E}_g - [2 \times h(T - T_{fl}) + e\sigma(T^4 - T^4_{sur}) + \frac{\acute{k}}{L}(T - T_{fl})]A_s = \rho V c \frac{dT}{dt} \quad (1\text{-}13)$$

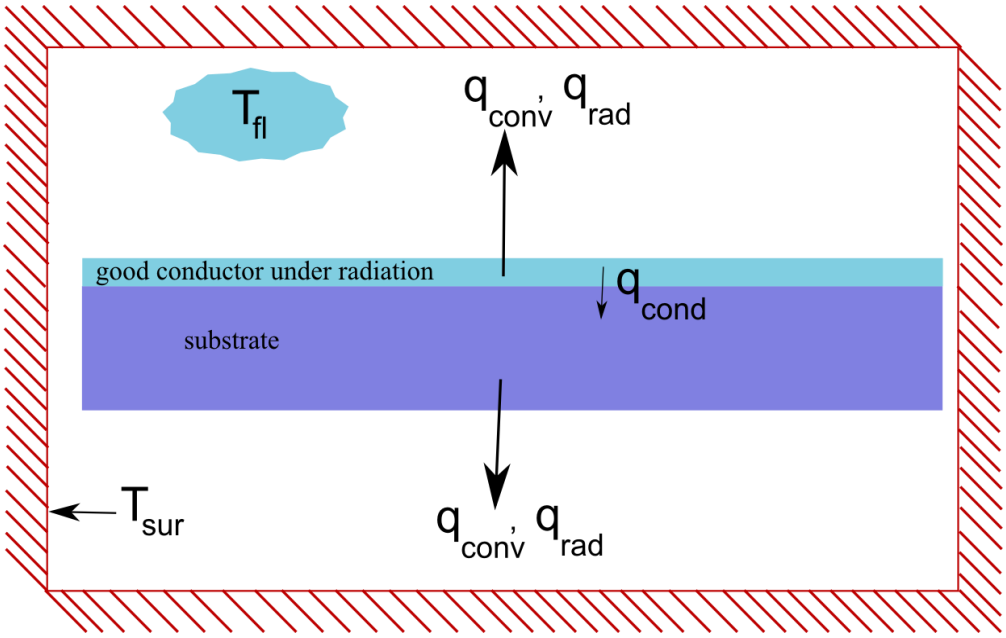

Figure 1-6 – Heat transfer model

where the symbols are as follows: $\acute{\rho}$ is the density (kg/m^3); c (J/kg.K) is the specific heat at constant pressure; V is the volume (m^3); A_s is the surface area (m^2); L is the thickness of the substrate (m); $\acute{k}$ is thermal conductivity (W·m^{-1}·K^{-1}); T_{fl} is the air (fluid) temperature (K); T_{sur} is the surroundings temperature(K); h is the convection heat transfer coefficient; $\dot{E}_g$ is the generated energy flux in the material (W) (in this case equal to P^t (derived in equation 1-10)) ; t is the time; $\acute{\sigma}$ is the Stefan–Boltzmann constant (W m^{-2} K^{-4}) and e is the emissivity of the material.

In cases when radiation can be neglected equations 1-13 will become in the form of a non-homogenous Linear Time-Invariant system (LTI) differential equation [36]:

$$\frac{\mathbf{d\Delta T}}{\mathbf{dt}} + \mathbf{a_1 \Delta T} + \mathbf{a_2} = \mathbf{0}\ ;\ \mathbf{\Delta T} = \mathbf{T} - \mathbf{T_{fl}} \qquad (1\text{-}14)$$

In this case the solution for the conductor material temperature is [36]:

$$\frac{T - T_{fl}}{T_i - T_{fl}} = \exp(-a_1 t) - \frac{a_2/a_1}{T_i - T_{fl}} \times [1 - \exp(-a_1 t)] \quad (1\text{-}15)$$

where T_i is the initial temperature.

For bonding experiments in which the *good electrical conductor* layer is sandwiched between two solid substrates (Figure 1-1) the primary source of heat loss during the transient state will be purely conductive to the substrates.

1.3.2 Earlier Works in Microwave Bonding

The first experiment conducted based on the microwave heating concept was silicon-silicon bonding using gold intermediate layers (Figure 1-7) [7]. Each intermediate layer (on each of the substrates) consisted of an adhesion promoter layer to bond gold to silicon (15 nm of chrome) and a susceptor layer (120 nm of gold).

In the experiment, substrates (4 inch silicon wafer) and intermediate stacked layers are put inside a custom-built single mode cavity in high vacuum (~25 μTorr) without any pressure application. Substrates were successfully bonded after 3 seconds of microwave radiation at 2.45GHZ and 300 Watts power.

The same approach has also been applied for PMMA-PMMA bonding. PMMA is one of the most common thermoplastics used in fabrication of microfluidics due to its optical transparency, chemical compatibility, relatively low price and wide accessibility [17]. One of the biggest challenges in fabrication of microfluidics is

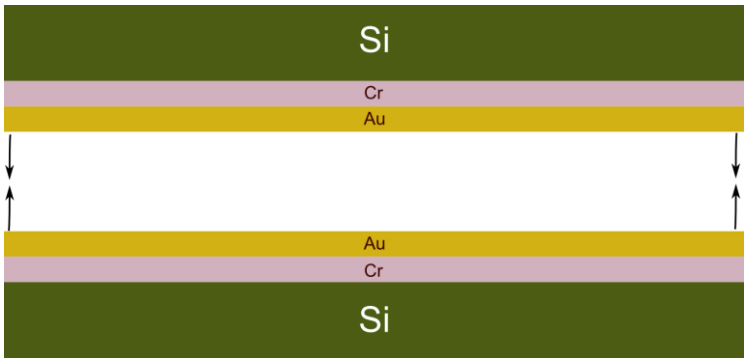

Figure 1-7 – Silicon-Silicon microwave bonding approach used in [7].

achieving high yield bonding processes with minimum damage to the channels. Similar to Budraa et al.'s approach, Lei et al. [8], [37], used chrome (50nm, adhesion promoter) and gold (50nm, susceptor) as intermediate layers between two PMMA substrates. In this approach, a micro-channel is fabricated on one of the PMMA substrates using the hot-embossing technique [38–40] before chrome and gold deposition and therefore the channel is coated with gold (Figure 1-8). The substrate stack is then bonded inside a custom-built single mode cavity at 2.45 GHz and 10 Watts power after approximately 120 seconds.

In addition to metal intermediate layers, conductive polymers have also been used for microwave bonding purposes. Yussuf et al. [41], used surrounding channels containing polyaniline suspension solvent (conductive polymer) around the target micro-channel to supply the required local heat for PMMA bonding. Using this approach, after 15 seconds of microwave radiation (2.45 GHz) they successfully bonded PMMA microfluidic channels (Average failure pressure of 1.18 MPa) together in a custom-built single mode cavity powered by a 300 W microwave source. PMMA substrates were attached together under a pressure of 0.12 MPa for the bonding experiment.

The idea of using surrounding channels as the heat source avoids channel contamination but it is a limiting factor for bonding of multiple microfluidic

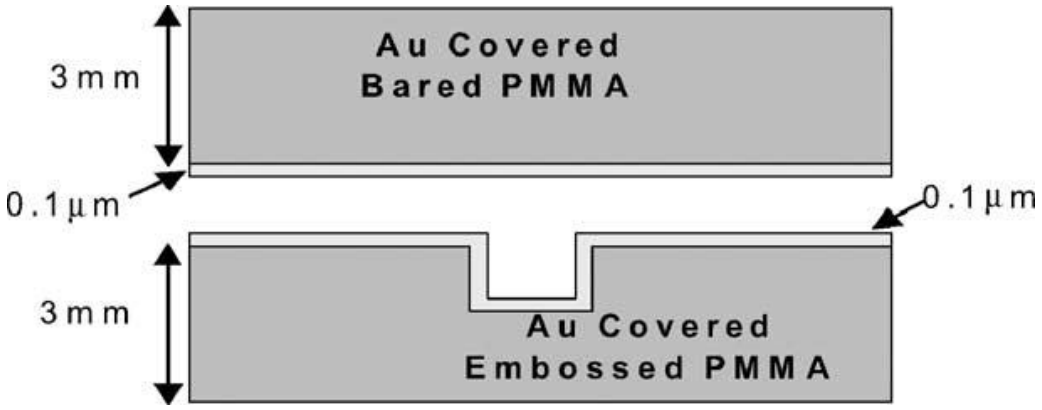

Figure 1-8 – PMMA-PMMA microwave bonding approach used in [8], [37]. (Reprinted from [37] with permission from Elsevier)

channels in close proximity (uniformity of heating and bonding quality is challenged).

Holmes et al. [42] also used conductive polymers (Polyaniline with up to 100um particle size) as microwave susceptors. In their approach, a relatively inexpensive commercial microwave oven (900 W) is being used as energy source.

In the experimental setup PMMA substrates (with micro-channel features) are clamped together using acrylic screw threads and wing nuts (Figure 1-9). The channels are then filled with polyaniline solution in methanol via capillary action. In their reported experiment, channels were successfully bonded after 30 seconds of microwave operation at 900 W. Although this technique has the advantage of using inexpensive equipment, it also has the disadvantage of leaving polyaniline particle residues (contamination) inside the channels after the bonding process.

Microwave heating has also been used to assist other bonding methods. Rahbar et al. [21] used microwave heating to enhance solvent bonding of the PMMA microfluidics. In their technique, an inexpensive commercial microwave oven has been used as an energy source. Off-the-shelf ferromagnetic miniature binder clips are used as microwave susceptors. In the bonding experiment PMMA substrates are clamped together having a poor solvent (alcohol) inserted at their interface. The substrate stack is held together using the binder clips attached all around the

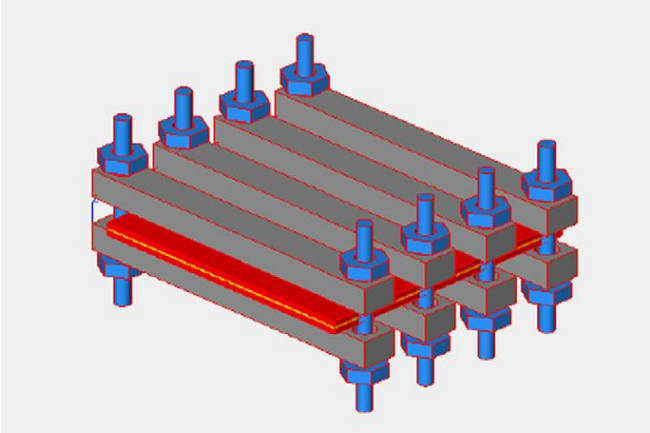

Figure 1-9 – PMMA-PMMA microwave bonding approach used in [42]. (Reprinted from [42] with permission from Elsevier.)

stack (Figure 1-10). Unlike the previous methods, this time the interface of the metal (in this case stainless steel) and the PMMA substrate is located on the outer surface of the substrates (external heating instead of localized heating). The heat generated by the binder clips propagates through the substrate and helps the solvent (alcohol) bonding process at the inner interface of the PMMA substrates. The bonding process based on this method takes up to 90 seconds. The PMMA substrates' bond achieved by this method has greater bond strength than direct solvent bonding with ethanol. One of the drawbacks of this technique is that it does not produce localized heating. Additionally, as mentioned earlier, using alcohol can damage PMMA substrates.

Dielectrics (instead of electrically conductive materials) have also been used for Microwave/RF bonding. Bayrashev et al. [43], proposed to bond two silicon substrates with a thick layer (2-20um) of polyimide in between. In their experiment a 500 watts RF source (14 MHz) was used to heat the dielectric up to its glass transition temperature (325-400℃℃ [43]) in order to bond the two

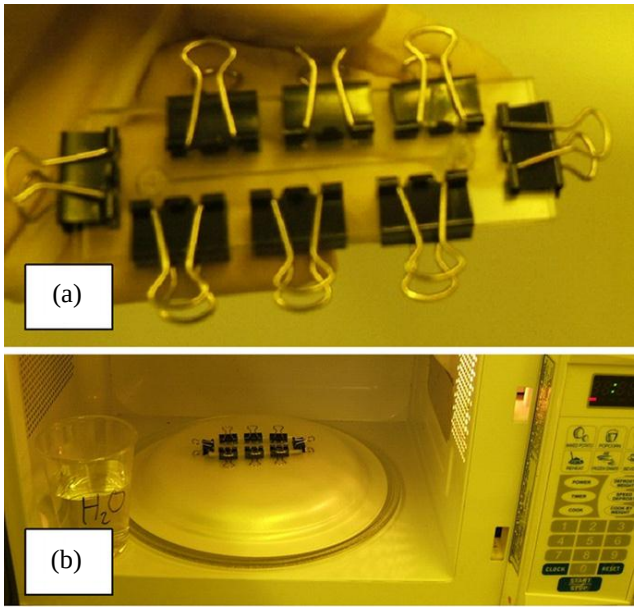

Figure 1-10 - PMMA-PMMA microwave bonding approach used in [21]. (a) PMMA substrates attached with binder clips (b) Bonding experiment setup (Reprinted from [21] with permission from authors and IOP Publishing Ltd.)

wafers (acting as an adhesive). The bonding process took 7 minutes to complete and the silicon substrates temperature stayed below 280℃.

In [44], Parylene was used as an intermediate layer for wafer bonding instead of polyimide. Parylene (glass transition temperature <90℃ [44]) is a crystalline and thermoplastic polymer in comparison with polyimide which is amorphous and a thermoset polymer. In the bonding experiment a commercial variable frequency microwave (VFM) has been used for enhanced uniform heating. Using Parylene as an intermediate layer, silicon wafers bonding is achieved at 160℃ and in ten minutes. In comparison with a polyimide intermediate layer, this was a lower temperature, making it better for thermally sensitive applications. However regardless of the temperature, they both require relatively long time for the bonding process which allows the localized generated heat to transfer to the devices and channels across the wafer.

In conclusions, electrically conductive susceptors show a faster and more selective heating process compared to direct heating. However, they have been mostly employed in bonding using customized microwave cavities and microwave sources, which are relatively costly and less accessible for widespread use. Commercial microwave ovens have been recommended as an alternative in few studies [21], [42]. However, these methods can contaminate the device and channels. In the next section we propose our solution to these problems.

1.4 Proposed Work

***Objective**: The objective of this thesis is to introduce a new technique to use microwave field and generate low cost, rapid, selective and localized heating for wafer bonding applications.*

In this study, we introduce a new category of designed metallic microwave susceptors added to the substrate interface to generate efficient and rapid selective heating. Figure 1-11 depicts the application of the electrodes on the surface of the substrate for device packaging and microfluidic bonding. We show that the substrate bonding can happen in localized areas and in less than 1 min. For this study, we utilize conventional microwave ovens as the energy source due to their relatively low cost and wide accessibility. To prototype the samples we propose using a commercial CO_2 laser cutter system for low cost metal electrode patterning.

The structure of the thesis is as follows. Chapter 2 will focus on the basics of the sample development technique using CO_2 laser cutter. To our knowledge, we for the first time are proposing to use such type of laser cutters for metal electrode patterning. Chapter 3 explains the proposed category of electrodes to use for microwave substrate bonding. Their characterization and performance is explained in details. Then, the proposed electrodes are used to bond the substrates and the results are presented in Chapter 4. At the end, our conclusions and summary of the thesis work along with the proposed future work is presented.

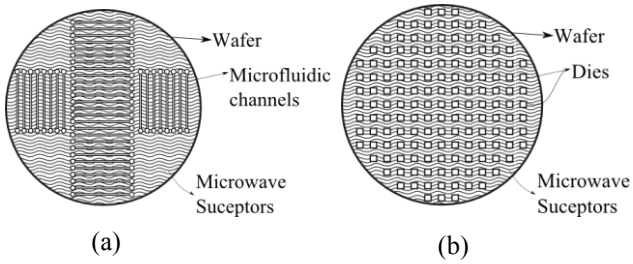

Figure 1-11 – Demonstration of using microwave susceptor for (a) microfluidics bonding (b) die

Chapter 2: A Low Cost Rapid Prototyping Method for Metal Electrode Fabrication using a CO_2 Laser Cutter[1]

Discussed in Chapter 1, our proposed microwave susceptors are comprised of a patterned thin metal film on top of a PMMA substrate. Therefore, there is a need for a suitable metal patterning prototyping technique for the experimental study of the designed susceptors.

One common solution is use of lithography and etching process, which requires relatively expensive clean room facilities and takes a long time. Less expensive substitutes are transparency photomask lithography ([45], [46]) and hot embossing lithography [47]. Although they reduce the fabrication cost, these techniques still require clean room facilities with multiple fabrication steps. Therefore, an alternative cost effective and rapid prototyping technique is very advantageous. This was particularly vital for our application in which initial experimental design rules were unknown and because failure modes like arcing could not be simulated using tools like HFSS.

Laser-machining is a direct-write patterning technique, which provides rapid electrode fabrication and significantly reduces the time interval between the design and implementation steps. Laser machining of metal electrodes has been previously performed using different laser types such as excimer ([48], [49]) femto-second [50] and ND:YAG ([51], [52]) lasers. In this study, we are proposing the use

[1] A version of this chapter has been submitted for publication to Journal of Micromechanics and Microengineering

of a commercial CO_2 laser cutter system for metal electrode patterning. Although CO_2 laser cutters have a relatively large kerf value (due to their spot size and thermal damage) compared to femto-second and ND:YAG lasers, they are more commercially accessible and do not require a custom experimental setup for their operation.

In this chapter, we present the use of commercial CO_2 laser cutters for thin aluminum (~100nm) electrode patterning such as the ones shown in Figure 2-1.

The ability to process materials with certain lasers is dependent on the operating laser wavelength absorption in the material. Absorptivity is defined as the ratio of beam energy that is absorbed by the material to the total energy of the beam. Absorptivity of materials for normal angles of radiation can be calculated as [53]:

$$\mathbf{A}(\boldsymbol{\lambda}) = \mathbf{1} - \mathbf{T}(\boldsymbol{\lambda}) - \mathbf{R}(\boldsymbol{\lambda}) \qquad (2\text{-}1)$$

for opaque materials (T=0):

$$\mathbf{A} = \mathbf{4n}/[(\mathbf{n}+\mathbf{1})^{\mathbf{2}} + \mathbf{k}^{\mathbf{2}}] \qquad (2\text{-}2)$$

where A is the absorptivity, T is the transmittance and R is the reflectivity of the material; n is the refractive index of the material and k is the extinction coefficient.

Table 2-1 shows the absorptivity values for bulk aluminum [53] and gold [54] (with no transmittance assumption) at wavelengths of 1.06 μm and 10.6 μm.

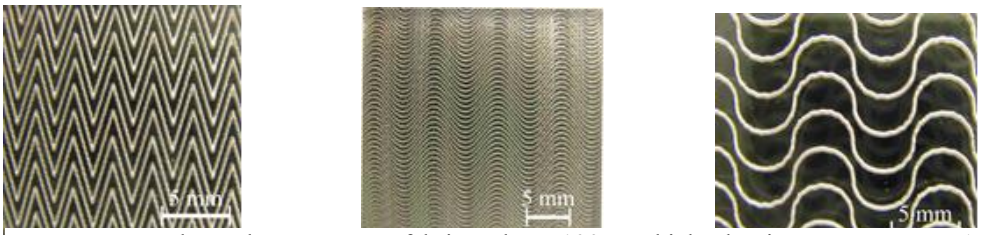

Figure 2-1 – Electrode prototypes fabricated on 100nm thick aluminum on a PMMA substrate (CO_2 laser cutter settings: vector cutting mode, Pulses per Inch (PPI) = 500, 15% power, 25% speed)

Table 2-1 – Refractive index, extinction coefficient and absorptivity values of aluminium and gold (no transmittance assumption) [61],[62]

Wavelength	Material	n	k	A
1.06 µm	Al	1.75	8.5	0.877
10.6 µm	Al	0.108	34.2	0.00037
1.06 µm	Au	0.256	6.9346	0.0206
9.919 µm (maximum wavelength provided by Palik [62])	Au	12.24	54.7	0.01545

However, the no transmittance assumption is not true for thin metal films. Axelevitch et al. [55] studied the effect of metal film thickness changes on transmittance at optical frequencies (Figure 2-2).

The concept of metal patterning using CO_2 laser systems is based on laser ablation of the underlying substrate. Although CO_2 laser beam's absorptivity is small for aluminum [53], [56], when the laser beam hits the thin aluminum layer a portion of the energy is reflected while another portion is transferred through the metal to its underlying substrate. If enough energy reaches to the substrate that is

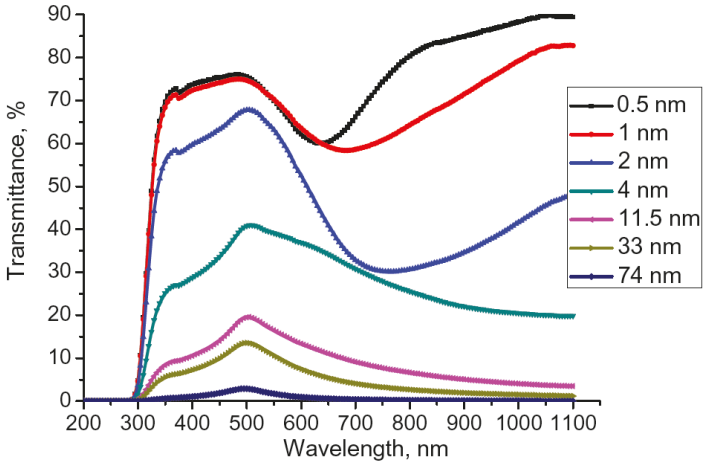

Figure 2-2 – Transmittance percentage of thin film gold with respect to wavelength (Reprinted from [55] with permission from Elsevier)

a good absorber of the CO_2 laser wavelength, (depending on the energy level) a small thickness of the substrate and its aluminum coating is removed from the substrate.

CO_2 laser wavelengths are absorbed by wide range of materials including Pyrex ([57], [58]), polymers and plastics such as polymethylmethacrylate (PMMA) ([59–62]) and Si-rubber [62]. In this study we have used PMMA as our substrate material.

In the following sections, the CO_2 laser cutter metal patterning is experimentally characterized for various laser power levels and pattern critical dimensions. A successful prototyping example for microwave heating applications is presented. The manufacturing method paves the way for use of CO_2 laser as an inexpensive alternative to the existing techniques for patterning thin metal films.

2.1 Characterization of CO_2 Laser Cutter for Metal Patterning

Our experimental setup for metal electrode patterning characterization consisted of VLS 3.50 Versa Laser CO_2 laser cutter [63] (Figure 2-3) and polymethylmethacrylate (PMMA) substrates coated with aluminum. The VLS 3.50 Versa Laser consists of a 50 W CO_2 laser mounted on a mechanical arm capable of two dimensional (in plane) movements; a 24 in. x 12 in. work surface area (perpendicular to the laser beam) with vertical movement capability; and a High Power Density Focusing Optics (HPDFO) (Figure 2-4) attachment for

Figure 2-3 – Electrode prototypes fabricated on 100nm thick aluminum on a PMMA substrate (CO_2 laser cutter settings: vector cutting mode, Pulses per Inch (PPI) = 500, 15% power, 25% speed)

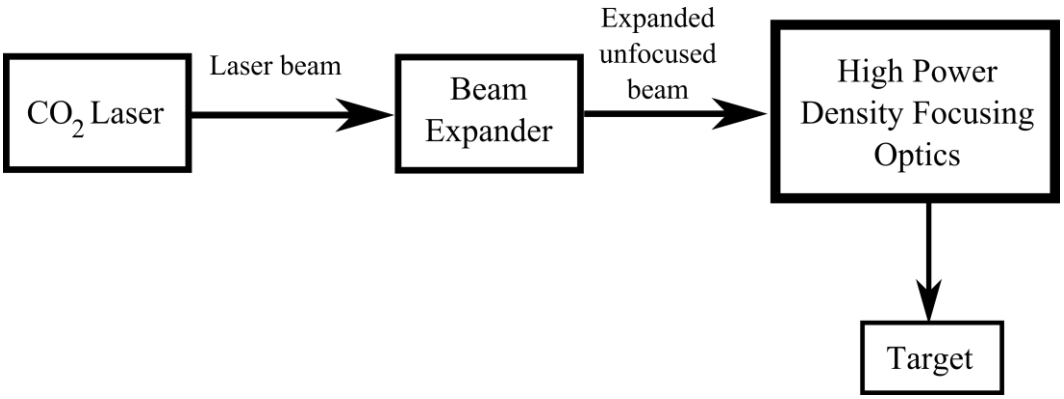

Figure 2-4 – High Power Density Focusing Optics (HPDFO) block diagram [64]

enhancing cutting precision (by reducing the spot size of the laser beam) and increasing the power density [64]. The HPDFO optics used with the 1.5 focus lens, available on the VLS 3.50 laser cutter, can produce a spot size diameter as small as 75 μm for very flat surfaces [64].

Test samples are prepared using a magnetron sputtering system in two aluminum layer thicknesses of 20nm and 100nm. Layouts are drawn in Corel Draw© software which is the CAD tool associated with the laser cutter for pattern transfer.

The VLS 3.50 laser cutter system operates in two modes that can be utilized based on the width of the lines required in the layout: vector cutting for line widths below 200μm and raster engraving for line widths above 200μm. In vector cutting mode the laser source follows a two dimensional path based on the designed CAD pattern while in raster engraving mode the designed CAD pattern image is divided into an array of dots (with a resolution of up to 1000 dpi) for cutting [65]. Vector cutting mode is mostly used for cutting thin lines or making through cuts in the substrate while raster engraving mode is commonly used for engraving relatively large (line width larger than 200μm) features in the substrate. In this study, both modes are characterized for metal patterning.

2.1.1 Vector Cutting Mode

Assuming that CO_2 laser optics are focused on the target substrate, three variables can influence the characteristics of a vector cut: number of pulses per inch (PPI), the speed of the cutting and the laser power level. Speed and power are specified with percentages of the maximum values. The maximum power value on the VLS 3.50 laser is 50 W and the maximum speed is approximately 10 mm/s [65].

VLS 3.50 Versa Laser CO_2 laser cutter has a maximum value of 1000 PPI. Figure 2-5 shows the cut traces using various values of PPI. As shown in Figure 2-5-(a), selecting low values will result in having discrete circular cuts in a straight line pattern instead of a continuous line cut.

Increasing the PPI value will generally increase the resolution of the cut pattern. However, for low melting point substrates increasing the PPI value may result in

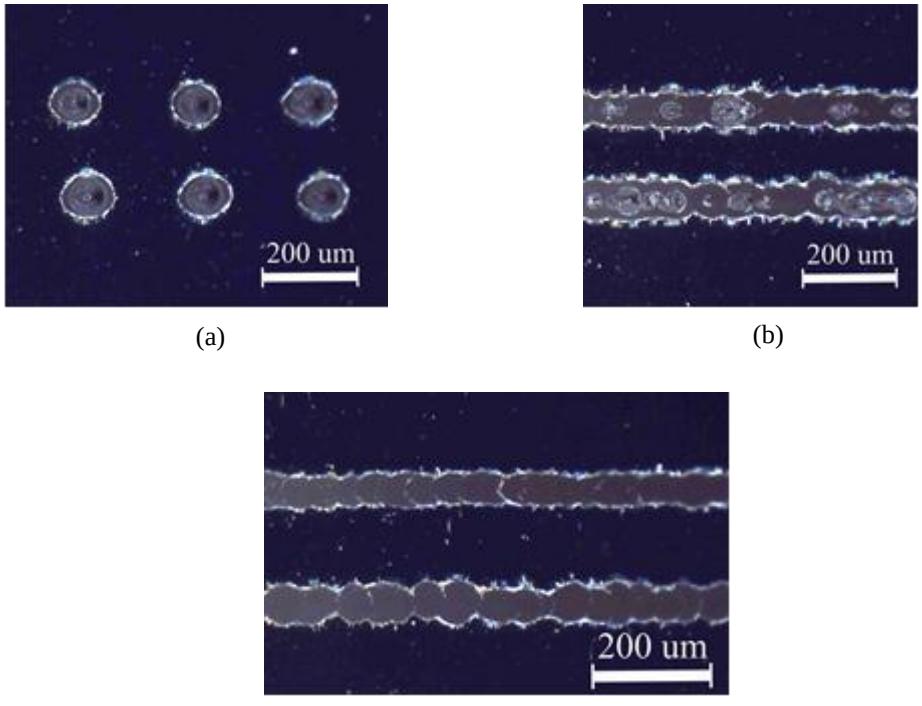

(a) (b)

(c)

Figure 2-5- Removing two parallel horizontal lines of 20nm aluminum layer in vector cutting mode with different PPI settings (a) PPI equal to 100 (b) PPI equal to 500 (c) PPI equal to 1000 (maximum value)

having larger areas of the substrate molten or deformed.

As mentioned earlier, cut patterns designed in CAD (Corel Draw) with line width of less than 200 μm are cut using the vector cutting mode. In this mode, patterns are cut using a constant line width (regardless of their original width settings), also known as hair line, which is less than 100μm wide (equal to the laser beam spot diameter on the target surface (Gaussian-based beam size), Figure 2-6).

The minimum power and speed level required for completely removing aluminum from the substrate is characterized based on electrical insulation criteria. For this purpose, a relatively large (4 square inch) non-patterned aluminum coated substrate was chosen as our experiment ground plane. Then an array of 0.5 cm x--0.5 cm square patches (square outline cut pattern) was cut on the aluminum sheet using different speed and power level settings.

The resistivity of the aluminum square patches was then measured (with respect to the ground plane (outside of the cut pattern)). The minimum power and speed settings, providing insulation (high resistivity) were selected as the minimum threshold for removing aluminum.

To remove 20 nm of aluminum using the laser cutter in vector cutting mode, 0.2% power and 30% speed was required. For a layer of aluminum 100nm thick, the

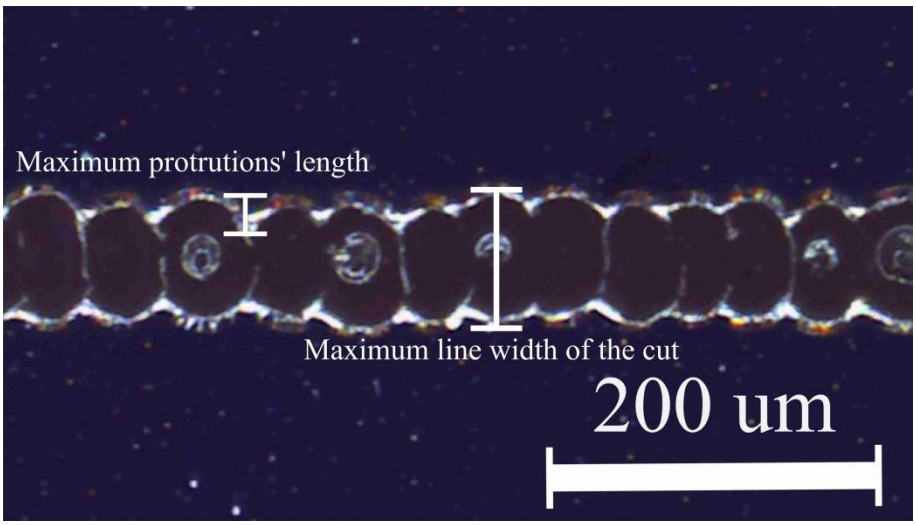

Figure 2-6 - A *hairline* wide line vector cut showing the characterization variables. 20nm Al, PPI: 500, power: 0.5%, speed: 30%.

required settings were 2% power and 30% speed. It is worth noting that both power and speed levels are chosen based on the required effective power delivered to the aluminum surface and therefore, other equivalent combination sets can be alternatively chosen. However, lower power levels and medium speed is desired in general for optimum cutting quality as higher power levels lead to an increase in the minimum feature size that can be cut.

In contrast with conventional lithography-etching techniques, CO_2 laser cut patterns will have jagged edges along the cut as shown in Figure 2-6. The jagged edge characteristics depended on two main factors: PPI value and ventilation flow power and direction.

As shown in Figure 2-7, the laser cut pattern is comprised of circular dots (laser beam spot) with a diameter of less than 100 μm. Therefore, increasing the PPI value leads to an increase in the density of laser beam spots along the cutting pattern. This increase in spot density, results in having smaller jagged edges near the margins of the cutting pattern.

Based on this concept, protrusions are always smaller than 50 μm long (laser beam spot radius). This is consistent with our experimental observations shown in figures Figure 2-5 and Figure 2-6. Based on our experiments, the protrusions' length for PPI 1000, 0.2% power, 30% speed on a 20nm aluminum sample are

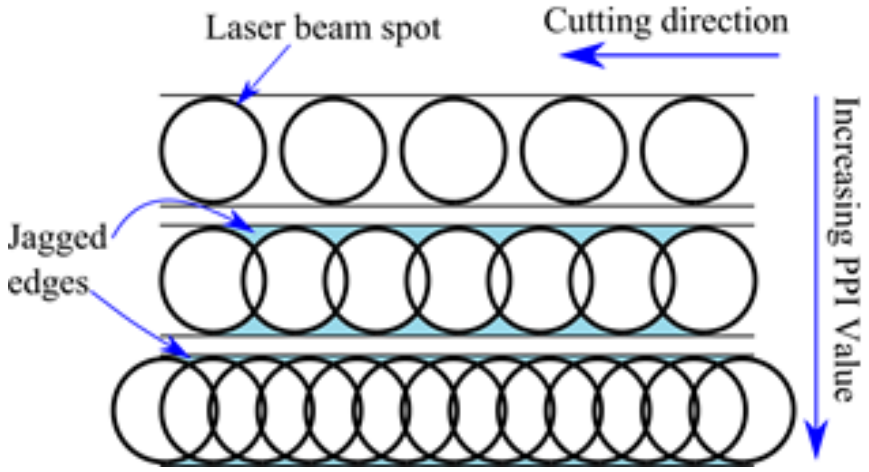

Figure 2-7 - Jagged edge area changes by PPI value variations

approximately 20 μm. This parameter is characterized for various fabrication parameters and illustrated in Table 2-2.

The ventilation flow is supposed to blow away the vaporized debris of the laser cutting process. Flow power and its direction can also affect the jagged profiles of the laser cut edges as small amounts of cutting debris may be re-deposited on the surface of the sample. To avoid this problem, ventilation flow should be strong and, if possible, directed along the cutting direction. Although the direction of the flow within the Versa Laser could not be controlled directly, the orientation of the design could be arranged to ensure the flow was in the most preferential direction.

The metal electrode width (between cutting patterns) is defined as electrode feature size. The minimum feature size characterization results of the laser cut electrodes for the sample with 20nm aluminum coating are shown in Table 2-2 and Figure 2-8. Table 2-3 shows the characteristics of the hairline cuts in the same conditions.

Table 2-2 - Minimum feature size of laser cut aluminium (20nm thickness, PPI: 1000, 0.2% power, 30% speed)

Orientation of the cut (note: ventilation flow is along Y axis)	Parallel line spacing in the design	Minimum electrode width	Jagged edge protrusion's maximum length relative to electrode width
X axis	200 μm	130 ± 5 μm	14.4%
X axis	450 μm	375 ± 5 μm	5%
X axis	1 mm	925 ± 5 μm	2%
Y axis	200 μm	125 ± 5 μm	12%
Y axis	450 μm	375 ± 5 μm	4%
Y axis	1 mm	930 ± 5 μm	1.6%

Table 2-3 - Hairline cut characteristics (20nm thickness, PPI: 1000, 0.2% power, 30% speed)

Cut orientation	Minimum cut width	Jagged edge protrusion's maximum length relative to cut width
X axis	70 ± 5 μm	26 %
Y axis	70 ± 5 μm	21 %

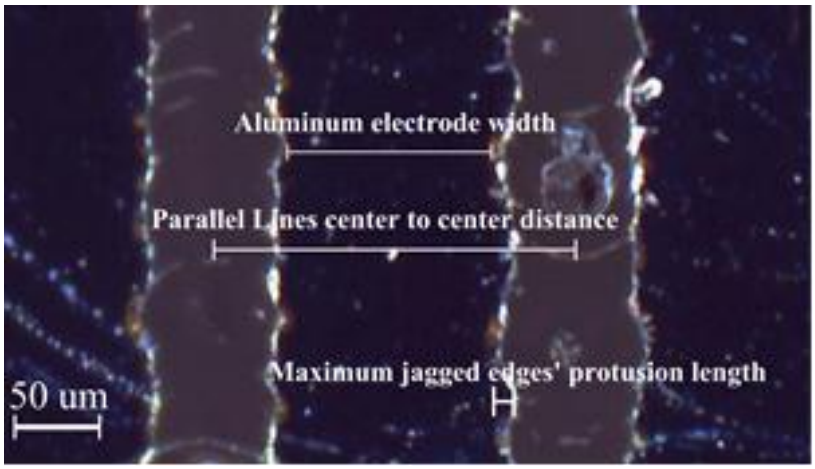

Figure 2-8 - Minimum feature size characterization variables of an electrode cut along Y axis

2.1.2 Raster Engraving Mode

Characteristics of raster engraving mode of the laser cutter are controlled by power level and processing speed settings [65].

It is worth noting that the VLS 3.50 versa laser only rasters in 1 direction (annotated by x axis on VLS 3.50 software) and as a result of that, the laser cutter grids the pattern by horizontal lines and rasters it row after row. Rastering row by row requires turning the laser source on and off based on the pattern along the horizontal line which results in a reduced cut quality for vertical lines compared with horizontal lines (Figure 2-9).

We used the same technique as our previously explained vector cutting mode characterization to find the optimum power/speed setting. For 100nm and 20 nm thick aluminum layers, 9% power and 30% speed and 6% power and 30% speed levels were required respectively.

2.2 CO_2 Laser Cutter Application for Rapid Prototyping

A CO_2 laser cutter can be used for wide variety of applications. This section illustrates one of the applications for microwave susceptors and appendix A will present an alternative application for antenna prototyping.

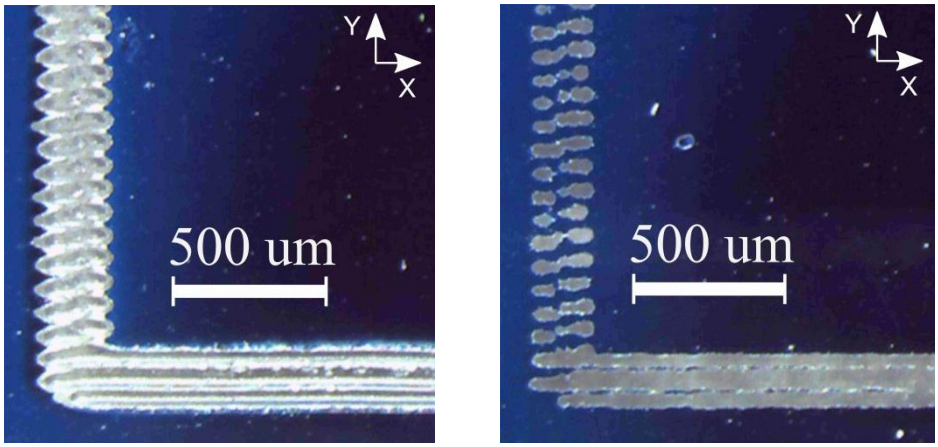

(a) (b)

Figure 2-9 - 25 mm^2 squares with 200um thick edges (20nm aluminum) (a) Rastered with 6% power and 30% speed settings (b) Rastered with 3% power and 30% speed settings

As discussed earlier in chapter 1, in this study, commercial microwave ovens (as an inexpensive and widely accessible energy source) are being used for microwave bonding. In this respect, specific metallic microwave susceptor patterns are required to be fabricated and used to produce rapid localized heating. For such applications that inexpensive prototyping is required, we propose the use of CO_2 laser patterning technique.

To further reduce the prototyping cost, low-cost acrylic mirrors (FABBACK® Acrylic Mirror Clear) are used to prepare the metallic susceptors. The FABBACK acrylic mirrors have the advantage of wide accessibility, as they are commercially available off-the-shelf in retail stores. The acrylic mirrors used consist of 2.85 mm thick PMMA, approximately 100nm thick aluminum and an approximately 30 μm thick protective paint layer on top of the aluminum as shown in Figure 2-10.

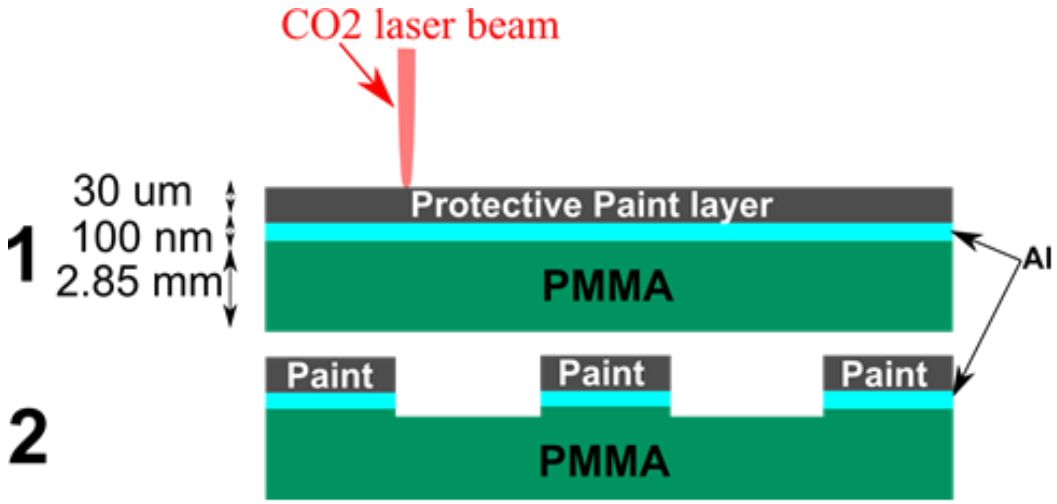

Figure 2-10 - Microwave susceptor prototyping steps on FABBACK© acrylic mirror using CO_2 laser cutter

To apply the CO_2 laser metal patterning technique to the acrylic mirror substrates, the settings required for removing aluminum and the protective paint layer are obtained using the same procedure described in section 2.1 and 2.2. In vector cutting mode, 4% power, 25% speed and PPI equal to 1000 and in raster engraving mode, 12% power and 25% speed are the minimum required values to remove the aluminum and the paint from the surface of the substrate. Figure 2-11 shows a sample of susceptor prototypes produced using VLS 3.50 laser operating in vector cutting mode with 15% power and 25% speed on acrylic mirrors. Aluminum patterns are initially transferred into a relatively large substrate area

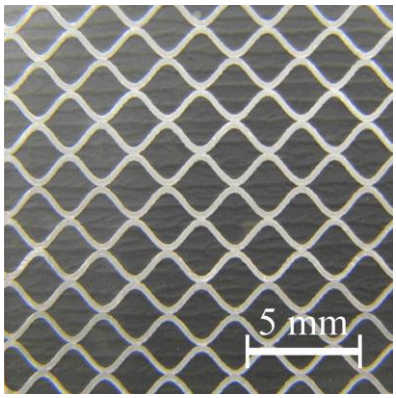

Figure 2-11 - 1 in^2 microwave susceptor sample fabricated on FABBACK© acrylic mirror. Figure shows front of the sample with protective paint on it. Cutline patterns are sine-waves with *period/amplitude* of 2.5.

and then the substrate is diced into smaller one square inch pieces using the laser cutter. To cut through the metal and 2.85 mm thick PMMA, the laser cutter is used in vector cutting mode with 50% power, 5% speed and PPI equal to 500.

Fabricated susceptors using this technique were then tested for heating inside the microwave oven cavity. More information on the design, simulation and experimental results of the metallic susceptors are provided in chapter 3.

Susceptor fabrication using CO_2 laser patterning technique significantly facilitates the prototyping steps and saves both time and fabrication cost.

2.3 Summary

Metal electrode patterning using a CO_2 laser cutter provides a relatively rapid, low cost and accessible prototyping method. Although CO_2 laser cutters are widely used for dielectric patterning and are widely accessible with no need to any custom setup, they have not been previously investigated for patterning thin metal layers. In this study it is shown that using this technique, electrode feature sizes larger than 450 μm can be fabricated with less than 5% dimension error. This can provide a rapid prototyping method beneficial for the design optimization processes and reduce both the fabrication time and cost compared to the existing prototyping techniques.

Chapter 3: Microwave Susceptor Design and Characterization[2]

As discussed in chapter 1, several microwave bonding techniques reported utilize customized microwave cavities and microwave sources, which are relatively costly and less accessible for widespread use. Commercial microwave ovens have been recently recommended as an alternative [21], [42]. They combine either external susceptors and solvents, or conducting polymers to heat up and weld polymer based microfluidics substrates. However, these methods can contaminate the device and channels under test through manual deposition of liquids (solvents or conductive polymer solutions) on the device surfaces prior to bonding.

We propose to use conventional microwave ovens and add a patterned metallic susceptor to the substrate interface to produce localized heating. For a typical microwave oven power level, solid metal films are very vulnerable to sudden arcing and explosions and cannot be directly used for controllable heating. Therefore, customized metallic susceptors are required to produce localized controllable, efficient, and selective heating without arcing. Although the microwave susceptor concept has been earlier used in the microwave cooking industry ([67], [68]), there is not much academic information available on them and to our knowledge, specific susceptor designs have not been previously applied to bonding of substrates in any reported work.

In this chapter, the goal is to design susceptors to be used in commercial microwave ovens to generate low cost, rapid, selective and localized heating for substrate bonding applications with a focus in this work on thermoplastic substrates which find wide use in microfluidics. First we present our results for different susceptor patterns and compare their efficiency at a fixed location in the

[2] A version of this chapter has been published [66]

microwave cavity. The effect of the test location is then studied and an efficient design with improved heating uniformity and significantly enhanced heating rate will be introduced. We will discuss susceptor element size effect and selectivity in detail. The rapid heating of the improved susceptor demonstrates that the generated heating is localized, selective, and far more controlled than solid metal films.

3.1 Microwave Heating System Simulation Model

Our microwave heating system includes: a microwave oven, a microwave susceptor and the substrate material. A Panasonic NNSA630W (inverter® technology) (Figure 3-1) microwave oven [69] was chosen for our initial experiments because its power level may be controlled in a continuous manner when operated at 50% of its maximum power rather than through duty cycle. The microwave oven cavity walls (including the interior metallic parts of the door) are grounded for safety purposes. However its safety can be compromised if the cavity walls or the door lock are intentionally manipulated or damaged. It is worth noting that in the case that arcing occurs in the cavity first safety step is to **disconnect the power from the plug while the doors of the microwave is kept closed** [69].

Figure 3-1- Panasonic NNSA630W microwave oven used in this study

A thin layer of aluminum (100nm) was selected as our susceptor material for initial tests and for the simulation. The substrate material used in this thesis, polymethylmethacrylate (PMMA), was chosen due to its transparency to microwave power (low RF power loss) [37] and wide application in polymer microfluidics.

The microwave susceptor design is done using electromagnetic simulations because the electromagnetic fields in the microwave are too complex to solve for analytically. To complete these simulations, ANSYS HFSS© software was used to determine the field distribution in the cavity based on measurements of the interior and the waveguide of our microwave oven.

As shown in Figure 3-2, a rectangular waveguide operating at 2.45GHz and on its dominant TE_{10} mode is used to feed the cavity. The glass turn-table has been removed from our model both in the simulation and experimental phases of the

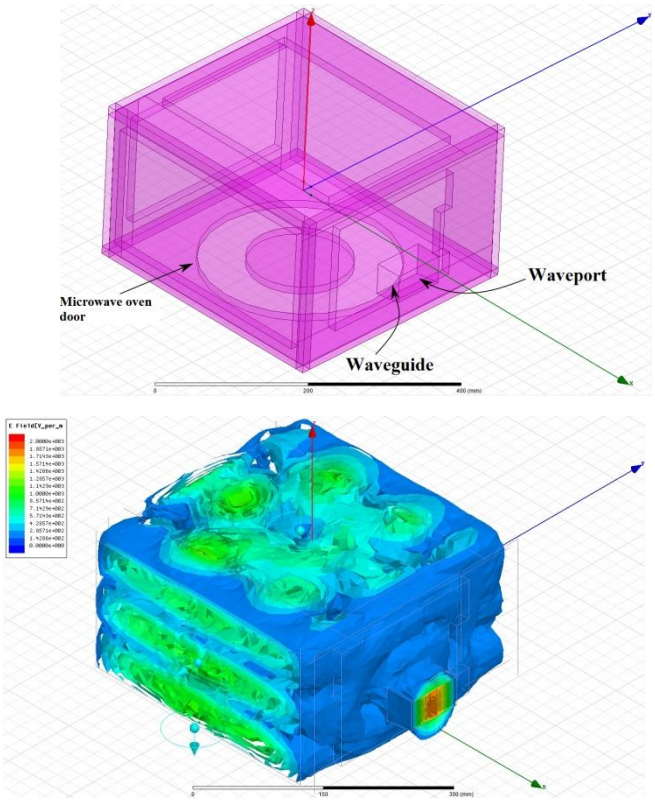

Figure 3-2- Microwave oven EM modeling (Reproduced from [75], Copyright © 2012, IEEE)

Figure 3-3 – Wet heat-sensitive fax paper experimental results and simulation results (showing Magnitude of Volumetric Current Density (MVCD)) of 15 cm x 10 cm x 150 μm of water placed at the same location inside the cavity

project. The wave port excitation in all of our simulation results is normalized to 1 W. The simulation model of the cavity has been verified with damp heat-sensitive fax paper tested in the microwave oven. A 15 cm x 10 cm sheet of damp fax paper was placed inside the microwave oven and heated for 30 sec at 50% power (600 W). The parts of the damp fax paper that heat up turn black while cooler areas remain white. Figure 3-3, shows an image of the damp fax paper after the experiment overlaid on the simulation results showing magnitude of volumetric current density (MVCD) of water at the same location. As shown in the figure, simulation results have acceptable consistency with the results obtained in the experiments. It is clearly seen that the areas with highest field intensity have turned black first, as would be expected from the higher heating rates at those locations.

In our simulation model instead of the actual thickness of the aluminum layer, a surrogate material 10μm thick but with the same surface resistance as the aluminum was used to allow acceptable computation time with a coarser mesh size [70].

3.2 Susceptor Designs for Controllable and Efficient Heating

The goal in the design of a susceptor for ultimate use in bonding applications is to be able to control the generated heat from the current flow on the metal patterns which ultimately should produce efficient and rapid heating without arcing. When done correctly, this produces localized and highly selective melting of the polymer substrate at the interface to be bonded while leaving other areas relatively cool.

The simulations for the samples are completed based on the details provided in section 3.1. For the initial studies, the sample is located in an area of intermediate intensity of electric field (avoiding hot and cold spots) as shown in Figure 3-4. Based on our simulation results, it is observed that the electric field variation, over the area that contains the sample, is less than 15%. Additionally, our sample sizes are chosen to be much smaller than our wavelength (<~0.2□) to avoid resonances and obtain a limited current with controllable heat generation.

In the initial experiments, as described in chapter 2, a CO_2 laser metal electrode prototyping technique was used. Low-cost acrylic mirrors (FABBACK® Acrylic Mirror Clear) purchased from Home Depot were used to prepare metallic susceptors. The mirrors consist of 2.85mm thick PMMA, approximately 100nm thick aluminum on the PMMA and a protective paint layer on top of the aluminum. The susceptor designs were transferred onto the aluminum sheet using Versa Laser VLS3.50 CO_2 laser cutter (50W laser power), using a power level of

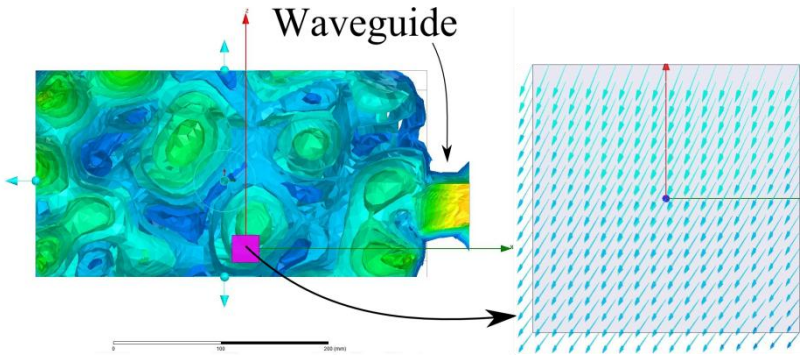

Figure 3-4 - Cross section view of the field distribution and the location of our sample (test location #1) (Reproduced from [75], Copyright © 2012, IEEE)

15% and speed setting of 25% of the laser maximum values.

To position the sample at selected locations inside the microwave oven cavity a sample holder structure was prepared that allowed for various positions and orientations. The structure was fabricated from PMMA (using the CO_2 laser cutting) as it was required that the support structure would not heat up under microwave oven operation or transfer significant heat from the sample under test (Figure 3-5).

Based on our experimental results, susceptor patterns are classified into three categories: 1-*non-controlled,* 2- *inefficient,* and 3-*efficient and controllable.* Among these categories, the first and second ones represent undesirable results and the third category is our preferred proposed patterns.

1-*Non-controlled* heating: As shown in Figure 3-2, during the microwave oven operation, a non-uniform field distribution forms inside the cavity. This characteristic can lead to non-uniform current generation and therefore, uncontrolled joule heating on continuous large conductive layers. To demonstrate an example of this situation, a 1 in^2 continuous sheet of aluminum was simulated.

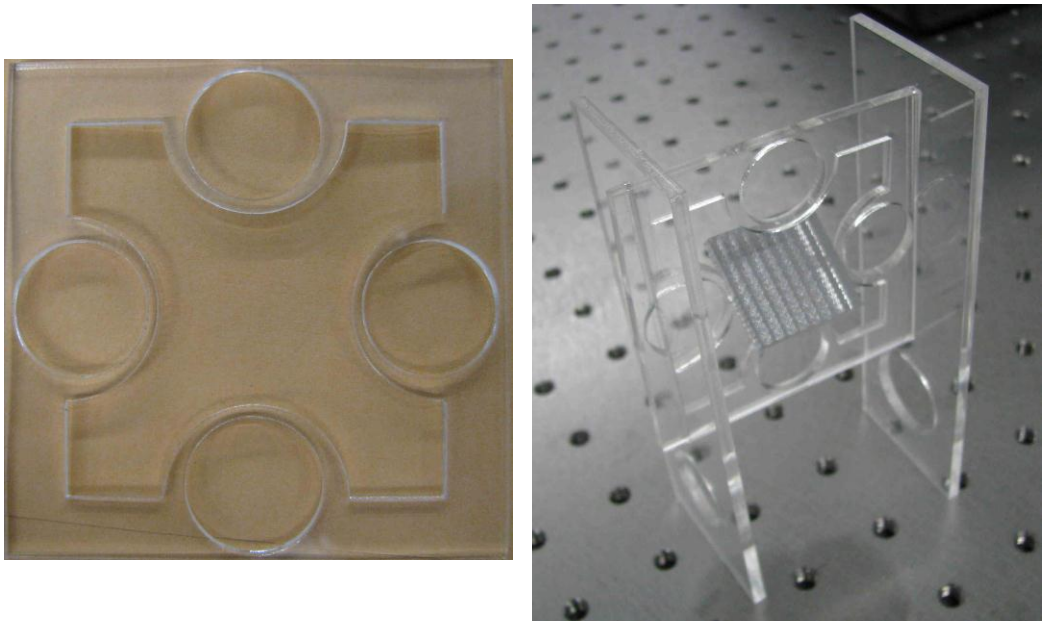

Figure 3-5 – PMMA sample holder structure

The complete sheet showed a considerable amount of current density magnitude variation on its surface (see Figure 3-6(a)) with the highest values (and therefore heating rates) located at the perimeter. Having large magnitude differences along the surface is very likely to cause arcing along the conductor. This has been also experimentally verified, as arcing across the film is observed almost immediately after the microwave cavity is excited at 50% power (600 W) (shown in Figure 3-6(b)). Therefore, large (>0.2λ) individual metal areas are avoided to reduce the chance of arcing which mainly occurs across an individual metal susceptor, rather than between susceptors.

Moreover, metal susceptor patterns having sharp, concave acute angles should be

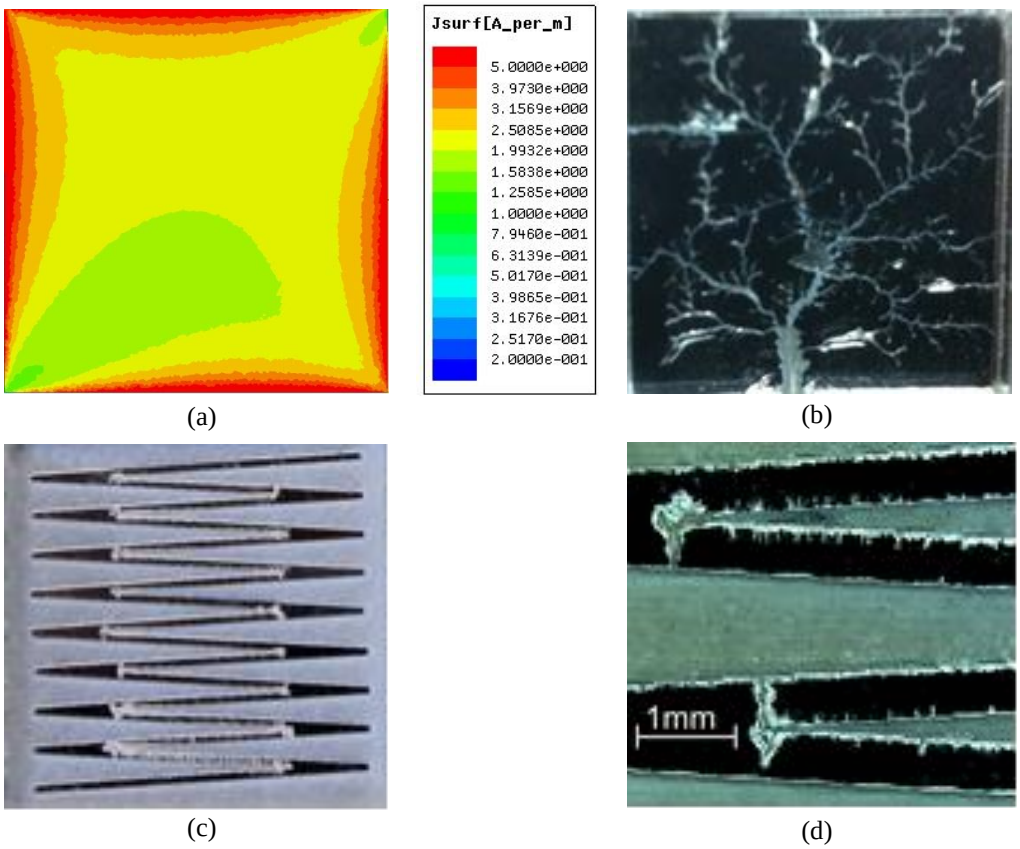

(a) (b)

(c) (d)

Figure 3-6 - Non-patterned sheet of Al, (a) Simulated magnitude of surface current density of the sample (Reproduced from [75], Copyright © 2012, IEEE) (b) A picture of the fabricated sample after the test (Reproduced from [75], Copyright © 2012, IEEE) (c) A susceptor with aluminum zigzag patterns after the test showing damage at the corners (d) closer image of the corners of the zigzag sample

avoided, as micro-sized arcing appears common on those locations due to the very high localized current density generated. Figure 3-6(c) illustrates a sample of a zigzag pattern with sharp edges while Figure 3-6(d) demonstrates a close view on the damaged spots by micro-arcing.

2-*Inefficient* Pattern: As individual susceptor elements shrink in size they become less efficient at generating significant current densities and can take several minutes to heat up to the point where the temperature can be measured (Figure 3-7(c)).

Obviously, the inefficient heating size threshold is dependent both on the heat sink variables (such as substrate thickness) as well as heating variables (such as the density of small susceptor elements on the substrate surface). The fact that negligible heating will occur with very small susceptor elements and that large and uncontrollable heating or arcing occurs with large elements, it was hypothesized that there would be an intermediate size and design of susceptor that could be rapidly heated but would not arc under typical microwave oven field densities. These elements were considered to be in our third category below.

3-*Efficient and controllable:* Many initial designs were conceived and tested, but only a few are demonstrated here for brevity. Most of these efficient designs have a high perimeter where highest induced RF current densities are expected. The criteria mentioned in the first category have also been taken into account during the efficient and controllable susceptor design to avoid non-controlled heating outcomes. As confident predictions of arcing cannot be made using electromagnetic simulations, these maximum dimensions have been mostly found through experimental trials, increasing the size of the elements until arcing is observed, and then keeping the maximum dimensions below this size threshold. To experimentally determine the temperatures of our samples as they are heated in the microwave, multiple *Nichiyu Giken Kogyo co.* thermo-labels [71] attached to the samples during microwave heating trials and recorded with video during each trial.

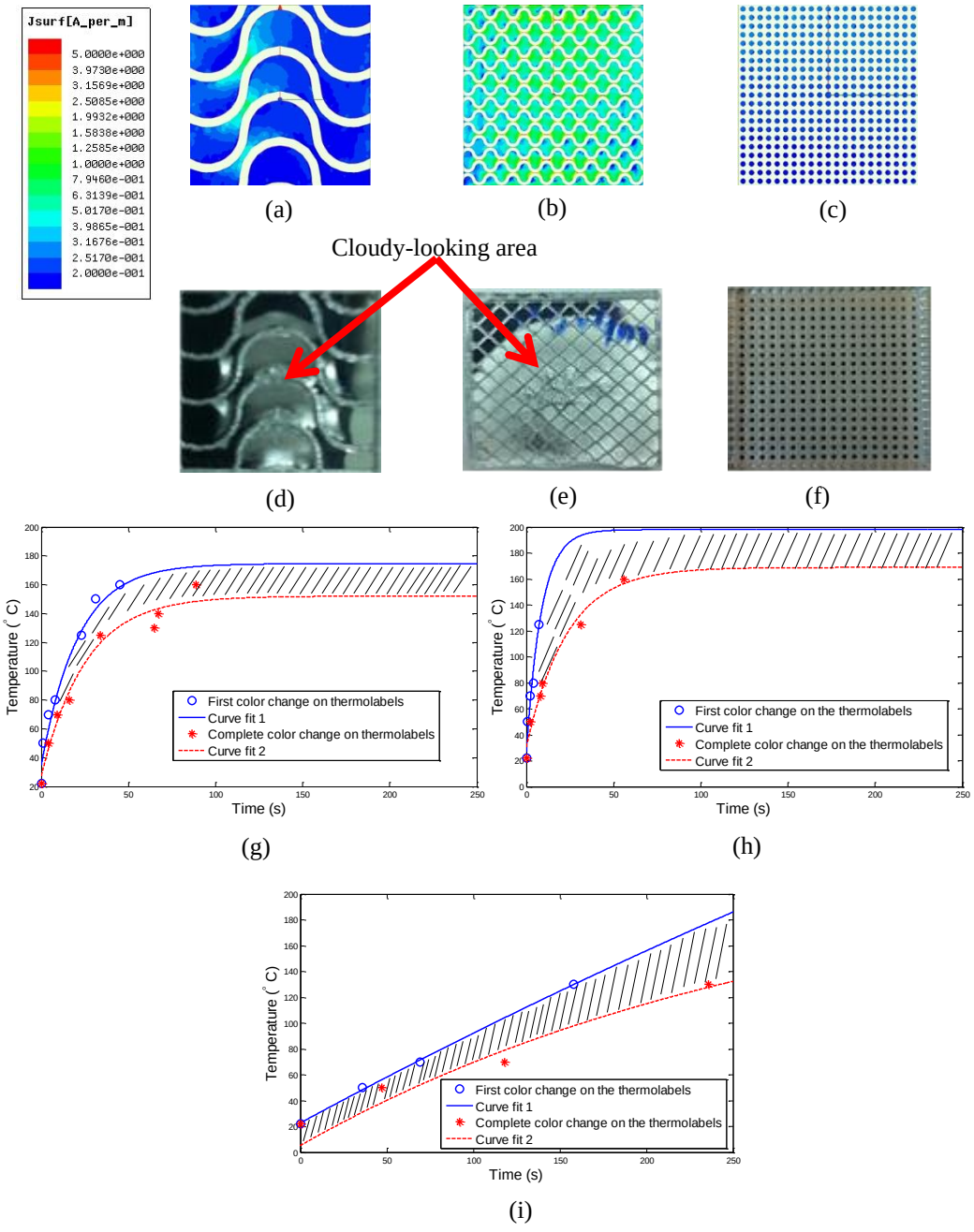

Figure 3-7 - Simulation and measurements results of samples tested at test location #1 (Figure 3-4) (a) Magnitude of Surface Current Density(MSCD) of a 1 cm x 1 cm semi-circular sine-wave pattern (b) MSCD of the 1 in x 1 in back-to-back sine-wave pattern (c) MSCD of the 1 in x 1 in array of dots pattern (d) A semi-circular wave pattern susceptor after the test (e) A back-to-back sine-wave pattern susceptor after the test (f) An array of dots susceptor after the test (g) temp vs. time measurements data of semi-circular wave pattern (h) temp vs. time measurements data of the back-to-back sine-wave pattern (i) temp vs. time measurements data of array of dots pattern (Reproduced from [75], Copyright © 2012, IEEE)

The microwave door blocks most infrared light, preventing direct infrared temperature measurement and thermocouples and other metallic temperature sensors could not be placed on the samples without affecting the electromagnetic fields, or acting as additional heat sinks to the samples.

Originally, an infrared thermometer was used to try and measure the sample temperature immediately after removal from the microwave, but rapid cooling of the sample, and very high temperature differences across the sample prevented accurate readings. In contrast, the thermal labels can be used to provide a high contrast visual indication of when the surface has reached a specific temperature. When different labels that responded to different temperatures were placed in close proximity to one another, a heating curve could be estimated from the video recordings. The labels change color once a specific temperature is reached and testing on pure PMMA under the same microwave conditions indicated no significant thermal heating of the labels themselves or pure PMMA under microwave operation.

Each of the graphs in Figure 3-7 consists of two curves, one showing temperature vs. time for the first recorded temperature change on each thermo-label when the microwave is running at 600 W and the other for when the complete 5 mm diameter circle (thermo-label surface size) has changed color (Figure 3-8). The

Figure 3-8–Thermolabel with 125℃ threshold. The white circle at the center of the thermolabel changes color (black) when temperature passes the threshold

area in between the two graphs is an indicator of heating uniformity. The closer the two curves on each graph are the more uniform the heating process. Cloudy areas indicated that the PMMA was heated beyond 150 °C and the aluminum wrinkled (Figure 3-9), giving a secondary visual indication of the uniformity of heating.

3.3 Test Location and Its Influence on Heating

In this section, the effect of the test location selection (inside the microwave oven cavity) on heating characteristics is examined. As mentioned earlier, the current (and the heat) generated on the susceptors depends on the intensity of the field. Therefore, considering the non-uniform field distribution of the microwave oven cavity, the position of the susceptor with respect to the fields inside the cavity strongly influences the heating characteristics.

In order to demonstrate this influence a second test location (test location #2) was selected based on the cavity simulation model and similar samples as shown in Figure 3-7 are tested at this location. As shown in Figure 3-10, the new location has approximately twice the electric field intensity compared to our previous test location for the same microwave power.

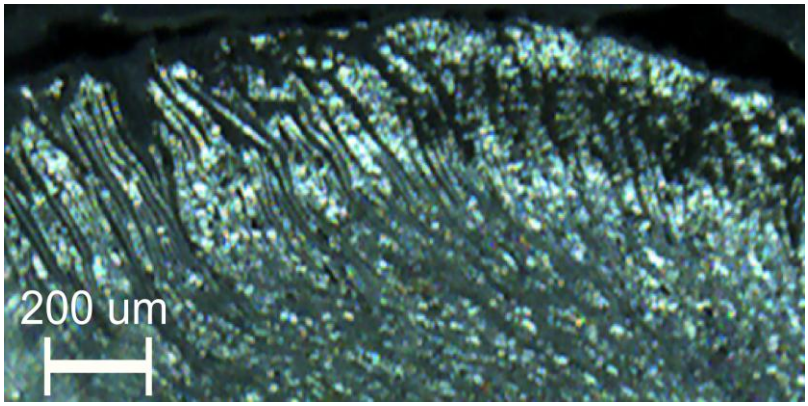

Figure 3-9 - Close view on the cloudy looking parts showing the wrinkles on aluminum surface when heating up to 160 degrees inside the microwave oven

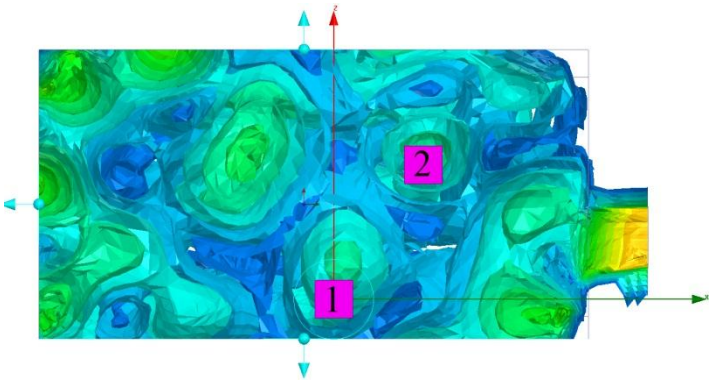

(a)

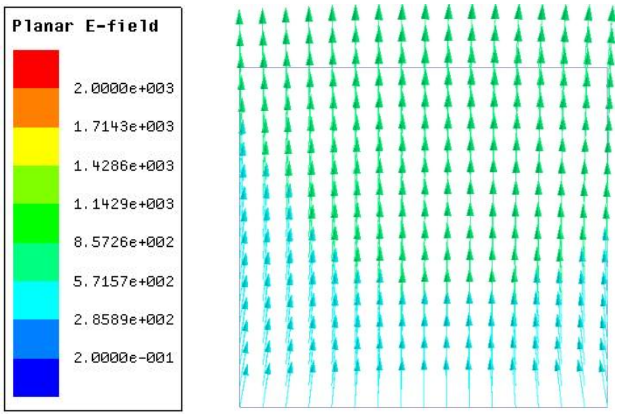

(b)

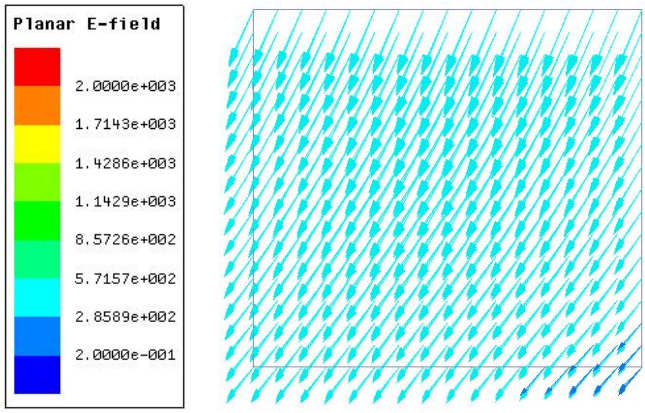

(c)

Figure 3-10 - (a) Simulation results showing electric field distribution at different test locations (1 in^2 surface area) in the microwave oven cavity (b) electric field distribution at test location #2 (c) electric field distribution at test location #1

Figure 3-11 presents the test results in the new location indicating a significant

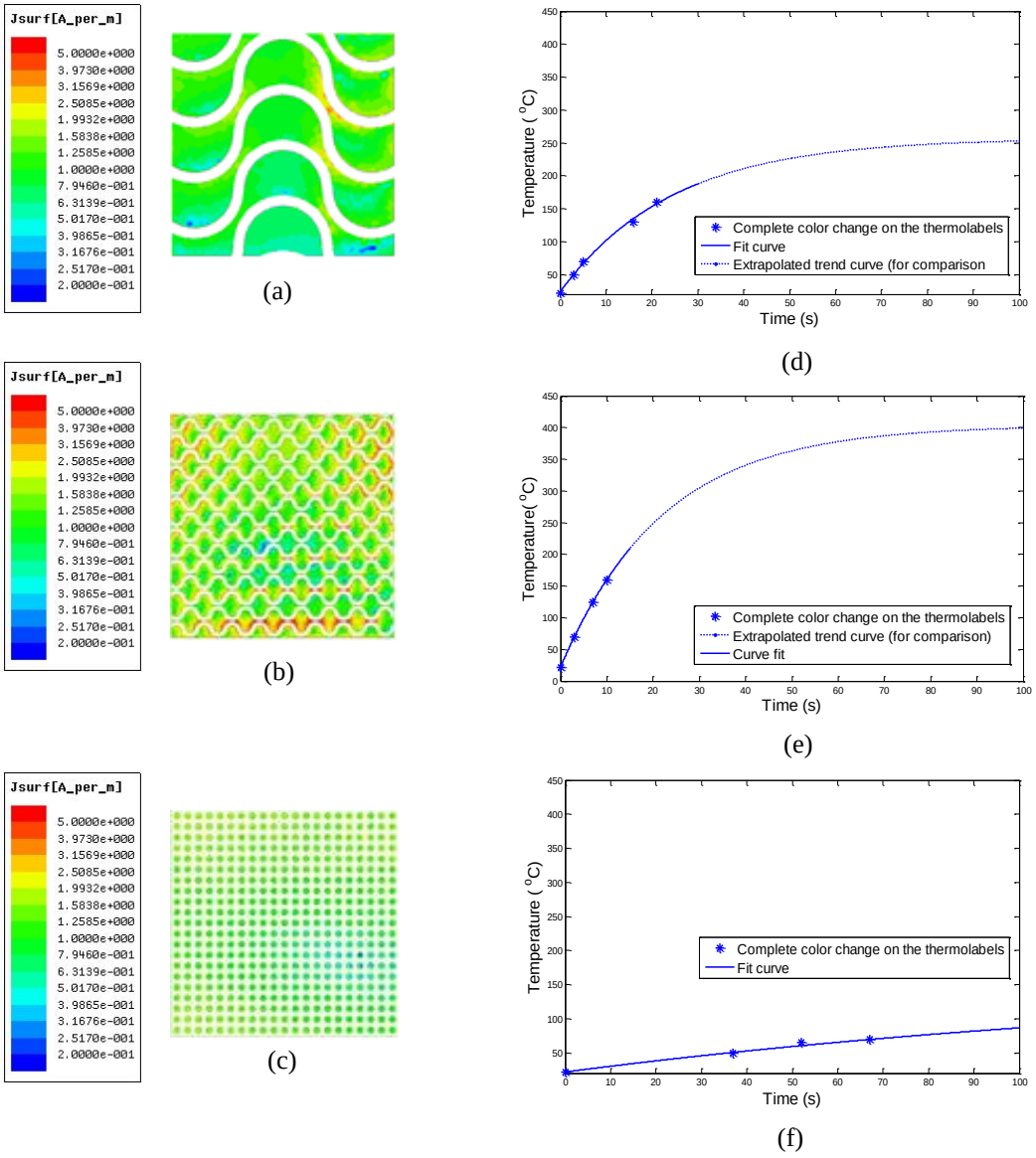

Figure 3-11- Simulation and measurements results of samples tested at test location #2. Dotted lines represent the extrapolated trend curves for better comparison between the graphs not temperature predictions. At temperatures above substrate melting point (160℃) our model may change (a) Magnitude of Surface Current Density(MSCD) of semi-circular sine-wave pattern (b) MSCD of the back-to-back sine-wave pattern (c) MSCD of the array of dots pattern (d) temp vs. time measurements data of semi-circular wave pattern (e) temp vs. time measurements data of the back-to-back sine-wave pattern (f) temp vs. time measurements data of array of dots pattern

enhancement in their heating rate due to the larger field intensity. Increased simulated current density of the samples shown in the Figure 3-11 (a) –(c) is also an indication of this fact. In this experiment (sample at test location#2), due to

much faster thermolabel color change (compared to those shown in Figure 3-7), the time difference between the first and complete color change is nearly indistinguishable and only one fit line is plotted.

3.4 Susceptor Size and Its Influence on Heating

As discussed in section 3.2, susceptor size plays an important role in heating efficiency and its controllability. Large, non-patterned metal films are vulnerable to arcing (Figure 3-6) and therefore to provide heat over those dimensions patterned metal susceptors are proposed. The arcing size threshold is a function of input power, test location and susceptor pattern (i.e. angles). In the susceptor pattern design step, electromagnetic simulation tool can help minimize the MSCD non-uniformity along the susceptor and avoid non-controllable heating (arcing). However accurate size threshold to avoid arcing can only be found from experimental characterization of a certain susceptor pattern at a specific test location and input power.

In the design of metal susceptor arrays, with the constant spacing (between metal elements) assumption , increasing the area of each susceptor element results in higher total MSCD and therefore heating rate for the susceptors. In practice, the spacing between the susceptor elements is mainly defined and limited by the prototyping fabrication technique (CO_2 laser cutting for this study). Figure 3-12 shows simulation results for susceptor array made up of squares where the individual element area is being doubled while spacing is kept constant. The samples are simulated at test location #2 (higher field intensity). Although MSCD patterns of the illustrated samples are similar, the ratio of '*metal area/total substrate area'* is changing and the average MSCD value on the larger susceptors is also larger for the same field strength. As the area of the susceptor array element increases, the percentage of the area covered with metals relative to substrate area increases as well. Having a larger percentage of the substrate's area covered with heating elements, each having higher surface current density leads to a faster heating rate overall.

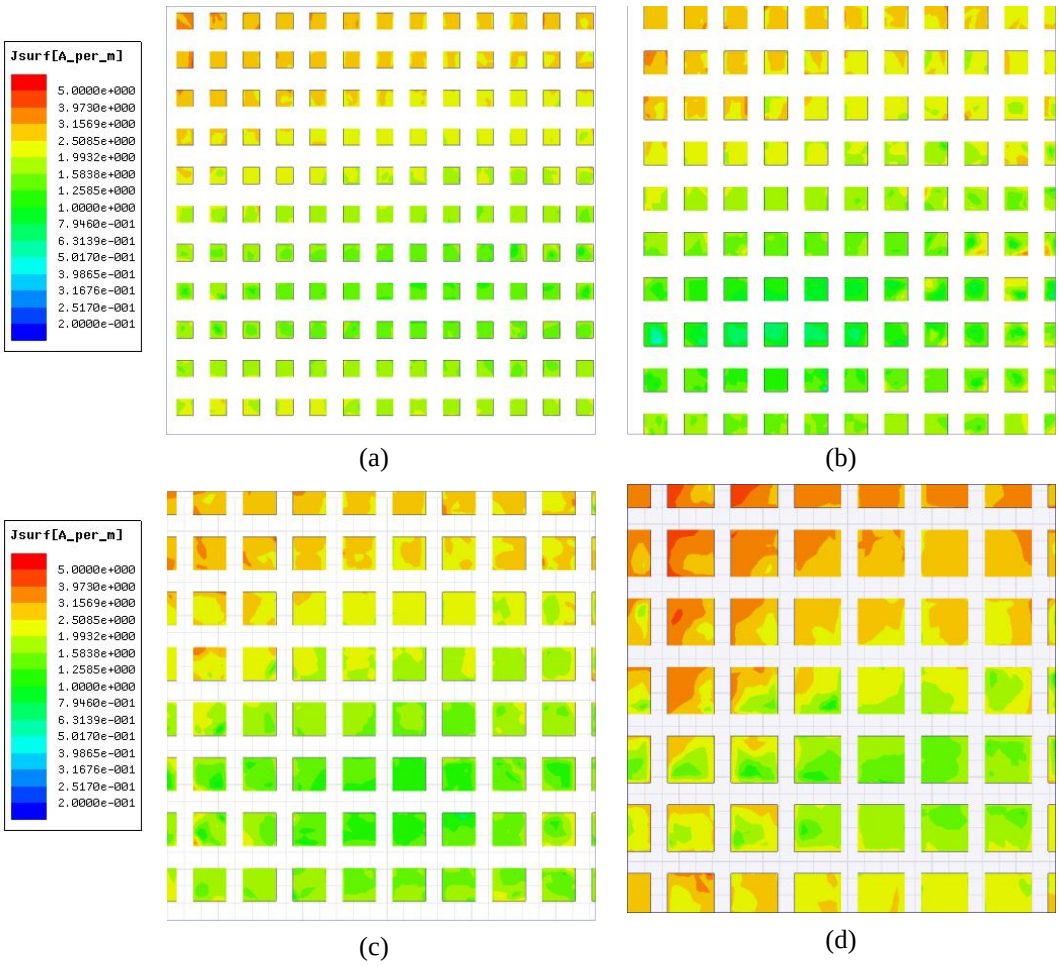

Figure 3-12 – Effect of susceptor size on heating (a) Simulation result (MSCD) of array of 2 mm^2 squares at test location #2. Metal area/ total susceptor area = 21% (b) Simulation result (MSCD) of array of 4 mm^2 squares at test location #2. Metal area/ total substrate area = 33.5%. (c) Simulation result (MSCD) of array of 8 mm^2 squares at test location #2. Metal area/ total substrate area = 37.8%% (d) Simulation result (MSCD) of array of 16 mm^2 squares at test location #2. Metal area/ total substrate area = 51%
Metal area/total substrate ratio was calculated using IMAGEJ, image analysis software.

3.5 Susceptor Pattern Design and Orientation and Its Influence on Heating

In general, an efficient susceptor design for bonding applications should heat up uniformly and quickly to ensure that local heat sink effects from the substrates is minimized and heating/melting is limited only to the susceptor areas near the

PMMA surface. Suitable susceptor pattern design can enhance the efficiency, uniformity and controllability of heating. Microwave current behavior is the basic concept behind the designing process of an efficient susceptor pattern. When an electromagnetic wave hits a perfect electrical conductor boundary, the following equations are valid [29], [32]:

$$\hat{\mathbf{n}} \times \mathbf{E_2} = \mathbf{0} => \mathbf{E_{2t}} = \mathbf{0} \quad (3\text{-}1)$$

$$\hat{\mathbf{n}} \times \mathbf{H_2} = \mathbf{J_s} \quad (3\text{-}2)$$

where E_2 is the electric field intensity on the perfect electrical conductor (PEC) (V/m); H_2 is the magnetic field intensity on the PEC medium (A/m); J_s is the surface current (A/m) and $\hat{n}$ is the normal vector of the perfect electrical conductor plane.

Equations 3-1 to 3-2 represent the fact that after putting the susceptor at the test location, the tangent electric field on the PEC becomes zero (or very small for good conductors). Thus, an electric current is produced to satisfy the new condition. To optimize the produced current, the susceptor should be orientated in a way that maximally perturbs the field. The maximum current is produced when the susceptor orientation is tangent to the electric field direction. Figure 3-10 shows the selected test locations inside the cavity for our study. As shown in Figure 3-10(a), the direction of the electric field vectors at the test location #2 is in +z direction (towards the top of the microwave oven cavity). Thus the sample should be located in '*zx*' plane for more heat generation. This has also been experimentally verified and observed that by locating our sample perpendicular to the electric field less heating is achieved, as compared to the tangent orientation.

Another important factor in the optimization is the current flow at the edges of the pattern. As RF currents primarily flow at the edges of the conductors, it is expected that we see higher current densities along the edges of the conductor that are perpendicular to the electric field. This can be explained by equations 1-1 to 1-4 (Maxwell's equations) which represent the fact that the electric and magnetic fields directions are always perpendicular. Additionally, equation 3-2 also represents the fact that current and magnetic field directions are also

perpendicular. Therefore, having the electric field in the z direction and the magnetic field in the y direction (normal to the susceptor plane) produces a current flow in x direction (tangent to the horizontal edge of the susceptor). A similar concept is described in [72].

To prove the above discussion, a simple simulation is carried out. Figure 3-13, Figure 3-14 and Figure 3-15 show the effect of the susceptor pattern on MSCD value and distribution by illustrating two arrays of rectangles with the same area but different orientations, at test location #2.

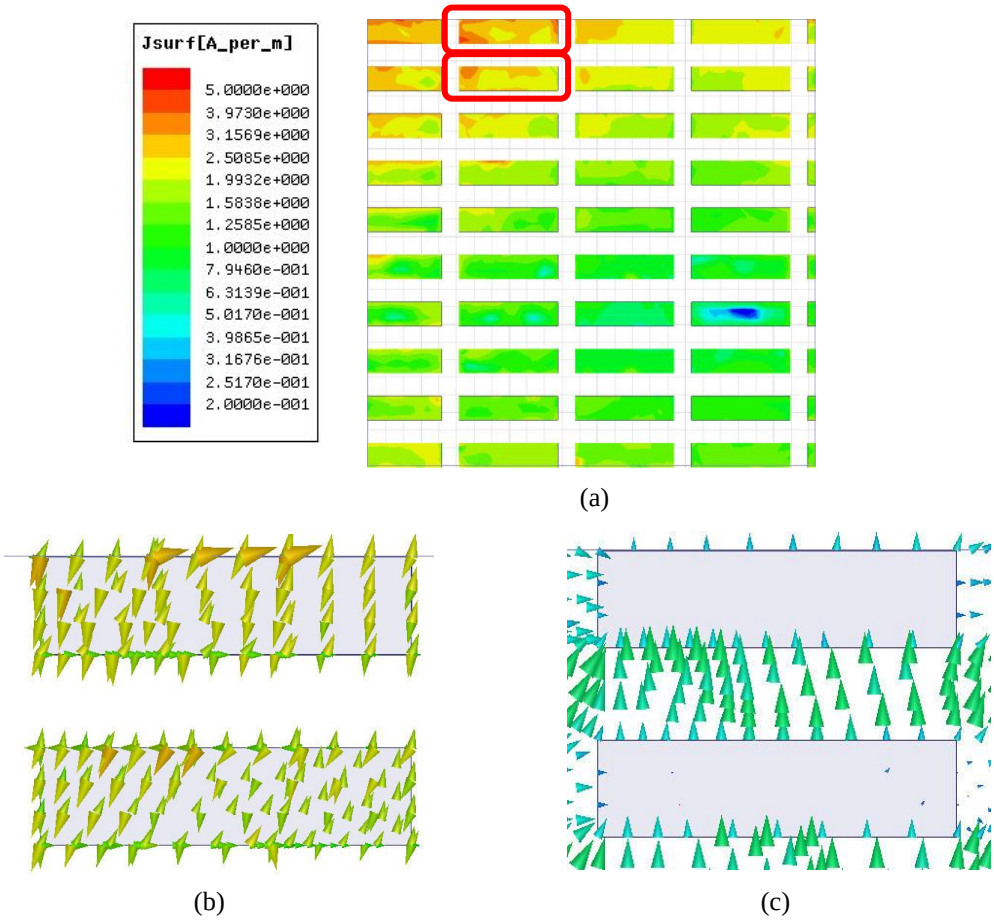

Figure 3-13 - Effect of pattern on surface current density (a) Simulation results (MSCD) of an array of 8 mm^2 rectangles with horizontal orientation located at test location # 2 (b) Surface current density direction for the susceptor elements with red rectangles around in figure(a). (c) Electric field directions shown around the elements with red rectangles around in figure (a).

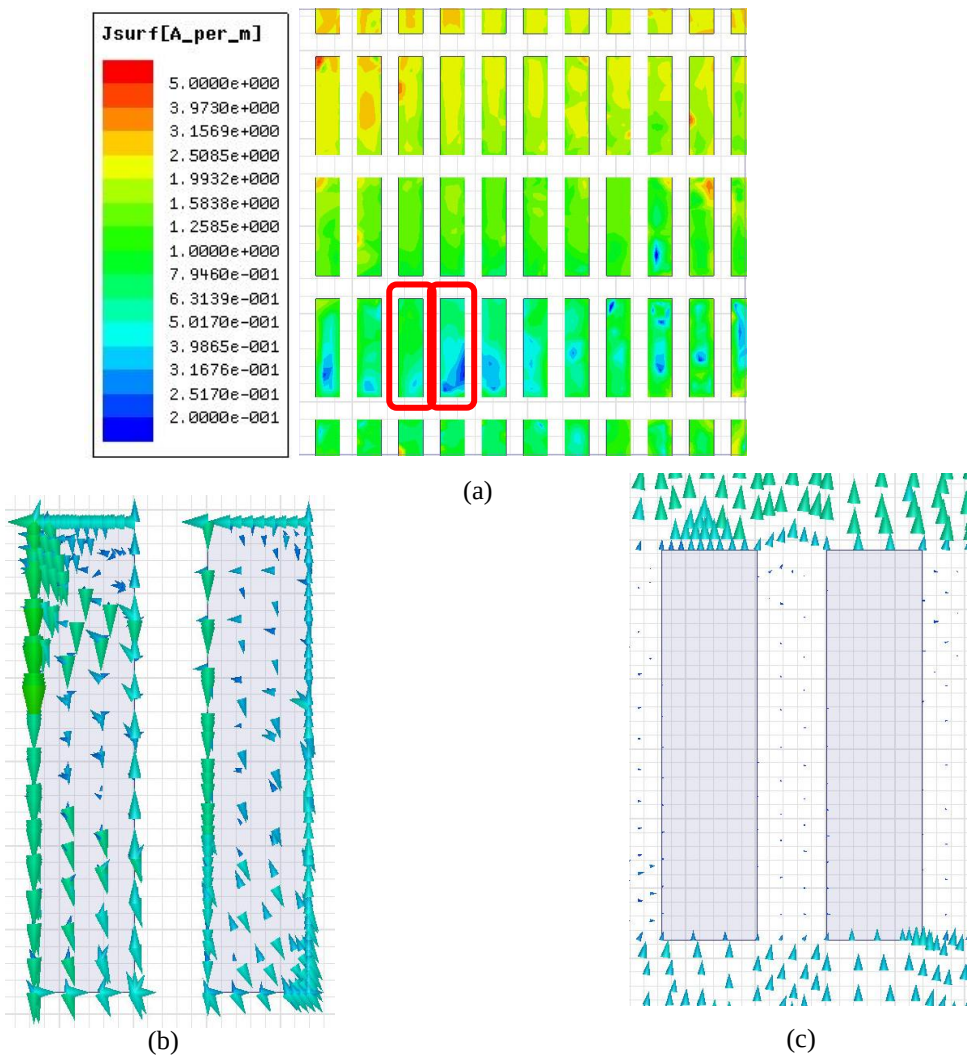

Figure 3-14 – - Effect of pattern on surface current density (a) Simulation results (MSCD) of an array of 8 mm^2 rectangles with vertical orientation located at test location # 2 (b) Surface current density direction for the susceptor elements with red rectangles around in figure(a). (c) Electric field directions shown around the elements with red rectangles around in figure (a).

The average MSCD current of the horizontal rectangles is 1.78585 A/m and the average for the vertical rectangles is 1.5945 A/m. Figure 3-14 also show the electric field and surface current density directions.

The simulation results also confirmed that currents mostly flow close to the edges that are perpendicular to the electric field and therefore having longer perpendicular edges to the electric field will result in higher MSCD values and thus higher heating rates. As a result, the patterns that are in-plane with E field

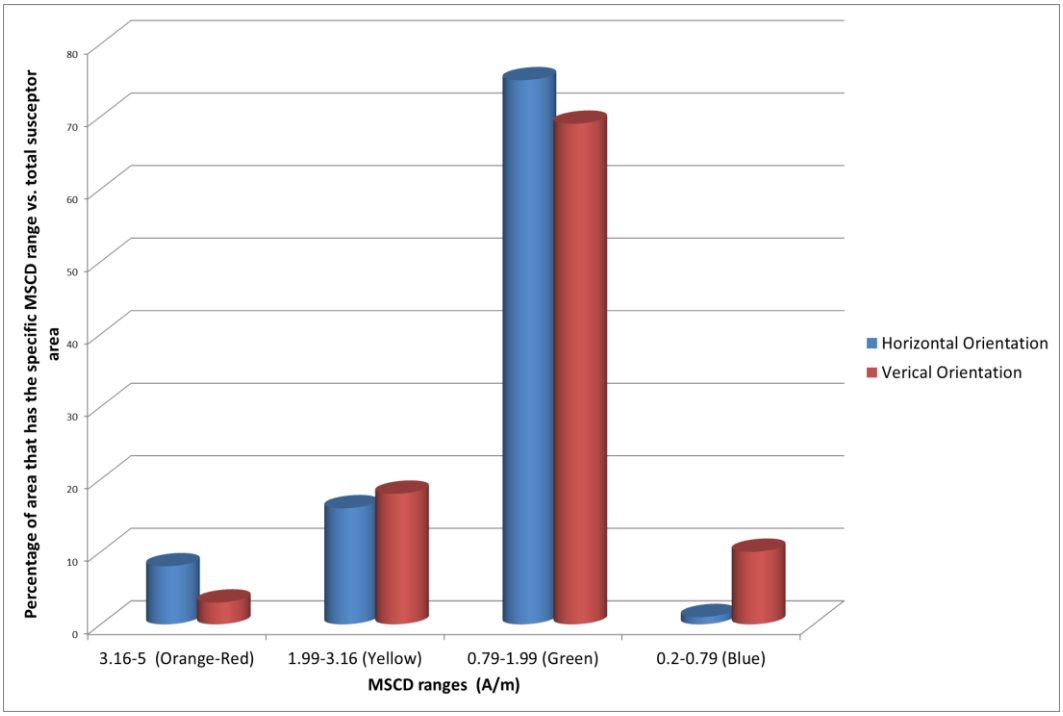

Figure 3-15 – Simulation results (shown in Figures 13 and 14) analysis using IMAGEJ image analysis software

with maximum perimeter perpendicular to the field direction should provide the highest heat generation. For instance for test location #2, an efficient microwave susceptor pattern should be designed by maximizing the length of top and bottom edges of the pattern.

3.6 Eye-Shape Pattern for Enhanced Efficiency

In order to design an efficient microwave susceptor pattern for test location #2 we are proposing the use of an eye-shape pattern. The eye-shape pattern susceptor shown in Figure 3-16 can be defined using its major (D_L) and minor (D_S) axes. The pattern is produced by cutting out two tangent back-to-back sine waves with the period/amplitude ratio of 5 kept as a constant but with different sizes of the major axis. For our experiments, the width of the cut line is kept constant at 500 μm (Figure 3-16). Based on the concept explained above, the advantage of the proposed eye-shape pattern is the fact that it has higher perimeter across the electric field direction than regular patterns such as rectangles with the same area.

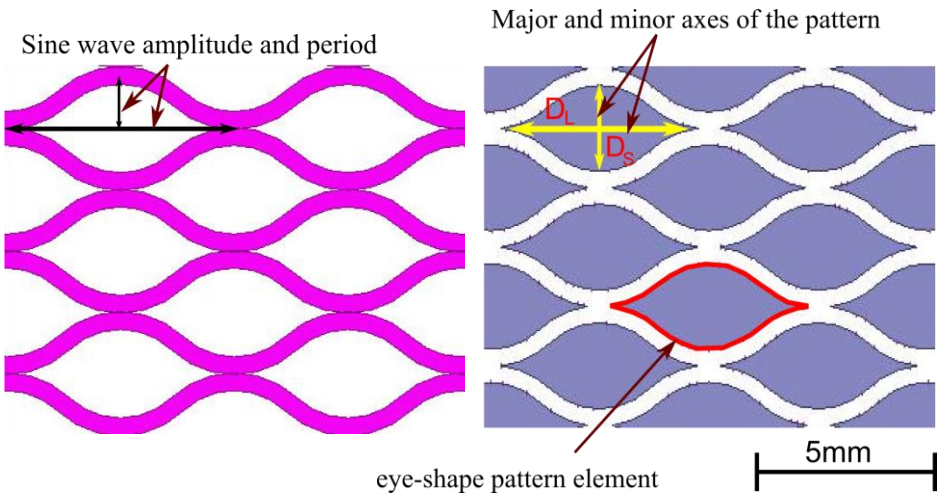

Figure 3-16 - (a) Tangent sine-wave patterns separating the eye-shape features with the line width of 0.5 mm (b) An array of eye-shape pattern susceptor model showing the major and minor axes of the eye-shape feature

Additionally the pattern is smooth and has fewer sharp corners than rectangles. It can also be cut with a continuous laser cutter motion, and doesn't require rastering to produce the pattern (which is much slower than the vector cutting process that was used).

The current distribution and heating rate for a sample of 1x1 inch is also illustrated. The new susceptor pattern provides significantly higher efficiency and faster heating rate. As is clear in Figure 3-17(c), the sample reaches at least 160 °C in less than 8 seconds. It is worth noting that edges of the susceptors reach 125℃ in 1 second. This shows the potential of susceptor pattern design for higher temperature targets.

a)-Eye-shape Element Size Effect: As previously discussed in section 3.2, metal feature size affects the efficiency of the heating. Very small features are less efficient in heating and very large ones are prone to arcing (inside the building block unit) and non-controlled heating.

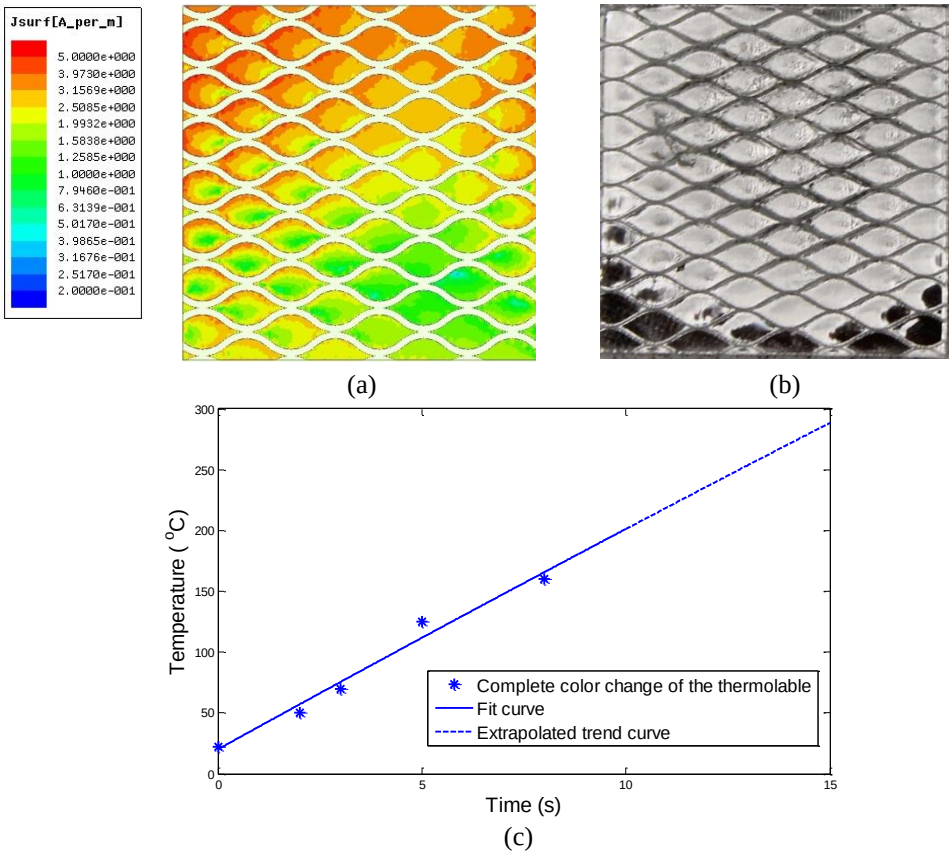

Figure 3-17 - Simulation and measurements results of the eye-shape pattern susceptor (with D_L = 5.6 mm) tested at test location #2 (a) Simulation results showing MSCD of the sample (b) A photo of the 1 in x 1 in sample after 14 seconds of microwave operation at 600 W input power (c) Temperature vs. time measurement results of the test including measured points, fit curve and extrapolated trend.

In order to optimize the eye-shaped pattern, the effect of its size is studied. The effect of *eye-shape element size* (with constant aspect ratio) on the heating rate is studied using 1 in^2 fabricated sample with arrays of eye-shape features of different sizes.

All of the experiments were carried out at 600 W input power. The target temperature for different susceptor patterns is selected to be 160℃ (the PMMA substrate melting point). Figure 3-18 presents the measured results.

It is clear that the features with small dimensions have very slow heating rate and require very long time to reach the target temperature. This area is shown as the inefficient heating area. As the building block size increases, the heating rate

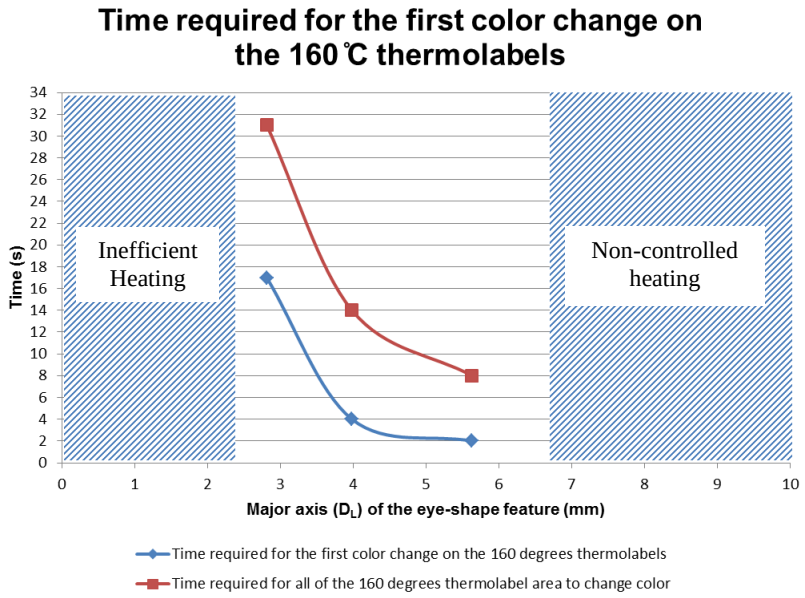

Figure 3-18 – Characterization of effect of eye-shape pattern element size on heating rate at the test location #2

improves and the total required time is reduced. The samples with feature D_L larger than 6.9 mm exhibit arcing and therefore are not acceptable for controllable heating. An example of the damaged features after arcing is shown in Figure 3-19(a).

(b)-Reusability: This is the second criterion of the eye-shape patterned susceptors that has been characterized. The goal is to determine if the patterns can be heated to the same temperature after cooling down and can be used as heaters repeatedly. It is important because the substrate material (PMMA) characteristics might change with temperature and could damage the susceptor. PMMA has a glass transition temperature of approximately 105℃ and a melting point of approximately 160℃.

For these experiments, efficient eye-shaped patterned susceptors (D_L = 5.6 mm) are used. Four temperature steps are selected and at each temperature the same susceptor is tested three times. As shown in Table 3-1, the time required to reach to temperatures up to 160℃ (sufficient for PMMA-PMMA bonding) has not changed significantly after three trials. This means that the designed susceptors

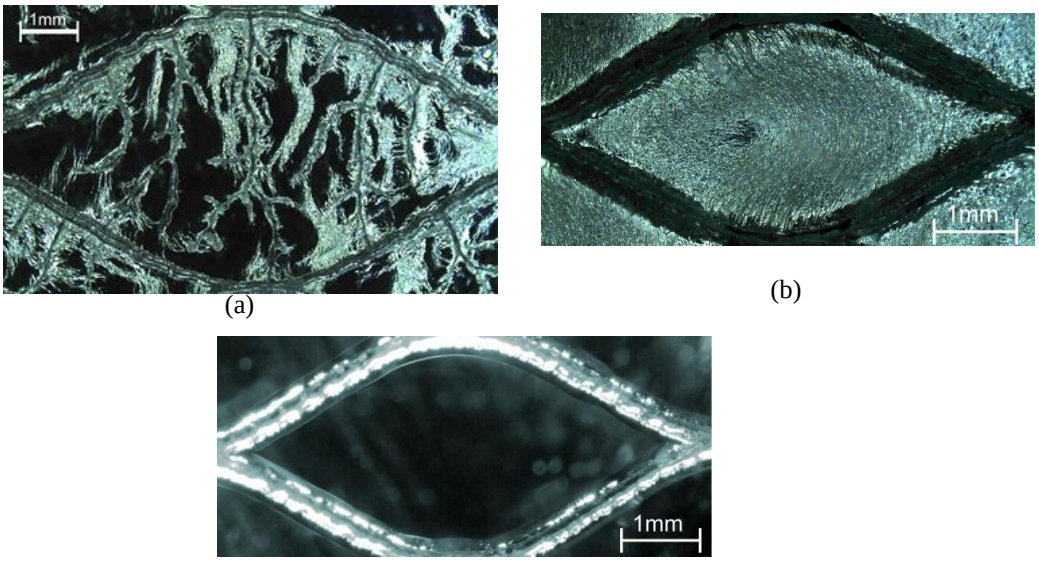

(a) (b)

(c)

Figure 3-19 - (a) Damaged susceptor with eye-shape element (D_L= 9 mm) after the test (non-controlled) (b) Efficient susceptor with eye shape element (D_L=5.6 mm) after the test (c) The susceptor with eye-shape element (D_L=5.6 mm) before the test

remain undamaged even when they are heated close to the melting point of the substrate material.

3.7 Size of the Uniformly Heated Area

As discussed earlier, the non-uniform field distribution inside the microwave cavity causes non-uniform heating across the sample with uniform susceptor

Table 3-1 - Reusability Characterization of the Eye-Shape Susceptors

	Number of trials	70°C	100°C	120°C	160° C
First color change on the thermolabels	1st	1s	1s	1s	2s
	2nd	1s	1s	1s	2s
	3rd	1s	1s	1s	2s
All of the thermolabel changed color	1st	3s	4s	5s	7s
	2nd	3s	4s	5s	8s
	3rd	3s	4s	5s	8s

designs. Up to this point, a relatively small sample size (0.2 wavelength) has been selected with minimum amount of field variations. As shown in Figure 3-7 and Figure 3-17, relatively uniform heating was achieved over the susceptor area of 1 in^2. However, for larger sample sizes, achieving uniform heat distribution becomes more challenging.

In order to achieve a larger uniformly heated area of the susceptor, the sample can be moved back and forth along a path inside the microwave oven cavity. Relocation inside the cavity can compensate for the field non-uniformity by passing the various parts of the sample through the hot-spots and cold-spots. This concept is similar to the microwave oven turntable that is used to enhance the uniformity of food heating.

As a proof of concept, a path was selected inside the microwave oven cavity for a 4 in^2 sample to move vertically in a range of 1 in (Figure 3-20).

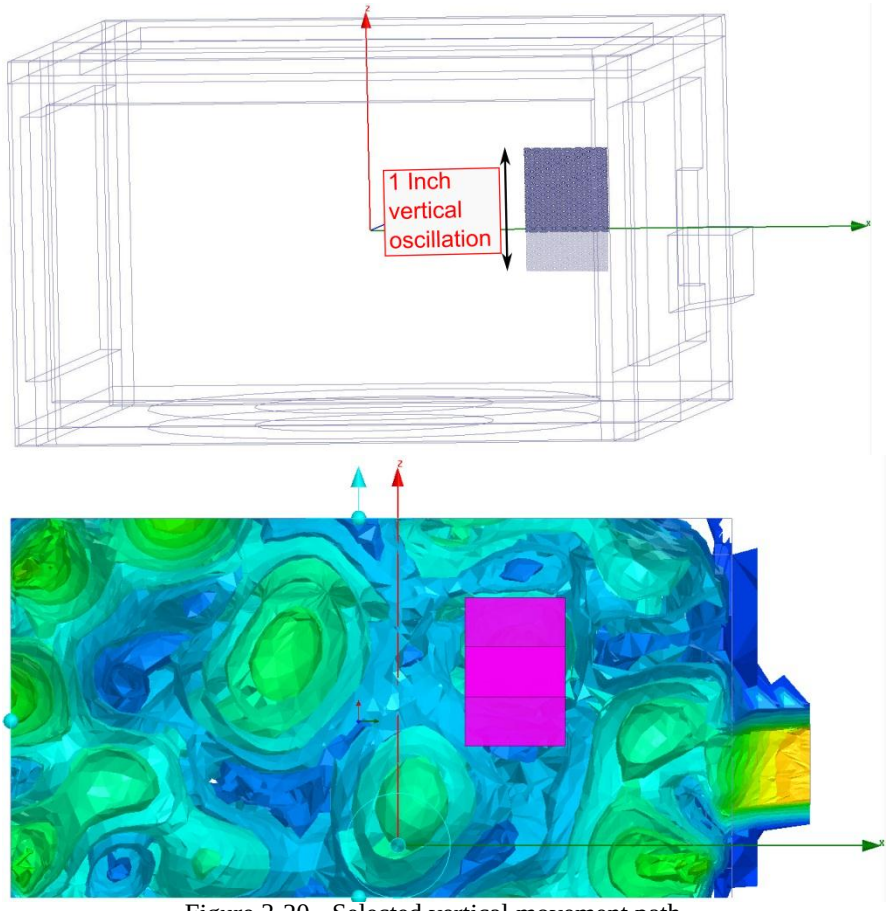

Figure 3-20 - Selected vertical movement path

To achieve this, a set of gears was designed and built from PMMA to convert the horizontal rotation of the microwave oven rotor to vertical oscillation (Figure 3-21).

A 4 in^2 eye-shape patterned susceptor (D_L = 5.6 mm) was fabricated and tested inside the microwave oven both for stationary and moving scenarios. As shown in Figure 3-22, moving the susceptor vertically with the span of 1 in has widened the uniformly heated area by approximately 1 in^2. For bonding applications where large substrate sizes are required, the best solution would be to modify the turn table or this particular translation system to move the samples at fast rates within the microwave cavity, so that the time average of the electromagnetic field intensity at each part of the bonded area is the same over the bonding duration. It is expect that faster motions within the cavity would be necessary for highly efficient bonding, as the sample would have to move through several hot and cold spots within the total bonding time to make the average heating uniform.

3.8 Heating Selectivity

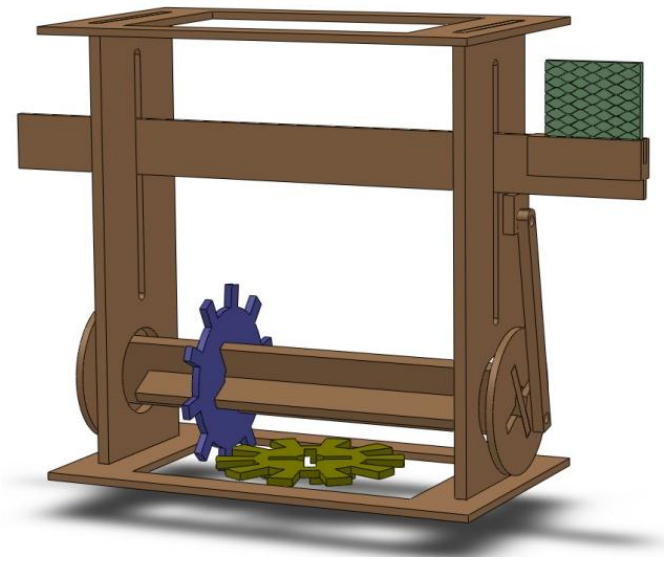

Figure 3-21 - Designed model of the fabricated system (from PMMA) producing vertical movement from the microwave oven rotor

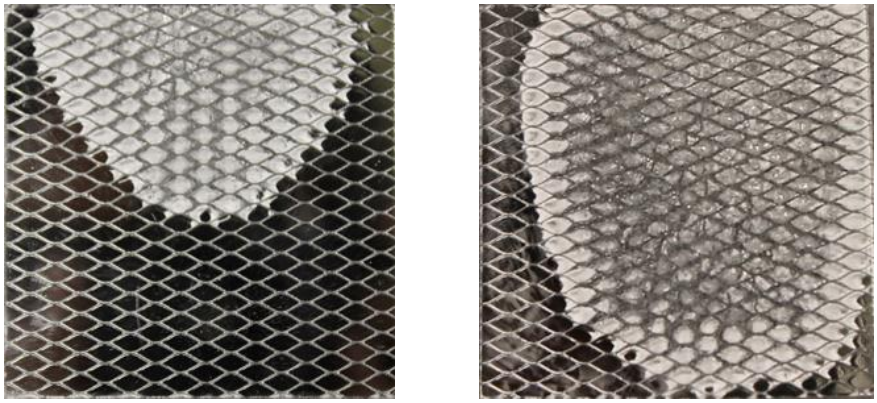

(a) (b)

Figure 3-22 - (a) 4 in^2 (2 in x 2 in) eye-shaped pattern susceptor tested inside microwave oven at a fixed position for 14 seconds (b) 4 in^2 eye-shape patterned susceptor tested inside microwave oven for 14 seconds by moving along the selected vertical path

As described in chapter 1, heating selectivity (susceptor vs. the device under packaging) is one of the main advantages of the microwave-heating concept for wafer bonding (Figure 1-11(b)) and therefore one of the main goals of our proposed technique. Consequently, this section investigates this criterion based on our designed susceptor patterns.

To test this, an experiment was completed using a 1 in^2 PMMA substrate coated with eye-shaped patterned susceptors (D_L = 5.6 mm) around its perimeter (representing a package) leaving an area of 1 cm^2 cleared of metal (but with PMMA) for actual devices (Figure 3-23). For actual die packaging, depending on its size and number of devices, this area and pattern could vary.

Under microwave radiation there will be current (and as a result joule heating) generated in electrically conductive materials. Therefore, one of the problematic scenarios for heating selectivity of microwave bonding could be having all metallic (conductive) structures in the device placement area. Based on our experiments it is known that the larger the metallic area, the higher is the heating potential. Considering these facts, two experiment scenarios were designed.

For the first experiment an array (total of 4) of 4 mm^2 square patches is included in the device placement area and for the second experiment an array of (total of 9)

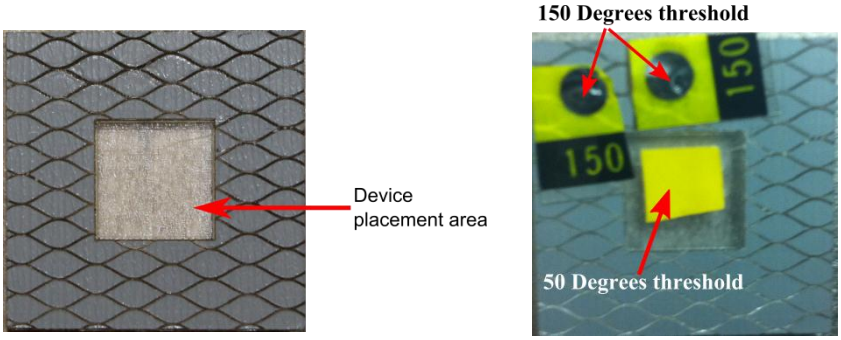

(a) (b)

Figure 3-23 - (a) Basic sample design for heating selectivity study showing the 1 cm^2 device placement area surrounded by microwave susceptors (b) sample with an empty device placement area shown after the test inside the microwave. Thermolabels indicate that the surrounding susceptors have reached 150℃ while the temperature of the device placement area (PMMA) is still below the 50℃ threshold (for color change).

1 mm^2 square patches are incorporated. In both experiments, the spacing between the square patches is constant. Samples are fabricated and tested inside the microwave oven cavity at test location #2. The temperature of the device and susceptor areas is measured using thermolabels (Figure 3-24). As shown in Figure 3-24(a), the surrounding susceptors reach 150° C while none of the 1mm^2 square patches' heat up to 50°C. The test involving 4 mm^2 square patches indicate that while the surrounding susceptor reaches 150°C, the patches heat up to at least 50 °C but they don't reach 70 °C (Figure 3-24(d) and (e)).

These results confirm that the proposed microwave bonding technique based on designed microwave susceptors could potentially offer high temperature selectivity and be used for substrates bonding.

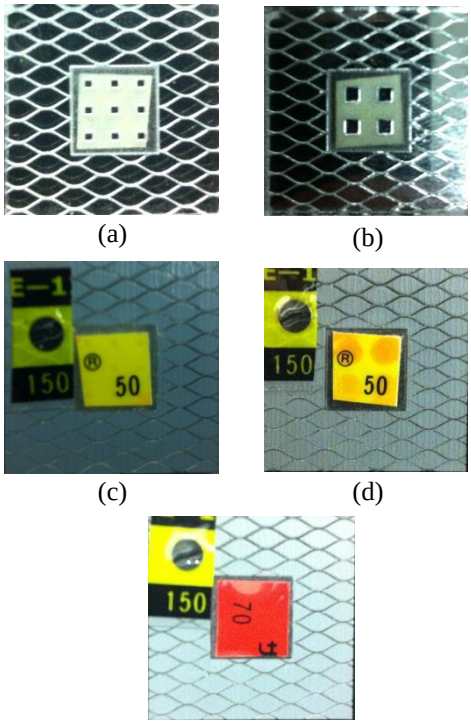

Figure 3-24 - Heating selectivity experimental results (a) sample (#1) with an array of 1 mm^2 square patches before the experiment (b) sample (#2) with an array of 4 mm^2 square patches before the experiment (c) sample #1 after the test. 150˚C thermolabel has changed color (white to black) while 50℃ thermolabel is unchanged (yellow) (d) sample #2 after the test. Both 150˚C and 50℃ thermolabels have changed color (white to black and yellow to orange) indicating that the 4 mm^2 square patches has reached 50℃ (e) sample #2 after the test showing the 70℃ thermolabel has not changed color (red) while the surrounding area has reached 150℃.

3.9 Summary

A new approach for generating localized heating using efficient metallic microwave susceptors in a commercial microwave oven is proposed. The structures have high potential for wafer and microfluidic bonding applications with further refinement. It is shown that the induced current densities and locations can be significantly affected by the susceptor designs. This implies that specific heat generation rate across the wafer can be controlled for known microwave sources, even with very basic commercial equipment. Based on this technique, efficient microwave susceptors are developed and characterized. It is demonstrated that the susceptor can generate localized efficient and selective

heating. In the proposed optimal eye-shaped pattern, a temperature of 160 °C can be achieved in less than 8sec at 50% microwave oven input power. In terms of heating selectivity, it is demonstrated that the designed eye-shape susceptors can reach 150℃ before an array of 1 mm^2 aluminum square patches would heat up to 50℃. This shows the potential of microwave susceptor design for packaging applications. It is also shown as a proof of concept that moving the sample along selected paths in the microwave cavity can compensate for non-uniformity of the field distribution and increase the uniformly heated area.

Chapter 4: Bonding of PMMA Microfluidics Using Microwave Susceptors[3]

The proposed susceptor in the previous chapter can be used for bonding two substrates. To test the concept, in this chapter the use of the proposed susceptors for bonding two PMMA microfluidic substrates is evaluated. PMMA is one of the most common thermoplastics used in fabrication of microfluidics due to its optical transparency, chemical compatibility, relatively low price and wide accessibility [17]. For thermally bonding thermoplastics, it is preferable to have the interface heated selectively and efficiently so as to minimize time and energy required.

Here, we demonstrate that the proposed metallic intermediate susceptor layer can provide fast, inexpensive and efficient bonding. To our knowledge, no previous study has been done on the design of intermediate metallic microwave susceptors for bonding microfluidics in commercial microwave ovens. As such, this work represents a significant step forward in the development of a rapid and reliable bonding method for thermoplastic substrates.

4.1 Microwave Heating System

Similar to the system described in section 3, the microwave heating system used in this study consisted of a commercial microwave oven (Panasonic NNSA630W and NNSD698S [74] microwave ovens, having identical cavity dimensions and input power) and PMMA substrates (1x1x0.06”Plaskolite© OPTIX Acrylic). Gold is used as the metallic material for microwave susceptors in these trials. This material was chosen because the deposition could be done very quickly using a

[3] A version of this chapter has been published [73]

Denton gold sputtering system commonly used for deposition on samples prior to scanning electron microscope (SEM) imaging. Doing so represented a significant reduction in cost per device fabricated, despite the higher cost of the material, because the throughput and fabrication turnaround time was much faster.

In chapter 3, microwave susceptor design details based on electromagnetic simulations were presented and for these trials a version of the eye shaped susceptor design was used.

In order to increase the surface area of the substrates that are in contact for bonding, the designed microwave susceptor patterns (eye-shape pattern) are produced by stencil sputtering (using shadow mask) rather than direct laser patterning. In this respect, the gold susceptor layer (15 nm thick) is sputtered on acrylic substrates through a patterned acrylic stencil (using a Denton gold sputtering system at vacuum pressure of 150 mTorr and 40 mA current for 120 seconds). The stencil is cut from 0.035 inch thick acrylic sheets using a Versa Laser VLS 3.5 CO_2 laser cutter (Figure 4-1 and Figure 4-2(a)). Laser cutter settings used for cutting the acrylic stencil are vector cutting mode, 12% power, 5% speed and PPI equal to 500.

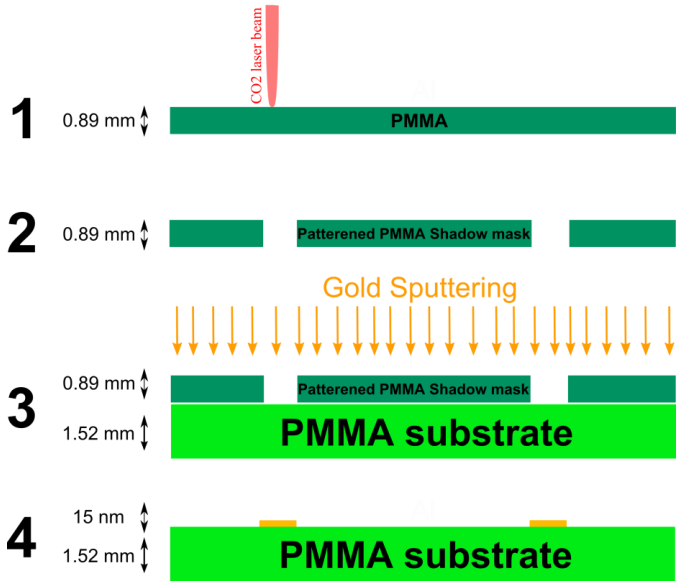

Figure 4-1 – Susceptor fabrication process using an acrylic shadow mask

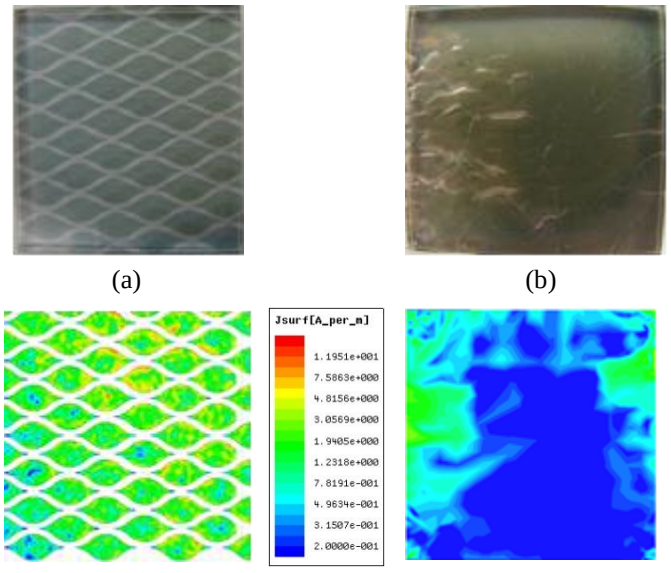

Figure 4-2 - (a) Picture of the fabricated microwave susceptor. (b) Picture of the non-patterned gold susceptor after the test, explosions are caused by large stress generations along the surface as a result of non-uniform heating. (c) Simulation results showing "Magnitude of Surface Current Density" (MSCD) of the susceptor at test location #2 (d) Simulation results showing MSCD of the non-patterned susceptor at the test location #2 (Figure 3-10).

The stenciling method was adopted for three main reasons: it could achieve the desired feature size and quality without the need for lithography or etching, it can be used for any metallic layer, and if the stencil was not in intimate contact, the edges of all metallic features would be gradually tapered in thickness, possibly producing fewer sharp step heights for subsequent bonding trials to overcome. While for the thicknesses used this would not be a severe issue, if thicker metallic layers were needed for other susceptor designs, this more gradual thickness change could have large benefits.

The heating profile of the fabricated microwave susceptors is illustrated in Figure 4-3.

4.2 Basic Bonding Experiment

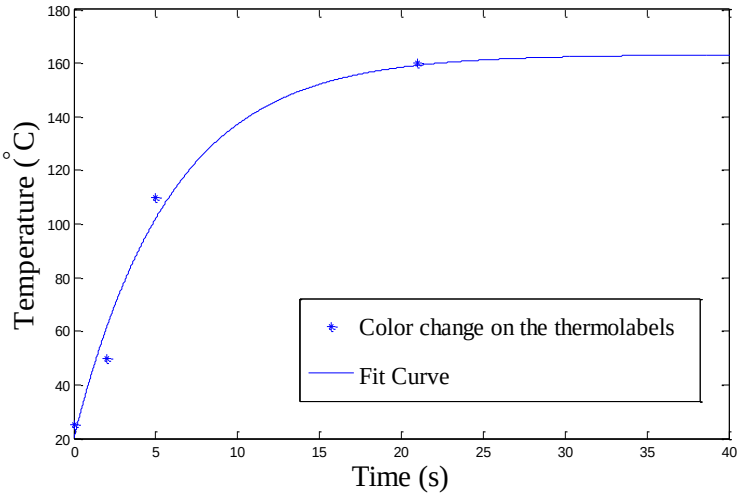

Figure 4-3 - Temperature vs. time of the designed microwave susceptor pattern

In the initial bonding experiments that were done to prove this bonding method was possible, two PMMA substrates, one with microfluidic channels and the other coated with gold susceptors were held together by elastic bands and two 1.5 in x 1.5 in PMMA sheets (2.95 mm thick) to exert moderate pressure (approximately 75 kPa) (Figure 4-4). Elastic bands are used for pressure application due to their

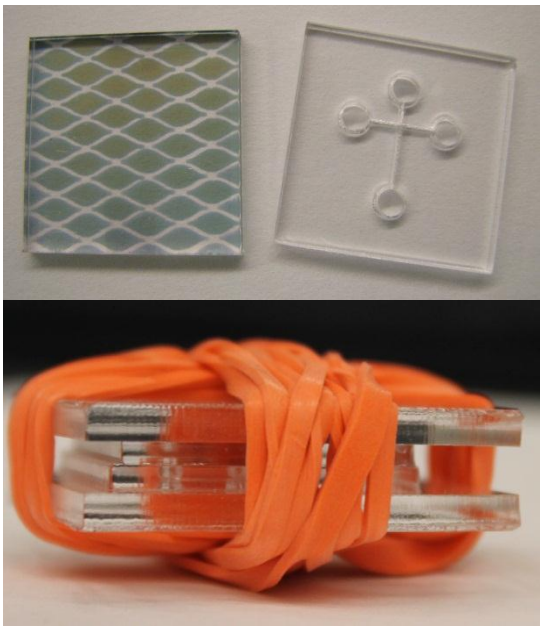

Figure 4-4 - Bonding samples and their attachment before the bonding test

relatively low RF loss and their low heating rate compared with the susceptors providing selective heating. The microfluidic channels are fabricated using the Versa Laser VLS 3.5 CO_2 laser cutter with raster engraving mode at 10% power and 5% speed. The reservoirs are cut using the laser cutter with vector cutting mode at 50% power and 5% speed.

The substrate stack is then placed at test location #2 (Figure 3-10) inside the microwave oven cavity for bonding. After running the microwave at 100% power (1200W) for 45 seconds the substrates were bonded and channels were sealed without leaks (Figure 4-5). In this manner, basic lessons were learned about the best methods for improving the bonding yield and strength in future designs, and efforts focused on an improved, microwave transparent clamping system that would apply more uniform pressure to the acrylic microfluidics and produce a more uniform bond. The following sections describe these bonding trials in more detail.

4.3 Substrate Bonding Characteristics

Section 4.2 showed that PMMA substrates with microfluidic channels can be bonded and sealed without leaks with the proposed microwave bonding technique. This section focuses on the substrates (without microfluidics) bonding

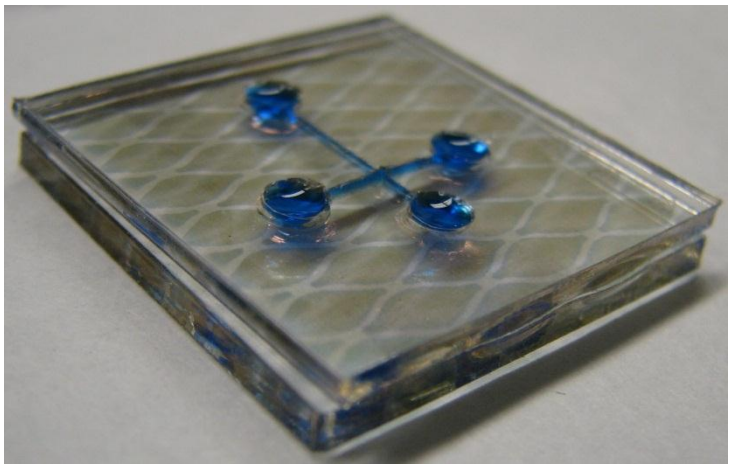

Figure 4-5 - bonded microfluidic channels filled with blue ink for leakage test

and its characteristics to improve the bonded area, minimize the bonding time and characterize the bonding strength.

Similar to section 4.2, in each experiment of this study two 1 in x 1 in PMMA substrates (one plain PMMA substrate and the other having susceptors fabricated on them using stencil sputtering) are used.

To achieve uniform pressure at the center of the substrates, PMMA (5.25 mm thick) pressure applicators are fabricated having a 2cm x 2cm contact area with the bonding substrates. By applying force away from the perimeter, the laser cut edges could be avoided, as these tended to have raised lips caused by reflow of PMMA that could be between 15 and 30 µm thick [18]. Moreover, 0.25mm thick silicone (Rogers Corporation HT-6135 performance solid silicone) intermediate layers are used between the pressure applicator and the substrates which eliminated some of the non-uniformity in the pressure and ensured better contact between the two acrylic pieces to be bonded(Figure 4-6). The substrate stack is then held together with an approximate constant pressure of 75 kPa applied using rubber bands (similar to Figure 4-4). An alternative force application method was also used for some experiments. In this method

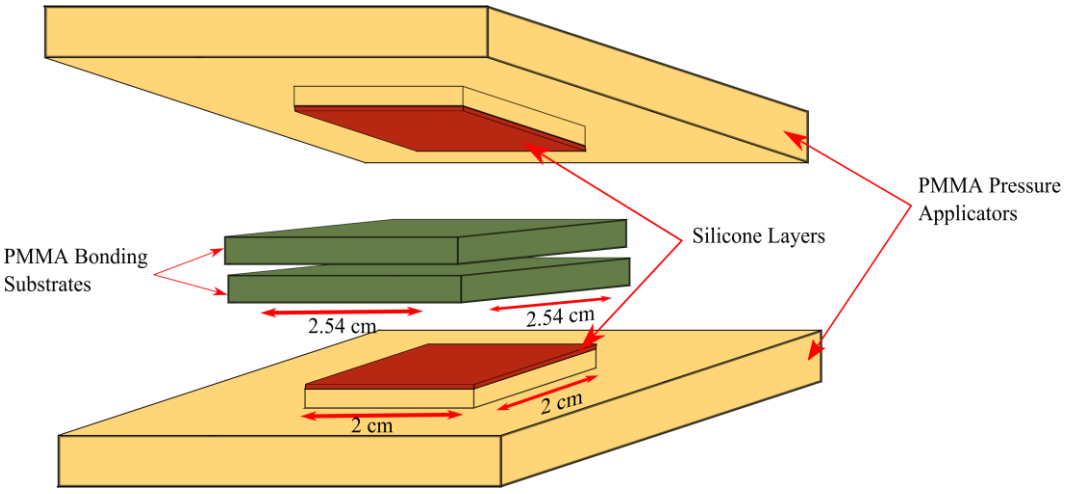

Figure 4-6 – Pressure applicator model for substrate bonding study

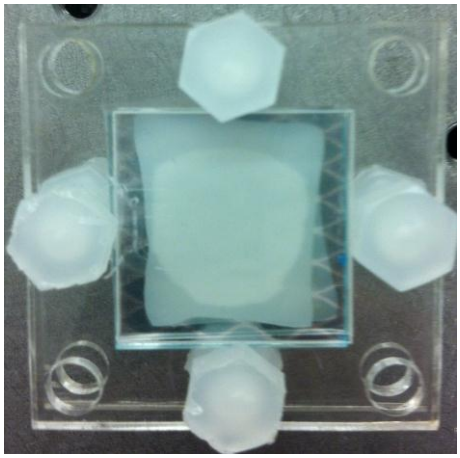

Figure 4-7 – Pressure application technique using polypropylene fasteners

polypropylene screws and nuts were used to attach the PMMA pressure applicators together (Figure 4-7). The advantage of using polypropylene bolts is their low RF loss characteristic, which keeps the materials unaffected during the microwave oven operation. In contrast with polypropylene, common nylon fasteners can melt in less than 1 minute under the microwave oven operation (Figure 4-8).

The substrate stack is placed inside the cavity at test location #2 for bonding experiments.

In order to characterize PMMA substrates bonding, four main bonding criteria are

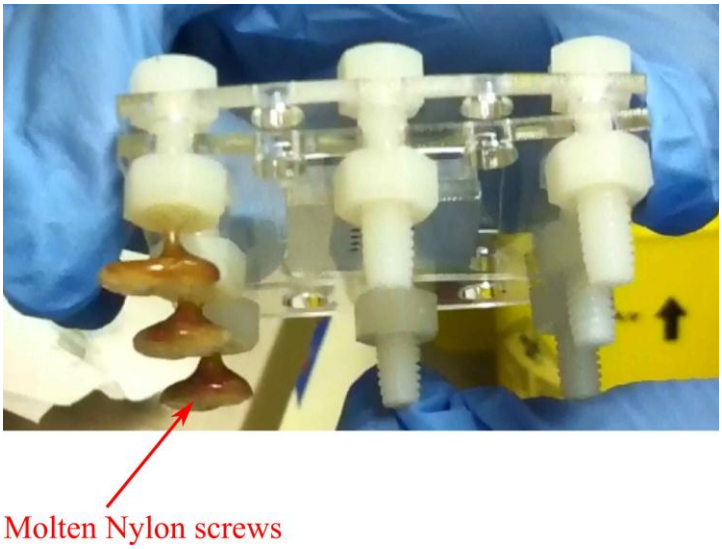

Figure 4-8 – Molten nylon screws after 1 minute of microwave oven operation

studied: *bond type*, *bonded area*, *bonding uniformity* and *bonding strength*. Moreover, alternatives are investigated for further reduction of the bonding temperature.

(a)Bond Type, Bonded Area and Bonding Uniformity: As discussed in chapter 3, the microwave susceptor layer at the interface of the two PMMA substrates is a heat source (Figure 4-3) which can cause bonding between the PMMA substrates and the gold intermediate layer or potentially cause the PMMA substrates to locally melt and fuse together.

As shown in Figure 4-3, the susceptor temperature is dependent on the time that it is being exposed to microwave radiation. Moreover, as shown in section 3.3, the heating rate is dependent on field intensity inside the microwave cavity and the field intensity itself is dependent on the input power of the microwave oven. In this section both of the effects of microwave *exposure time (operating time)* and *input power* of the microwave oven, on the bonded area is investigated.

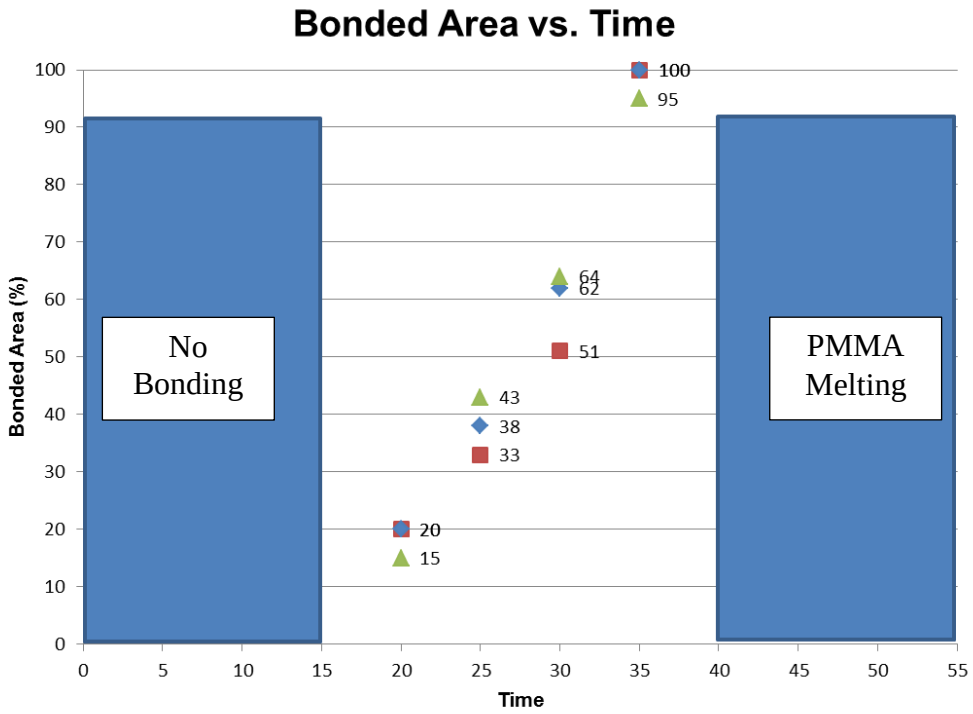

Figure 4-9 – Experimental results showing bonded area with respect to operating time of the microwave oven at 100% input power. Different symbols are only used for better visibility.

-Effect of exposure time on bonded area: Figure 4-9 shows the results of bonding experimental trials with different microwave exposure times (at 100% microwave oven input power (1200 W)). Approximate bonded area percentage is calculated with respect to the contact area of the two substrates (2 cm x 2 cm area at the center) from post-experiment image analysis of the samples using ImageJ software (Developed by National Institute of Health (NIH)) [75].

As shown in Figure 4-9, the experimental results show that PMMA substrate bonding using our proposed technique requires at least 20 seconds of microwave exposure time. Results showed that between 20 seconds and 30 seconds of exposure time a relatively weak bond forms between the PMMA substrate and the gold susceptor layer (Figure 4-10-(a)). Bonding samples exposed to microwave radiation for 35 seconds formed a stronger uniform bond over all of the contact area (2cm x 2cm area) (Figure 4-10-(b)) and susceptors heating up longer than 40

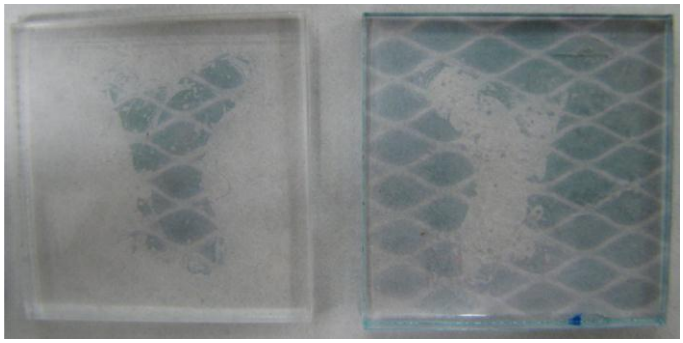

(a)

(b) (c)

Figure 4-10 – (a) Bonding samples after the test exposed to microwaves for 25 seconds at 100% power, showing weak PMMA-Gold bond (b) Bonded samples after exposed for 35 seconds at 100% power (c) Molten PMMA substrates after the test inside the microwave oven cavity for 45 seconds at 100% power.

seconds in the microwave oven melted the PMMA substrates (Figure 4-10-(c)). The obtained results are consistent with the measured temperature profile of the susceptors (Figure 4-3).

-Effect of input power on bonded area: As shown in Figure 4-11 decreasing the input power will increase the time required for PMMA substrate bonding. The change in microwave oven input power has a similar effect to the effect of field intensity changes (section 3.3) and therefore decreasing the input power results in lower field intensity at the same cavity location which slows the susceptor heating process.

Bonding uniformity is related to the pressure application mechanism (amount of pressure and its uniformity) as it has a relation with the contact area of the bonding substrates. Moreover, it is related to uniform heating of the susceptors as discussed in chapter 3. As shown in Figure 4-10-(b) PMMA substrates bonding using the microwave susceptors with the conditions described above can provide uniform bonding on a 2cm x 2cm area in 35 seconds.

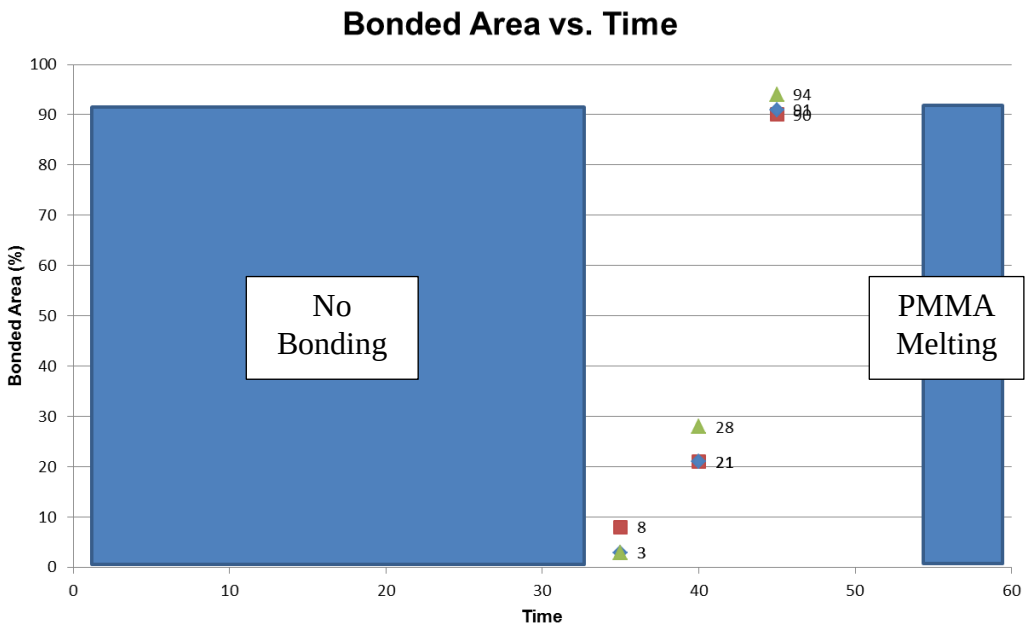

Figure 4-11– Experimental results showing bonded area with respect to operating time of the microwave oven at 70% input power. Different symbols are only used for better visibility.

(b) Bond Strength: The bond strength of the microwave bonded substrates was characterized by performing pulling test using an MTS 810 testing system. PMMA bonded substrates were attached to 1 inch diameter aluminum bars on both sides using Instant Krazy Glue. At the center of the surface of the free end of aluminum bars a hole was drilled and a 3 mm diameter steel cable was fixed through the hole using set screws. The other end of the cable was similarly attached to the grippers of the MTS 810 testing system for pulling (Figure 4-12). This system minimized torques from misalignments and allowed a nearly normal pulling force during the trials.

Pulling test were carried out on five samples with 2cm x 2cm bonded area and the bond strength data was extracted from their load vs. stroke curve. The minimum measured load causing the bond to break was 550 N which is equivalent to an overall pulling pressure of 1.375 MPa pulling pressure over the 2 cm x 2 cm bonded area. According to [76], a 1.0 MPa bond strength is sufficient for most of the microfluidics applications.

Observations after the pulling test indicated that the adhesion failures were primarily at the gold-PMMA interface (gold layers were transferred from one substrate to another during the bonding process). One solution to increase the bonding strength, can be to reduce the metal covered areas of the susceptor (in a new susceptor design) to allow for larger PMMA-PMMA contact area (Appendix B). Larger polymer contact area will increase the chance of polymer-polymer welding. Use of adhesion promoter layers such as chrome can also enhance the adhesion strength of gold to its underlying substrate. Alternatively, metals other

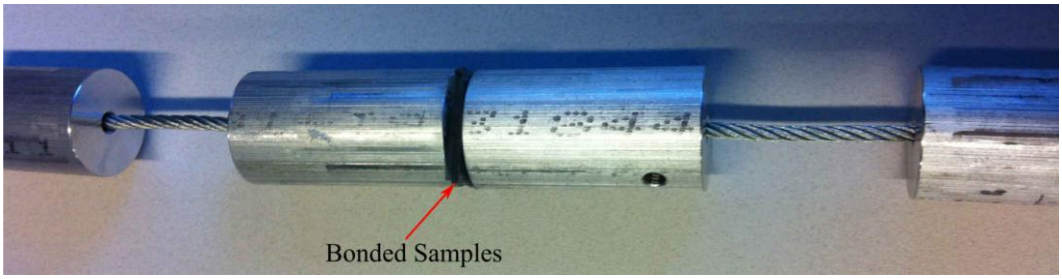

Figure 4-12 – Pulling test setup

than gold would normally have higher adhesion strength to the PMMA and could be explored in future work.

(c) *Bonding temperature reduction:* Bonding temperature reduction can decrease the chance of micro-channel deformation and provide faster bonding process. In this respect two alternatives were investigated for their potential use with the microwave bonding technique: *Using an intermediate layer with lower melting point than the substrates, and assisting a solvent bonding process with localized heating.*

(a) Using an intermediate layer with lower melting point: In order to investigate the effect of using low melting point intermediate layer, one of the substrates (without susceptor) is exposed to deep ultraviolet (UV) at 254 nm from a Stratgene 2400 DNA crosslinker. Deep UV exposed PMMA substrates start degrading from the exposed surface with time [77]. The glass transition temperature of the exposed areas is decreased and therefore the exposed surface of the PMMA acts as an intermediate layer with lower melting point. Experiments in a convection oven showed that eight hours of deep UV exposure at a nominal dose of 4 mW/cm^2 reduces the glass transition temperature of the exposed surface of PMMA to below 80℃.

The bonding experiment using the deep UV exposed PMMA with similar experimental conditions to section 4-3-(a) showed that the substrates bonded after 20 seconds at 100% power (Figure 4-13). This confirms the advantage of utilizing low melting temperature intermediate layers for bonding temperature (and bonding time) reduction. The controllability of this process was more challenging however, and would often result in voids in the bond. This may be partially due to the warpage of the PMMA substrate after long DUV exposures preventing full contact during the application of pressure in the microwave.

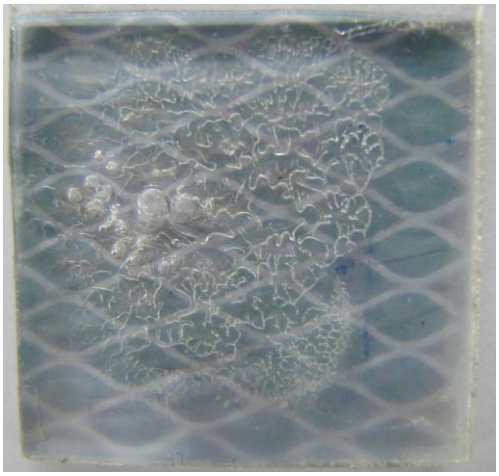

Figure 4-13–UV-Exposed PMMA substrate bonded in 20 seconds.

(b) Assisting solvent bonding process with localized heating: Thermally assisted solvent bonding can both enhance the solvent bonding process and bond the substrates at lower temperatures than PMMA glass transition temperature [19], [21]. To test this, a few drops of isopropanol alcohol (IPA) were placed between the PMMA substrates and the substrate stack was then bonded inside the microwave oven at the same conditions, as in section 4-3(a). The substrates were successfully bonded after 10 seconds at 100% power (Figure 4-14). Unfortunately, while the introduction of solvent speeds the bonding process, the quality of the area being bonded looks far worse, possibly due to evaporation,

Figure 4-14 – Thermally assisted (microwave susceptors) solvent (IPA) bonded PMMA substrates. The substrates were bonded after 10 seconds at 100% input power.

boiling and other localized damage caused by non-uniform heating in the susceptors. Additionally, the timing and operator skill required to ensure that the assembled stack didn't have too much or too little alcohol prevented this method from being worthwhile to pursue further at this time, although if lower powers are used, it could still be a viable alternative technique for bonding.

4.4 Microfluidics Bonding Characteristics

In this section PMMA microfluidics bonding characteristics such as *channel deformation* through the bonding process and *channel leakage* characteristics of the bonded microfluidics will be discussed.

(a) Channel deformation: In order to study the effect of microwave bonding using metallic susceptors on channel structure and dimensions, 1 cm long channels were fabricated on PMMA substrates using the Versa Laser VLS 3.50 CO_2 laser cutter (raster engraving mode, 1.5 pt (0.53 mm) CAD design line width, 10% power, 5% speed). The substrates were then used for bonding with the same experimental condition as section 4-3-(a). The substrates were bonded after 35 seconds at 100% microwave oven input power. Cross-section images of the micro-channel before and after the bonding step are shown in Figure 4-15 (a) and (c). As shown in Figure 4-15(c), the micro-channel side walls were deformed significantly during the bonding step causing the channel width to reduce by approximately 40% of its original dimension. Channel width before the bonding test is approximately 740 μm and its depth is approximately 710 μm.

The reason behind micro-channel deformation is the excessive heat generated and transferred to the channel structure by the susceptors which then causes the PMMA to reflow into the channel and reduce its dimensions. Therefore, one solution is to move the susceptors away from the channels. To test this hypothesis, a new shadow mask (stencil) was fabricated that removed the susceptors from the channel location.

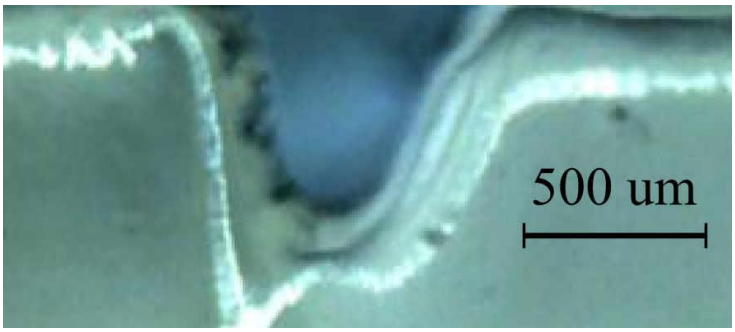

(a)

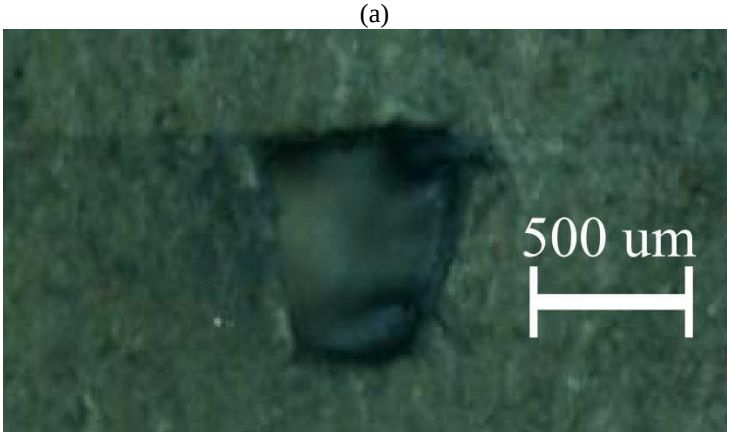

(b)

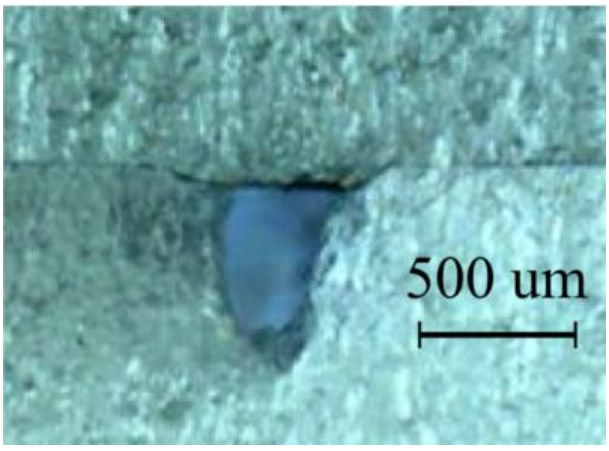

(c)

Figure 4-15 – (a) PMMA micro-channel fabricated using CO_2 laser cutter shown before the bonding experiment (b) PMMA micro-channel encapsulated using microwave susceptors surrounding (not directly on top of) the channel (Figure 4-16) showing less than 3% dimension change after the bonding process (c) PMMA micro-channel encapsulated using microwave susceptors (including ones directly on top of the channel) showing the deformations caused by the bonding process (channel width reduced by approximately 40%). *Substrates with bonded channels have been cut by a band saw for channel cross section imaging.*

The new substrates (one with micro-channels and susceptors around the channels

and the other, a plain substrate) were fully and uniformly bonded inside the microwave oven cavity after two microwave runs, each 35 seconds at 100% input power (Figure 4-16).

The substrates were cooled down to room temperature between the two runs. The substrates were bonded in two separate microwave runs instead of a longer continuous run to avoid the substrate melting possibility (Figure 4-9).

Cross section images of the channel before and after bonding are shown in Figure 4-15 (a) and (b). As shown in Figure 4-15(b), with the new susceptor configurations channel dimension changes during the bonding process is less than 5%.

Moving the microwave susceptors away from the microfluidic features has two advantages. One is providing a significant improvement in reduction of feature deformations and the other is avoiding potential channel contamination by removing gold susceptors from the micro-channel.

(b) Leakage test: In order to further characterize our proposed technique for PMMA microfluidics bonding, a leakage test was performed. First, simple microfluidic samples consisting of an inlet, outlet and a micro-channel were fabricated using the CO_2 laser cutter. Similar to the channel deformation

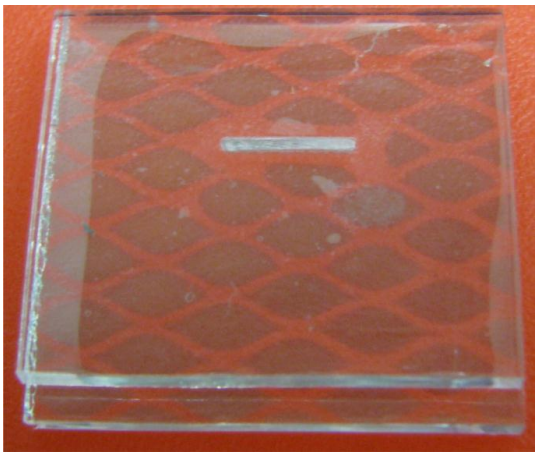

Figure 4-16 – Bonded substrates with micro-channels and surrounding susceptors

characterization, laser settings for channel fabrication were: raster engraving mode, 1.5 pt (0.53 mm) CAD design line width, 10% power, 5% speed.

Laser settings for fabrication of the reservoirs (inlet and outlet of the channel) were: vector cutting mode, *hair-line* CAD design line width, 50% power, 5% speed. Next, 15 nm of gold was sputtered on the surrounding areas of the channel. The prepared substrate was then attached to a plain PMMA substrate (Figure 4-6) for bonding. The substrates uniformly bonded after two runs of microwave operation each 35 seconds long (Figure 4-17).

For the leakage test a *Harvard Apparatus 11 Plus single syringe pump*, a 15 mL syringe, Cole-Parmer Tygon® silicone tubing (1/16"ID x 1/8"OD, YO-95702-01) and dyed (yellow) water (as the fluid) were utilized (Figure 4-18). The tubes were attached and sealed on to the reservoirs using *Instant Krazy Glue* gel (Figure 4-19).

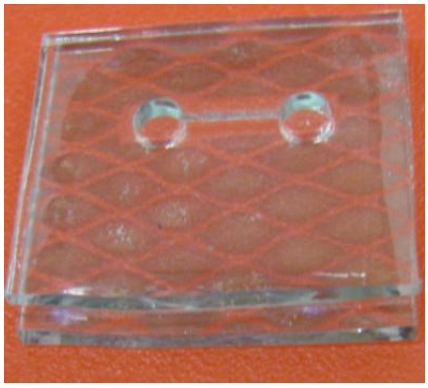

Figure 4-17 – Bonded PMMA microfluidics substrates

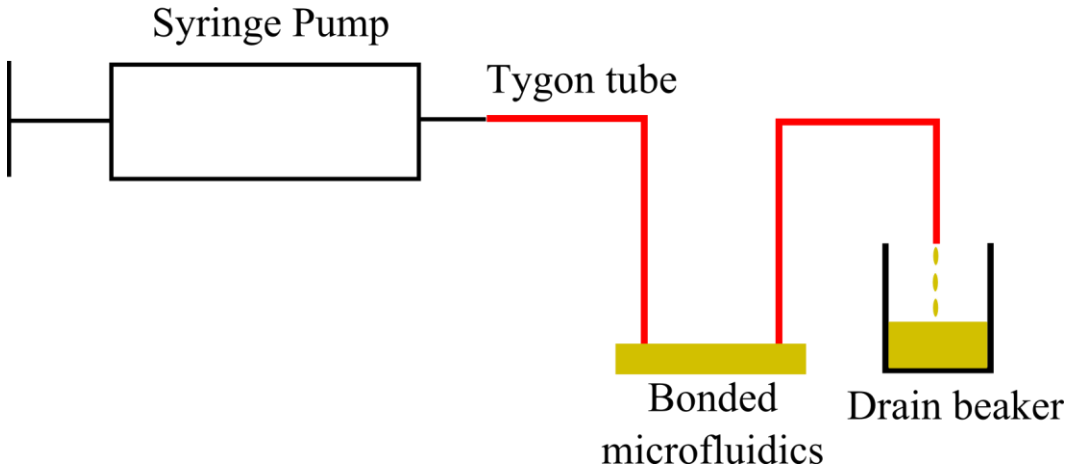

Figure 4-18 - Leakage test experimental setup

During the test no leakage was observed after increasing the flow rate of the fluid up to 9.7 mL/min (maximum for the syringe). This is further confirmation that the technique is viable for sealing PMMA microfluidics for both high pressures and high flow rates with optimal conditions.

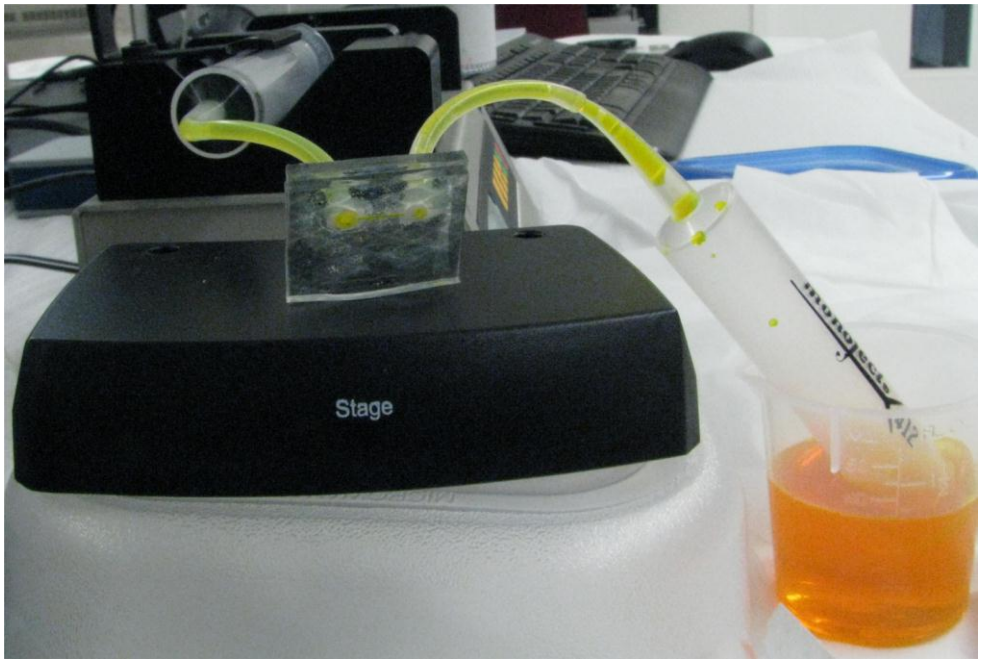

(a)

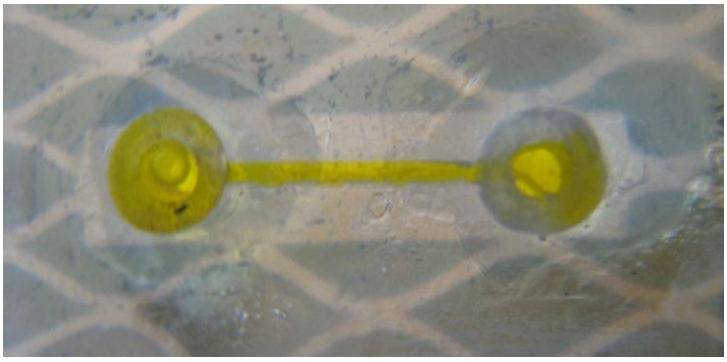

(b)

Figure 4-19 -(a) Leakage test setup (b) Microchannel filled with dyed water during the leakage test, cloudy areas around the reservoirs are external residues of the Instant Krazy Glue used for sealing the tubes connection.

4.5 Summary

In this chapter, the concept of using the designed microwave susceptors to bond thermoplastic microfluidics is demonstrated. Using a single susceptor design style to minimize our experimental variables, it was found that PMMA substrates can be bonded together in less than 35 seconds inside the commercial microwave oven at 100 % power without any evidence of arcing or uncontrolled heating.

The time required to fully bond the microfluidics was longer than the typical time required for heating a single susceptor without a matching substrate, which is expected as the effective heat sink of the PMMA is at least doubled in this arrangement. In future, more efficient designs with larger element areas, or higher perimeter to area ratios may be used to further enhance bonding selectivity and reduce time. As an alternative, several modifications to the bonding process were explored, including lowering the glass transition temperature of the bonded interface by deep UV exposure, and introducing a poor solvent for PMMA (IPA) which would initiate bonding at much lower temperatures than those in the absence of the solvent. Of these two options, the inclusion of a lower melting point intermediate layer is the more promising one, because of the controllability and possible safety challenges in using solvents in the microwave when arcing is a possibility. There was a significant advantage to placing the susceptors at a small distance away from the channels with respect to minimizing the deformation of the channels. With improved thermal modeling we can expect to get the best possible placement of heaters in close proximity to the channels so that the bulk of the microfluidics are strongly bonded, yet the channels will remain below the glass transition temperature of the PMMA for the duration of the bonding steps. Moreover, the substrates and microfluidics bonding processes were characterized for bonding strength, channel deformation and leakage test. It was shown that PMMA microfluidics bonding using microwave susceptors and commercial microwave ovens provides inexpensive, rapid and easy solution for microfluidic bonding.

Chapter 5: Conclusions

5.1 Summary:

This thesis introduces a novel approach for low cost microwave heating. A relatively low cost and widely accessible commercial microwave oven is used as the energy source and patterned metallic layers are used as microwave susceptors to generate heat. The proposed technique has the advantage of fast and local heating at the interface between substrates which makes it a good candidate for polymer bonding applications. The following sections summarize the main contributions of this project in more details.

5.1.1 Electrode Patterning Technique Using CO_2 Laser Cutter (Chapter 2):

A novel low cost rapid metal electrode prototyping technique is introduced which utilizes a widely accessible commercial CO_2 Laser Cutter (VLS 3.50 Versa Laser). This technique is based on heating the underlying substrate of the target metal layer instead of direct heating of metal. It is shown that electrodes with minimum feature size of 450um can be fabricated with less than 5% dimension error using this technique. Rapid (comparable with simulation time) susceptor fabrication using this technique significantly assists the design and optimization process of the susceptors. Other metal patterning applications such as antenna prototyping (Appendix A) can also benefit from this method.

5.1.2 Efficient Microwave Susceptor Design and Characterization (Chapter 3):

It is shown, both by simulation and experiments, that commercial microwave ovens have a non-uniform field distribution which results in non-uniform heating of the susceptors (in some cases can lead to arcing and micro-explosions). In order to overcome this challenge appropriate microwave susceptor patterns (rather

than large individual solid conductive layers) are designed based on electromagnetic simulations. Electromagnetic simulations provided acceptable estimations as a design tool for prediction of the current and thus heating distribution of the designed susceptors.

Using the explained design toolkit an efficient susceptor pattern is designed and optimized showing rapid, selective, localized heating. Characterization of the designed susceptor pattern showed acceptable reusability for temperatures below the melting point of the substrate.

The uniform heating area for susceptors with fixed position inside the microwave oven cavity was approximately 1 in^2. As a proof of concept, it was shown that moving the susceptor inside the cavity on a selected path can increase the uniform heating area on the substrate.

We also showed that using different designed susceptor patterns (inefficient and efficient) together on a substrate it is possible to achieve acceptable heating selectivity which is desirable for packaging applications.

5.1.3 Microfluidics Bonding Using the Designed Microwave Susceptors (Chapter 4):

An improved susceptor pattern (eye-shaped) was applied to PMMA-PMMA substrates and microfluidics bonding. It was demonstrated that PMMA substrates can be bonded within 35 seconds of microwave oven operation producing minimum measured bond strength of 1.375 MPa. In a similar approach, microwave susceptors were fabricated around a micro-channel for microfluidics bonding characterization. Post-experiment characterizations results showed that bonding process caused less than 5% deformation in channel dimensions when the susceptors are in close proximity but not under the micro-channels. Bonded microfluidic substrates did not show any sign of leakage under flow rates up to 9.7 mL/min.

5.2 Future Study

5.2.1 Design of the optimized susceptor pattern for higher temperature targets

Efficient microwave susceptors designed in this study, showed the potential for other microwave heating applications in microfabrication (such as hot-embossing) and material processing. In this project PMMA is used as our substrate material due to its wide usage in microfluidics applications. However, the PMMA melting point is around 160℃ and therefore our designs were limited by this temperature. Using other substrates with low RF loss and higher melting temperatures can allow for further design and characterization of microwave susceptors at higher temperatures.

Future studies can also investigate other substrate bonding materials for different applications.

5.2.2 Increasing the uniform heating area to achieve larger bonding area

As discussed in chapter 1, one of the potential applications of the proposed technique is in wafer level packaging [78–80] (Figure 1-11). In this respect considering the available standard wafer sizes, there is an interest to increase the uniform heating area.

Further field uniformity enhancements might be achieved by using designed custom built single mode cavity with larger operating wavelength.

As a proof of concept in this study we have shown that moving the substrate a selected path in the cavity can also enhance the bonding uniformity area (Section 3.5).

It was shown that heating rate and uniformity can be controlled using the designed patterns. In this respect one other solution can be designing hybrid susceptor patterns (efficient and inefficient patterns) together in a way to compensate for field non-uniformity.

5.2.3 Bonding devices such as MEMS and RF devices using this technique

As shown in section 3.6 designed susceptor patterns can provide heating selectivity for bonding metallic structures. In this respect further studies can be carried out on actual Micro Electro-Mechanical Systems (MEMS) and RF devices bonding and their challenges.

5.2.4 Using low melting point intermediate layers for bonding

In chapter 4 it was demonstrated that a deep UV exposed PMMA layer can decrease the time required for bonding by reducing the bonding temperature. In a similar approach other low melting point materials can also be used at the interface for bonding at lower temperatures.

References

[1] C. Liu, 'Recent Developments in Polymer MEMS', *Advanced Materials*, vol. 19, no. 22, pp. 3783–3790, 2007.

[2] S. H. Ng, R. T. Tjeung, Z. F. Wang, A. C. W. Lu, I. Rodriguez, and N. F. Rooij, 'Thermally activated solvent bonding of polymers', *Microsystem Technologies*, vol. 14, no. 6, pp. 753–759, Nov. 2007.

[3] C. H. Yun, J. R. Martin, E. B. Tarvin, and J. T. Winbigler, 'AL to AL wafer bonding for MEMS encapsulation and 3-D interconnect', in *Micro Electro Mechanical Systems, 2008. MEMS 2008. IEEE 21st International Conference on*, 2008, pp. 810 –813.

[4] R. Truckenmüller, R. Ahrens, Y. Cheng, G. Fischer, and V. Saile, 'An ultrasonic welding based process for building up a new class of inert fluidic microsensors and -actuators from polymers', *Sensors and Actuators A: Physical*, vol. 132, no. 1, pp. 385–392, Nov. 2006.

[5] J. J. Shah, J. Geist, L. E. Locascio, M. Gaitan, M. V. Rao, and W. N. Vreeland, 'Capillarity Induced Solvent-Actuated Bonding of Polymeric Microfluidic Devices', *Analytical Chemistry*, vol. 78, no. 10, pp. 3348–3353, May 2006.

[6] Y. T. Cheng, L. Lin, and K. Najafi, 'Localized silicon fusion and eutectic bonding for MEMS fabrication and packaging', *Microelectromechanical Systems, Journal of*, vol. 9, no. 1, pp. 3 –8, Mar. 2000.

[7] N. K. Budraa, H. W. Jackson, M. Barmatz, W. T. Pike, and J. D. Mai, 'Low pressure and low temperature hermetic wafer bonding using microwave

heating', in *Twelfth IEEE International Conference on Micro Electro Mechanical Systems, 1999. MEMS '99*, 1999, pp. 490–492.

[8] Kin Fong Lei, W. J. Li, N. Budraa, and J. D. Mai, 'Microwave bonding of polymer-based substrates for micro-nano fluidic applications', in *TRANSDUCERS, Solid-State Sensors, Actuators and Microsystems, 12th International Conference on,* 2003, vol. 2, pp. 1335– 1338 vol.2.

[9] G. Wallis, 'Field Assisted Glass-Metal Sealing', *Journal of Applied Physics*, vol. 40, no. 10, p. 3946, 1969.

[10] A. Gerlach, D. Maas, D. Seidel, H. Bartuch, S. Schundau, and K. Kaschlik, 'Low-temperature anodic bonding of silicon to silicon wafers by means of intermediate glass layers', *Microsystem technologies*, vol. 5, no. 3, pp. 144–149, 1999.

[11] S. Farrens and S. MicroTec, 'Metal based wafer level packaging', in *Proceedings of the International Wafer-Level Packaging Conference (IWLPC), San Jose (CA)*, 2008.

[12] H. Shao, D. Kumar, S. A. Feld, and K. L. Lear, 'Fabrication of a Fabry-Perot Cavity in a Microfluidic Channel Using Thermocompressive Gold Bonding of Glass Substrates', *Journal of Microelectromechanical Systems*, vol. 14, no. 4, pp. 756 – 762, Aug. 2005.

[13] F. Niklaus, P. Enoksson, E. Kälvesten, and G. Stemme, 'Low-temperature full wafer adhesive bonding', *Journal of Micromechanics and Microengineering*, vol. 11, p. 100, 2001.

[14] R. Knechtel, ‘Glass frit bonding: an universal technology for wafer level encapsulation and packaging’, *Microsystem Technologies*, vol. 12, no. 1, pp. 63–68, 2005.

[15] L. Martynova, L. E. Locascio, M. Gaitan, G. W. Kramer, R. G. Christensen, and W. A. MacCrehan, ‘Fabrication of plastic microfluid channels by imprinting methods’, *Analytical chemistry*, vol. 69, no. 23, pp. 4783–4789, 1997.

[16] H. F. Zhang, X. W. Liu, Z. C. Peng, W. Wang, and Y. F. Chen, ‘Investigation of Thermal Bonding on PMMA Capillary Electrophoresis Chip’, *Advanced Materials Research*, vol. 60–61, pp. 288–292, 2009.

[17] C.-W. Tsao and D. L. DeVoe, ‘Bonding of thermoplastic polymer microfluidics’, *Microfluidics and Nanofluidics*, vol. 6, no. 1, pp. 1–16, Nov. 2008.

[18] H. Klank, J. P. Kutter, and O. Geschke, ‘CO2-laser micromachining and back-end processing for rapid production of PMMA-based microfluidic systems’, *Lab on a Chip*, vol. 2, no. 4, p. 242, 2002.

[19] Y.-C. Hsu and T.-Y. Chen, ‘Applying Taguchi methods for solvent-assisted PMMA bonding technique for static and dynamic μ-TAS devices’, *Biomedical Microdevices*, vol. 9, no. 4, pp. 513–522, 2007.

[20] R. K. Roy, *Design of Experiments Using The Taguchi Approach: 16 Steps to Product and Process Improvement*. John Wiley & Sons, 2001.

[21] M. Rahbar, S. Chhina, D. Sameoto, and M. Parameswaran, ‘Microwave-induced, thermally assisted solvent bonding for low-cost PMMA microfluidic

devices', *Journal of Micromechanics and Microengineering*, vol. 20, no. 1, p. 015026, Jan. 2010, doi:10.1088/0960-1317/20/1/015026.

[22] M. T. Koesdjojo, Y. H. Tennico, and V. T. Remcho, 'Fabrication of a Microfluidic System for Capillary Electrophoresis Using a Two-Stage Embossing Technique and Solvent Welding on Poly(methyl methacrylate) with Water as a Sacrificial Layer', *Analytical Chemistry*, vol. 80, no. 7, pp. 2311–2318, Apr. 2008.

[23] B. Bilenberg, T. Nielsen, B. Clausen, and A. Kristensen, 'PMMA to SU-8 bonding for polymer based lab-on-a-chip systems with integrated optics', *Journal of Micromechanics and Microengineering*, vol. 14, p. 814, 2004.

[24] P. Turmezei, A. Polyakov, J. R. Mollinger, M. Bartek, A. Bossche, and J. N. Burghartz, 'Microfluidic device constructed from photosensitive BCB for erythrocyte membrane deformability measurement' *in Proc. of Eurosensors XVII, Guimarães, Portugal, University of Minho, September 21, 2003*, pp. 193-196 (2003).

[25] J. Han, S. H. Lee, A. Puntambekar, S. Murugesan, J. W. Choi, G. Beaucage, and C. H. Ahn, 'UV adhesive bonding techniques at room temperature for plastic lab-on-a-chip', in *7th International Conference of Miniaturized Chemical and Biochemical Analysis Systems, October 5-9, 2003, Squaw Valley, California, USA*, 2003.

[26] L. Gutierrez-Rivera, J. Martinez-Quijada, R. Johnstone, D. Elliott, C. Backhouse, and D. Sameoto, 'Multilayer bonding using a conformal adsorbate film (CAF) for the fabrication of 3D monolithic microfluidic devices in photopolymer', *Journal of Micromechanics and Microengineering*, vol. 22, no. 8, p. 085018, Aug. 2012.

[27] J. Kim, B. Jeong, M. Chiao, and L. Lin, 'Ultrasonic Bonding for MEMS Sealing and Packaging', *IEEE Transactions on Advanced Packaging*, vol. 32, no. 2, pp. 461 –467, May 2009.

[28] Z. Zhang, X. Wang, Y. Luo, S. He, and L. Wang, 'Thermal assisted ultrasonic bonding method for poly(methyl methacrylate) (PMMA) microfluidic devices', *Talanta*, vol. 81, no. 4–5, pp. 1331–1338, Jun. 2010.

[29] D. M. Pozar, *Microwave engineering*. Wiley, 1997.

[30] H. A. Wheeler, 'Formulas for the Skin Effect', *Proceedings of the IRE*, vol. 30, no. 9, pp. 412 – 424, Sep. 1942.

[31] T. L. Bergman, F. P. Incropera, A. S. Lavine, and D. P. DeWitt, *Fundamentals of Heat and Mass Transfer*. John Wiley & Sons, 2011.

[32] C. A. Balanis, *Advanced Engineering Electromagnetics*. Wiley, 2012.

[33] M. Mehdizadeh, *Microwave/RF Applicators and Probes for Material Heating, Sensing, and Plasma Generation: A Design Guide*. William Andrew, 2009.

[34] Y. V. Bykov, K. I. Rybakov, and V. E. Semenov, 'High-temperature microwave processing of materials', *Journal of Physics D: Applied Physics*, vol. 34, p. R55, 2001.

[35] S. Marinel and E. Savary, 'In situ measurement of the shrinkage during microwave sintering', *Journal of Materials Processing Technology*, vol. 209, no. 10, pp. 4784–4788, Jun. 2009.

[36] F. P. Incropera and D. P. DeWitt, *Fundamentals of heat transfer*. Wiley, 1981.

[37] K. F. LEI, S. AHSAN, N. BUDRAA, W. J. LI, and J. D. MAI, 'Microwave bonding of polymer-based substrates for potential encapsulated micro/nanofluidic device fabrication', *Sensors and actuators. A, Physical*, vol. 114, no. 2–3, pp. 340–346.

[38] S. Qi, X. Liu, S. Ford, J. Barrows, G. Thomas, K. Kelly, A. McCandless, K. Lian, J. Goettert, and S. A. Soper, 'Microfluidic devices fabricated in poly(methyl methacrylate) using hot-embossing with integrated sampling capillary and fiber optics for fluorescence detection', *Lab on a Chip*, vol. 2, no. 2, p. 88, 2002.

[39] M. Heckele, W. Bacher, and K. D. Müller, 'Hot embossing - The molding technique for plastic microstructures', *Microsystem Technologies*, vol. 4, no. 3, pp. 122–124, 1998.

[40] H. Becker and U. Heim, 'Hot embossing as a method for the fabrication of polymer high aspect ratio structures', *Sensors and Actuators A: Physical*, vol. 83, no. 1–3, pp. 130–135, May 2000.

[41] A. A. Yussuf, I. Sbarski, J. P. Hayes, M. Solomon, and N. Tran, 'Microwave welding of polymeric-microfluidic devices', *Journal of Micromechanics and Microengineering*, vol. 15, no. 9, pp. 1692–1699, Sep. 2005.

[42] R. J. Holmes, C. McDonagh, J. A. D. McLaughlin, S. Mohr, N. J. Goddard, and P. R. Fielden, 'Microwave bonding of poly(methylmethacrylate) microfluidic devices using a conductive polymer',

Journal of Physics and Chemistry of Solids, vol. 72, no. 6, pp. 626–629, Jun. 2011.

[43] A. Bayrashev and B. Ziaie, 'Silicon wafer bonding with an insulator interlayer using RF dielectric heating', in *Micro Electro Mechanical Systems, 2002. The Fifteenth IEEE International Conference on*, 2002, pp. 419–422.

[44] H. Noh, K. Moon, A. Cannon, P. J. Hesketh, and C. P. Wong, 'Wafer bonding using microwave heating of parylene for MEMS packaging', in *Electronic Components and Technology Conference, 2004. Proceedings. 54th*, 2004, vol. 1, pp. 924 – 930 Vol.1.

[45] V. Linder, H. Wu, X. Jiang, and G. M. Whitesides, 'Rapid Prototyping of 2D Structures with Feature Sizes Larger than 8 μm', *Analytical Chemistry*, vol. 75, no. 10, pp. 2522–2527, May 2003.

[46] T. Deng, H. Wu, S. T. Brittain, and G. M. Whitesides, 'Prototyping of masks, masters, and stamps/molds for soft lithography using an office printer and photographic reduction', *Analytical chemistry*, vol. 72, no. 14, pp. 3176–3180, 2000.

[47] H. Schift, R. W. Jaszewski, C. David, and J. Gobrecht, 'Nanostructuring of polymers and fabrication of interdigitated electrodes by hot embossing lithography', *Microelectronic Engineering*, vol. 46, no. 1–4, pp. 121–124, May 1999.

[48] L. Hanborough, 'Excimer laser patterning of thick and thin films for high density packaging', *Microelectronic packaging and laser processing: 25-26 June, 1997, Singapore*, vol. 3184, p. 176, 1997.

[49] C. J. Hayden, J. C. T. Eijkel, and C. Dalton, ‘An alternative method of fabricating sub-micron resolution masks using excimer laser ablation’, *Journal of Micromechanics and Microengineering*, vol. 14, p. 826, 2004.

[50] C. J. Hayden and C. Dalton, ‘Direct patterning of microelectrode arrays using femtosecond laser micromachining’, *Applied Surface Science*, vol. 256, no. 12, pp. 3761–3766, Apr. 2010.

[51] M. F. Shafique, K. Saeed, D. P. Steenson, and I. D. Robertson, ‘Laser Prototyping of Microwave Circuits in LTCC Technology’, *Microwave Theory and Techniques, IEEE Transactions on*, vol. 57, no. 12, pp. 3254 –3261, Dec. 2009.

[52] M. Schuettler, S. Stiess, B. V. King, and G. J. Suaning, ‘Fabrication of implantable microelectrode arrays by laser cutting of silicone rubber and platinum foil’, *Journal of neural engineering*, vol. 2, p. S121, 2005.

[53] W. M. Steen and J. Mazumder, *Laser Material Processing*. Springer, 2010.

[54] E. D. Palik, *Handbook of Optical Constants of Solids*. Academic Press, 1985.

[55] A. Axelevitch, B. Gorenstein, and G. Golan, ‘Investigation of Optical Transmission in Thin Metal Films’, *Physics Procedia*, vol. 32, no. 0, pp. 1–13, 2012.

[56] A. M. Prokhorov, V. I. Konov, I. Ursu, and N. Mihailescu, *Laser Heating of Metals*, 1st ed. Taylor & Francis, 1990.

[57] C. K. Chung and S. L. Lin, ‘CO2 laser micromachined crackless through holes of Pyrex 7740 glass’, *International Journal of Machine Tools and Manufacture*, vol. 50, no. 11, pp. 961–968, Nov. 2010.

[58] S. L. Lin, H. Y. Wang, and C. K. Chung, ‘Simulation and fabrication of pyrex glass drilling using CO2 laser’, in *Nano/Micro Engineered and Molecular Systems (NEMS), 2010 5th IEEE International Conference on*, 2010, pp. 333 –336.

[59] D. Snakenborg, H. Klank, and J. P. Kutter, ‘Microstructure fabrication with a CO2 laser system’, *Journal of Micromechanics and Microengineering*, vol. 14, p. 182, 2004.

[60] L. Romoli, G. Tantussi, and G. Dini, ‘Experimental approach to the laser machining of PMMA substrates for the fabrication of microfluidic devices’, *Optics and Lasers in Engineering*, vol. 49, no. 3, pp. 419–427, Mar. 2011.

[61] T.-F. Hong, W.-J. Ju, M.-C. Wu, C.-H. Tai, C.-H. Tsai, and L.-M. Fu, ‘Rapid prototyping of PMMA microfluidic chips utilizing a CO2 laser’, *Microfluidics and Nanofluidics*, vol. 9, no. 6, pp. 1125–1133, 2010.

[62] P. A. Atanasov, ‘CW CO’, 1997, vol. 3092, pp. 772–775.

[63] ‘Laser Cutting, Engraving and Marking Equipment, Machines and Software | Universal Laser Systems’, *Universal Laser Systems, Inc*. [Online]. Available: http://www.ulsinc.ca/. [Accessed: 04-Sep-2012].

[64] C. J. Risser, E. W. Gorham, and Y. P. Sukhman, ‘High resolution laser beam delivery apparatus’, U.S. Patent 706093413-Jun-2006.

[65] Universal Laser Systems Team, ‘VersaLASER® (VLS) User Guide VLS 2.30, VLS 3.50’. Universal Laser Systems, 2010.

[66] A. Toossi, M. Daneshmand, and D. Sameoto, ‘Microwave Susceptor Design for Wafer Bonding Applications’, in *Microwave Symposium Digest (MTT), 2012 IEEE International*, Montreal, QC, 2012, pp. 1-3.

[67] W. C. Winters, H. Chang, G. R. Anderson, R. A. Easter, and J. J. Sholl, ‘Microwave heating package, method and susceptor composition’, U.S. Patent 4 283 427 11-Aug-1981.

[68] A. N. Dodge, N. F. David, and J. Q. Mendoza, ‘Susceptor for microwaveable food’, U.S. Patent D545 125 S, 26-Jun-2007.

[69] ‘Operating Instructions of Panasonic NN-SA630W Microwave Oven’. Panasonic Home Appliances Microwave Oven (Shanghai) Co., Ltd., 2010.

[70] M. Soltysiak, W. Gwarek, M. Celuch, and U. Erle, ‘FDTD modelling of plain susceptors for microwave oven applications’, in *2010 18th International Conference on Microwave Radar and Wireless Communications (MIKON)*, 2010, pp. 1–4.

[71] ‘Nichiyu Giken Kogyo Co., Ltd.’ [Online]. Available: http://www.nichigi.com/. [Accessed: 01-Sep-2012].

[72] S. V. Egorov, A. G. Eremeev, I. V. Plotnikov, V. E. Semenov, A. A. Sorokin, N. A. Zharova, and Y. V. Bykov, ‘Edge effect in microwave heating of conductive plates’, *Journal of Physics D: Applied Physics*, vol. 39, no. 14, pp. 3036–3041, Jul. 2006.

[73] A. Toossi, D. Sameoto, and D. Daneshmand, ‘Low Cost Localized Bonding of PMMA Microfluidics Using Microwave Susceptors’, in *2012 Solid-State Sensors, Actuators and Microsystems Workshop Digest*, Hilton Head, SC, USA, 2012, pp. 252–253.

[74] ‘Operating Instructions of Panasonic NN-SD698S Microwave Oven’. Panasonic Home Appliances Microwave Oven (Shanghai) Co., Ltd., 2009.

[75] ‘ImageJ: Image Processing and Analysis in Java’. [Online]. Available: http://rsbweb.nih.gov/ij/. [Accessed: 09-Sep-2012].

[76] A. Han, O. Wang, M. Graff, S. K. Mohanty, T. L. Edwards, K.-H. Han, and A. Bruno Frazier, ‘Multi-layer plastic/glass microfluidic systems containing electrical and mechanical functionality’, *Lab on a Chip*, vol. 3, no. 3, p. 150, 2003.

[77] M. Haiducu, M. Rahbar, I. G. Foulds, R. W. Johnstone, D. Sameoto, and M. Parameswaran, ‘Deep-UV patterning of commercial grade PMMA for low-cost, large-scale microfluidics’, *Journal of Micromechanics and Microengineering*, vol. 18, no. 11, p. 115029, Nov. 2008.

[78] S. A. Audet and K. M. Edenfeld, ‘Integrated sensor wafer-level packaging’, in , *1997 International Conference on Solid State Sensors and Actuators, 1997. TRANSDUCERS ’97 Chicago*, 1997, vol. 1, pp. 287 –289 vol.1.

[79] Y.-K. Park, H.-W. Park, D.-J. Lee, J.-H. Park, I.-S. Song, C.-W. Kim, C.-M. Song, Y.-H. Lee, C.-J. Kim, and B. K. Ju, ‘A novel low-loss wafer-level packaging of the RF-MEMS devices’, in *The Fifteenth IEEE International Conference on Micro Electro Mechanical Systems, 2002*, 2002, pp. 681 –684.

[80] B. Lee, S. Seok, and K. Chun, ‘A study on wafer level vacuum packaging for MEMS devices’, *Journal of Micromechanics and Microengineering*, vol. 13, no. 5, pp. 663–669, Sep. 2003.

[81] B. Riddle, J. Baker-Jarvis, and J. Krupka, ‘Complex permittivity measurements of common plastics over variable temperatures’, *IEEE Transactions on Microwave Theory and Techniques*, vol. 51, no. 3, pp. 727–733, Mar. 2003.

[82] J. Capodagli and R. Lakes, ‘Isothermal viscoelastic properties of PMMA and LDPE over 11 decades of frequency and time: a test of time–temperature superposition’, *Rheologica Acta*, vol. 47, no. 7, pp. 777–786, Jun. 2008.

[83] A. Tanwar, K. Gupta, P. Singh, and Y. Vijay, ‘Dielectric measurements on PWB materials at microwave frequencies’, *Bulletin of Materials Science*, vol. 29, no. 2, pp. 181–185, 2006.

[84] D. H. Werner and S. Ganguly, ‘An overview of fractal antenna engineering research’, *Antennas and Propagation Magazine, IEEE*, vol. 45, no. 1, pp. 38 – 57, Feb. 2003.

[85] I.-K. Kim, J.-G. Yook, and H.-K. Park, ‘Fractal-shape small size microstrip patch antenna’, *Microwave and Optical Technology Letters*, vol. 34, no. 1, pp. 15–17, May 2002.

Appendix

A. Antenna prototyping using the CO_2 laser cutter

To demonstrate the possibility of using CO_2 laser cutter for other metal electrode patterning applications, microstrip patch antenna prototyping is selected. In this respect, two microstrip patch antennas are designed and simulated using ANSOFT Designer© software.

The first antenna is a standard patch antenna designed for 3.5 GHz on a 2.85 mm thick PMMA substrate. PMMA microwave frequency design variables used in the simulation process are ([81–83]): permittivity of 2.7 and loss tangent of 0.037. The second antenna is a first-iteration Koch fractal island microstrip antenna [84], [85] with an iteration factor of 0.25 which is designed for 8 GHz on a 2.85 mm thick PMMA substrate.

The designed antenna patterns are fabricated using the CO_2 laser patterning technique. To reduce the prototyping cost, similar to microwave susceptor prototypes, acrylic mirrors (FABBACK® Acrylic Mirror Clear) are used to fabricate the antennas. VLS 3.50 laser is used in raster engraving mode with 15% speed and 25% power to pattern the aluminum and protective paint layer. 3M™Aluminium foil tape 427 (0.07 mm thick aluminum foil) is attached to the back of the patterned substrate to be used as the ground plane of the antennas. Figure A-1 shows the fabricated antennas using this technique. To provide electrical connections to the feed line of the antennas, the protective paint layer of that area was removed using acetone and the connectors are attached using silver epoxy. The input return loss of the fabricated antennas is measured using Agilent Technologies© E8362B PNA series network analyzer. As illustrated in Figure A-2, simulation and measurement results of the return loss of the antennas are matched, indicating the capability of CO_2 laser cutter for such applications.

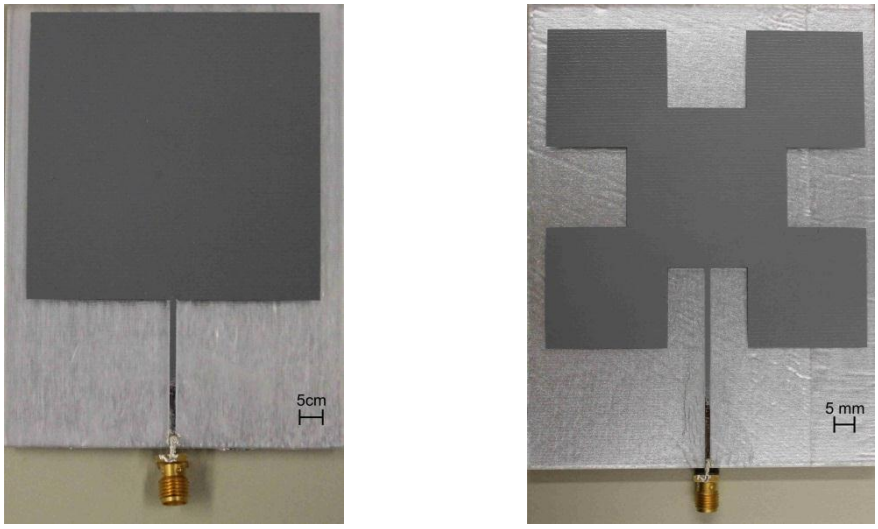

(a) (b)

Figure A-1 - (a) Simple microstrip patch antenna prototype fabricated using CO_2 laser cutter (b) first iteration Koch island microstrip patch antenna with the iteration factor of 0.25, fabricated using CO_2 laser cutter

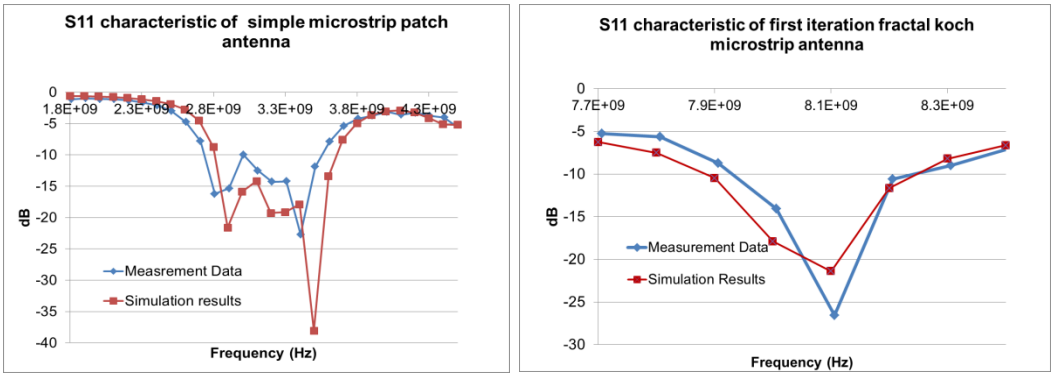

(a) (b)

Figure A-2 - Input return loss characteristics of fabricated microstrip antenna prototypes

B. Maximizing PMMA-PMMA contact area using efficient hollow susceptor patterns

As discussed in chapter 3, RF currents primarily flow near the edges of the conductor. Thus, removing part of the center of the conductor (furthest from the edges) is expected to have minimum influence on the heating efficiency of the susceptors. Having smaller areas of the substrate covered with metal has the advantage of having an increased PMMA-PMMA contact area which results in higher chance of producing a PMMA-PMMA bond (relatively strong) rather than a PMMA-Metal bond.

To verify this hypothesis a hollow-eye shape pattern was simulated at test location #2 (Figure B-1). A comparison between the simulation results of the eye-shape pattern and its hollow version, does not show a significant influence (caused by removing the center area of the conductor) neither on the pattern of the MSCD nor on its magnitude ranges. The hollow eye-shape pattern was also experimentally fabricated and tested at test location #2. While the hollow eye-shape pattern has a slightly smaller heating rate than the original eye-shape pattern (Figure B-1(d)), but it still has a relatively high heating rate.

Future studies can focus on different hollow patterns and their optimization to achieve rapid localized bonding with the minimum metal area required.

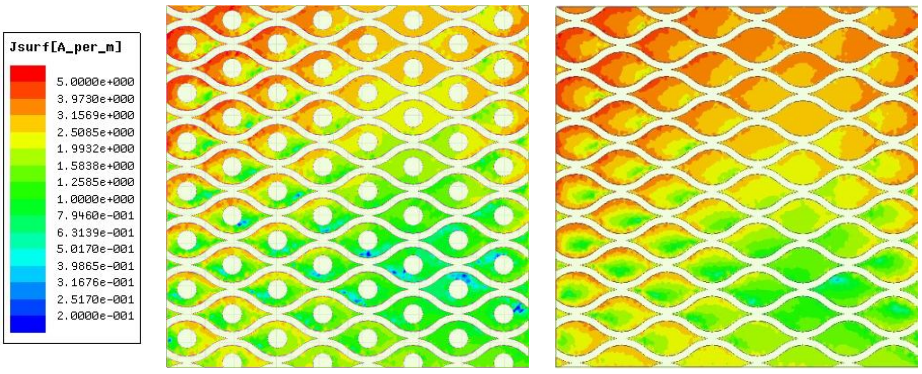

(a) (b)

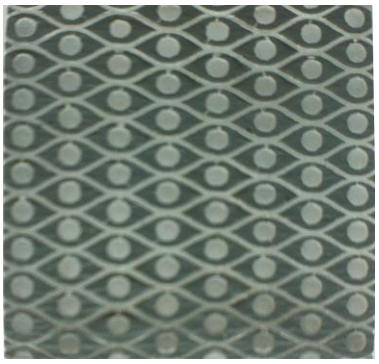

(c)

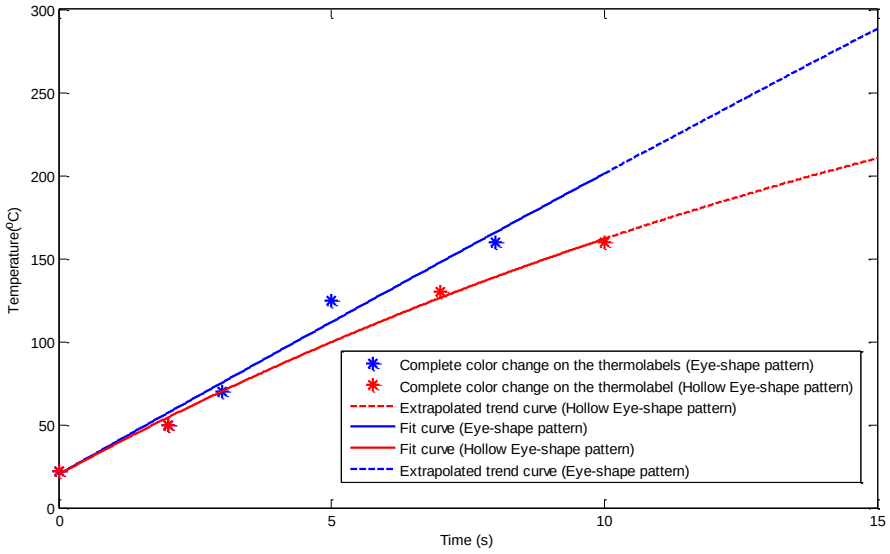

(d)

Figure B-1 – (a) Simulation results (MSCD) of a hollow eye-shape susceptor (D_L = 5.6 mm) (b) Simulation results of eye-shape susceptor (D_L = 5.6 mm) (c) Hollow eye-shape susceptor fabricated from FABBAK acrylic mirrors using CO_2 Laser cutter. (d) Temperature vs. time profiles of eye-shape susceptor and its hollow version